

THE COMPUTATIONAL THERMODYNAMIC MODELLING
OF THE PHASE EQUILIBRIA PERTAINING TO THE
TiO₂ – Ti₂O₃ – FeO SLAG SYSTEM

by

DAVID JOHANNES FOURIE

Thesis submitted in partial fulfillment
of the requirements for the Degree



MASTER OF SCIENCE IN ENGINEERING
(EXTRACTIVE METALLURGICAL ENGINEERING)

Department of Process Engineering

University of Stellenbosch

Supervised by:

Dr J.J. EKSTEEN (University of Stellenbosch, South Africa)

Dr J.H. ZIETSMAN (Ex Mente, South Africa)

Stellenbosch

December 2004

DECLARATION

I, the undersigned, hereby declare that the work contained in this thesis is my own original work and that I have not previously in its entirety or in part submitted it at any university for a degree.

DJ FOURIE

September 2004

SUMMARY

During the production of pure TiO_2 for the pigment industry, ilmenite, containing 35 – 60 % TiO_2 , is reduced to high titania slag, containing 85 – 95 % TiO_2 and pig iron. These ilmenite smelters are operated in very tight operating windows. Over reducing the slag may lead to the formation of TiC and reducing much of the TiO_2 to Ti_2O_3 . According to Namakwa Sands furnace operators, this does not only affect the grade of the product, but it can cause slag foaming and furnace eruptions. In under reducing conditions, the liquid slag is fluxed by the FeO and may corrode the furnace lining and consequently lead to run-outs. The reducing conditions in the furnace are not only controlled by carbon addition, but also by temperature. Standard practise in industrial ilmenite smelters is to operate the furnace with a slag freeze lining to protect the refractory lining from chemical and physical attack by the slag. It is therefore clear that it is of great importance to be able to predict the slag liquidus temperature at different compositions. This can help the operator to avoid dangerous operating conditions.

Over the past few decades, a number of solution models have been developed to describe non-ideal solutions. With the rapid increase in computer power, these models became more valuable and practical to use in advanced control and decision-support. In this study, some of the better-known models are discussed and evaluated for the $\text{TiO}_2 - \text{Ti}_2\text{O}_3 - \text{FeO}$ system, based on a critical review of properties and measurements published in literature.

Two of these models, the “modified quasi-chemical” model and the “cell” model were chosen to be applied to the high-titania slag system. Both these models are based on statistical thermodynamics with some differences in the initial assumptions. In this study, the model parameters for the cell model were regressed from experimental data.

The high-titania slag produced, consists mainly of titanium in different oxidation states and FeO , placing its composition inside the $\text{TiO}_2 - \text{Ti}_2\text{O}_3 - \text{FeO}$ ternary system. Reliable experimental data for this system are very limited. All three binary systems

contained in the $\text{TiO}_2 - \text{Ti}_2\text{O}_3 - \text{FeO}$ system were considered, namely $\text{FeO} - \text{TiO}_2$, $\text{TiO}_2 - \text{Ti}_2\text{O}_3$ and $\text{FeO} - \text{Ti}_2\text{O}_3$. Only liquidus data for these three binaries were used to regress the model parameters. Accuracy of the models was determined by calculating the root mean square (RMS) error between the experimental data point and the value calculated using the model and the newly determined model parameters. These errors corresponded well with the reported experimental error of the datasets for both the models and all the binary systems.

Due to the fact that this study focussed on the liquidus surface of the system, the results were also plotted in the form of binary phase diagrams and ternary liquidus isotherms. The cell model uses only binary interaction parameters to describe the ternary system. These parameters are not expanded to higher order polynomials, which makes this model more robust, but also less accurate than other models such as the modified quasi-chemical model.

OPSOMMING

Tydens die produksie van suiwer TiO_2 vir die pigmentbedryf, word ilmeniet, wat 35 tot 60 % TiO_2 bevat, gereduseer tot 'n hoë titaan slak, met 'n TiO_2 inhoud van 85 tot 95 % TiO_2 , en potyster. Hierdie ilmeniet smeltoonde word binne baie nou bedryfskondisies beheer. Oor-redusering van die slak kan lei tot the formasie van TiC en die redusering van TiO_2 tot Ti_2O_3 . Dit affekteer nie net die produk se kwaliteit nie, maar kan volgens Namakwa Sands oond operateurs ook slak skuiming en ontploffings tot gevolg hê. Gedurende onder-reduserende omstandighede in die oond, word die vloeibaarheid van die slak verhoog deur die hoër FeO inhoud in die slak. Dit maak die slak meer korrosief en kan lei tot faling van die vuurvaste stene. Die mate van redusering in die oond word nie net bepaal deur die toevoeging van koolstof nie, maar ook deur die temperatuur van die slak. Dit is 'n standaard praktyk van die industrie om die oond te bedryf met 'n gevriesde slak laag om sodoende die vuurvaste stene te beskerm teen chemiese en fisiese aanval van die slak. Dit is dus duidelik dat dit baie belangrik is om die slak se smeltpunt by verskillende samestellings te kan voorspel. Dit kan die operateur help om die oond binne veilige bedryfskondisies te hou.

'n Hele aantal oplossingsmodelle is oor die afgelope paar dekades ontwikkel vir die beskrywing van nie-ideale oplossings. Hierdie modelle het oor die afgelope paar jaar baie toegeneem in praktiese waarde as gevolg van die snelle toename in rekenaarkapasiteit en -spoed. Dit het veral groot waarde in gevorderde beheerstelsels en besluitneming steun. Sommige van die meer bekende modelle word in hierdie studie bespreek en ge-evalueer vir die $\text{TiO}_2 - \text{Ti}_2\text{O}_3 - \text{FeO}$ stelsel, gebaseer op 'n kritiese evaluasie van eienskappe en eksperimentele data gepubliseer in die literatuur.

Twee van hierdie modelle, die “gemodifiseerde kwasi-chemiese” model en die “sel” model, is gebruik om die hoë titaan slak stelsel te beskryf. Beide hierdie modelle is gebaseer op statistiese termodinamika en het klein verskille m.b.t. die aanvanklike aannames. Die model veranderlikes vir die sel model is in hierdie studie afgelei vanaf die eksperimentele data.

Die hoë titaan slak wat tydens hierdie proses geproduseer word, bestaan hoofsaaklik uit FeO en titaan in sy verskillende oksidasie toestande. Dit plaas die samestelling van die slak reg binne die $\text{TiO}_2 - \text{Ti}_2\text{O}_3 - \text{FeO}$ ternêre stelsel. Betroubare eksperimentele data vir hierdie stelsel is baie beperk. In hierdie studie word daar gekyk al drie binêre stelsels binne die $\text{TiO}_2 - \text{Ti}_2\text{O}_3 - \text{FeO}$ ternêre stelsel, naamlik: $\text{FeO} - \text{TiO}_2$, $\text{TiO}_2 - \text{Ti}_2\text{O}_3$ en $\text{FeO} - \text{Ti}_2\text{O}_3$. Slegs die smeltpunt temperatuur data vir hierdie twee binêre is gebruik in die afskatting van die model veranderlikes. Die akkuraatheid van die modelle is bepaal deur die wortel van die gemiddelde kwadraat van die fout tussen die eksperimentele waardes en die berekende waardes te bepaal. Albei die modelle het 'n relatiewe klein fout in vergelyking met die gerapporteerde eksperimentele fout gehad vir al die binêre stelsels.

Hierdie studie het gefokus op die smeltpunt temperatuur van die slak en die resultate is daarom ook in die vorm van binêre fasesdiagramme en isoterme projeksies op die ternêre fasesdiagramme gestip. Die “sel” model gebruik slegs binêre interaksie parameters om die ternêre stelsel te beskryf. Hierdie parameters word vir die “sel” model nie uitgebrei tot hoër order polinome en dit maak die “sel” model meer robuust, maar minder akkuraat as ander modelle soos byvoorbeeld die “kwasi-chemiese” model.

Aan Cozette

En in herinnering aan my goeie vriend

Boots (1975 – 2002)

ACKNOWLEDGEMENTS

I would like to acknowledge the contributions and support of many friends, colleagues and family who made the completion of this thesis possible. In particular, I would like to thank the following people and organisations for their support:

- I would like to express my sincerest gratitude to my two supervisors, Jacques Eksteen and Johan Zietsman, who throughout the project shared their insights, reminded me of the value of my contribution and kept me focussed on the job at hand.
- Not only the advice and help from Dr. Klaus Hack of GTT in Germany, but the friendly and patient way in which he gave it, is much appreciated.
- A special thank you goes to Mr Goosen, my high-school teacher, who translated an essential paper for me from German.
- I acknowledge the funding of the project and the financial support from Mintek.
- Thank you to my colleague and friend, Pranusha Pather, for proofreading the manuscript.
- I also want to thank all my friends and family, especially my parents, for their support and prayers throughout.
- Finally I want to thank my wife, Cozette, for her support and her faith in me that kept me going.

All the credit goes to my Creator, God Almighty, who gave me talents, opportunities, family and friends who made everything possible.

TABLE OF CONTENTS

1	INTRODUCTION.....	1
1.1	Titanium products.....	1
1.2	Titanium feedstock.....	2
1.3	Production of titanium dioxide pigment	4
2	LITERATURE REVIEW.....	6
2.1	General considerations	6
2.2	Structure of high titanium slags.....	8
2.2.1	General considerations	8
2.2.2	The co-ordination of titanium ions.....	9
2.2.3	Physical properties of titanium containing melts related to their structure 12	
2.2.3.1	The viscosity of titanium containing slags.....	12
2.2.3.2	The electrical conductivity of titanium containing slags	14
2.3	Thermodynamic models	15
2.3.1	The basic approach to thermochemical modelling.....	16
2.3.2	Raoult's law (ideal solution)	18
2.3.3	Henry's law (dilute solution)	20
2.3.4	The Regular solution model.....	22
2.3.5	The Sub-regular solution model.....	25
2.3.6	Temkin's theory	26
2.3.6.1	Electrical equivalent ion fraction	27
2.3.7	The Polymerization model	29
2.3.8	Two-Sub lattice Model.....	35
2.3.9	The Quasi Chemical model	37
2.3.9.1	Basic Quasi Chemical theory	37
2.3.9.2	The modified binary quasi chemical theory	39

2.3.9.3	Fixing the composition of maximum ordering.....	43
2.3.9.4	Composition dependence of ω and η	46
2.3.9.5	Partial molar properties	47
2.3.9.6	The modified quasi-chemical theory for ternary solutions	48
2.3.9.7	Partial molar properties	51
2.3.10	The Cell Model	52
2.3.10.1	Background	52
2.3.10.2	Basic Hypotheses	52
2.3.10.3	Energy of cells formation.....	53
2.3.10.4	Energy of cells interaction	53
2.3.10.5	Expression of the thermodynamic functions of the liquid mixture of oxides	54
2.3.11	Unified interaction parameter formalism	57
2.3.11.1	The standard interaction parameter formalism	57
3	THERMODYNAMICS/PHASE DIAGRAM DATA.....	62
3.1	Relating thermodynamics and phase diagrams	62
3.2	Thermodynamics and phase equilibrium in the Ti – O system	64
3.2.1	The Ti – TiO ₂ system	64
3.2.2	The TiO ₂ – Ti ₂ O ₃ system.....	69
3.3	Thermodynamics and phase equilibrium in the Ti – Fe – O system	71
3.3.1	The FeO – TiO ₂ system.....	71
3.3.2	The FeO – Ti ₂ O ₃ system	77
4	MODELLING TECHNIQUE AND PROCEDURE	78
4.1	Choosing a model	78
4.2	Model implementation on computers.....	82
4.2.1	ChemSAGE.....	82
4.2.1.1	The general structure of ChemSage (Bale et al., 2002)	83
4.2.1.2	Gibbs free energy minimization.....	89

4.2.1.3	Least squares parameter estimation	91
4.2.2	F*A*C*T.....	96
4.2.3	FactSage	97
4.2.4	Optimization procedure.....	99
5	A REVIEW OF THE DATA USED	101
6	MODELLING RESULTS AND DISCUSSION	103
6.1	The FeO – TiO ₂ binary	103
6.2	The TiO ₂ – Ti ₂ O ₃ binary	105
6.3	The TiO ₂ – Ti ₂ O ₃ - FeO ternary	107
7	CONCLUSIONS AND RECOMMENDATIONS.....	113
8	REFERENCES.....	115
9	APPENDICES	122
9.1	APPENDIX A: Thermodynamic data used for calculations.....	122
9.2	APPENDIX B: ChemSAGE datafiles used in the optimisations.	128
9.3	APPENDIX C: Pure component data used in the optimisations.....	137
	NOMENCLATURE.....	157

TABLE OF FIGURES

Figure 1: Activity - Composition diagram for a hypothetical binary solution $A - B$	21
Figure 2: Enthalpy and entropy of mixing of a binary system for different degrees of ordering about $X_A = X_B = 1/2$. Curves are calculated from the modified quasi-chemical theory at $T = 1000$ °C with $z = 2$ for the constant values of ω (kcal) and with $\eta = 0$. (Pelton and Blander, 1984).....	38
Figure 3: Two methods to approximate ω_{ij} and η_{ij} in the ternary system from their values in the binaries	50
Figure 4 The binary phase diagram for components A and B that are completely miscible over the entire composition range.....	62
Figure 5 Binary phase diagram for the system $Ti-TiO_2$ summarizing various data in the literature (after De Vries and Roy (1952)).....	64
Figure 6: Titanium-oxygen phase diagram (after Wahlbeck and Gilles, 1966).....	65
Figure 7: Assessed $Ti-O$ phase diagram (after Murray and Wriedt (1987)).....	66
Figure 8: Calculated $T-X$ phase diagram of $Ti-O$ and experimental data up to 0.62 mole fraction oxygen (after Waldner and Eriksson, 1999).	67
Figure 9: Calculated $T-X$ phase diagram of the system $Ti-O$ for $0 \leq x_o \leq 1$ and 1 bar total pressure. Predicted gas/liquid equilibria are also shown (after Waldner and Eriksson, 1999).....	68
Figure 10: $TiO_2 - Ti_2O_3$ phase diagram determined by Brauer and Littke (1960)	69
Figure 11: Optimised $Ti_2O_3 - TiO_2$ phase diagram. Composition in terms of components $TiO_{1.5} - TiO_2$ (after Eriksson and Pelton, 1993).....	70
Figure 12: $FeO - TiO_2$ phase diagram as postulated by Grieve and White (1939).....	71
Figure 13: $FeO - TiO_2$ phase diagram after MacChesney and Muan (1961).....	72
Figure 14: Liquidus points in the high titanium region of the $FeO - TiO_2$ binary, after Grau (1979)	73
Figure 15: Examples of cooling curves after Grau (1979)	74
Figure 16: High titanium region of the $FeO - TiO_2$ binary, after Grau (1979).....	75
Figure 17: Optimised $FeO - TiO_2$ phase diagram, after Eriksson and Pelton (1993). Experimental points from Grau (1979)	76
Figure 18: Comparison of MnO activity calculated by the Modified Quasi-chemical model with measured data in $SiO_2-MnO-CaO$ melts at 1500 °C and 1650 °C. Reference state: pure solid MnO . (after Li et al. 1998).....	78
Figure 19: Comparison of MnO activity calculated by the Cell model with measured data in $SiO_2-MnO-CaO$ melts at 1500 °C and 1650 °C. Reference state: pure solid MnO . (after Li et al. 1998)	79
Figure 20: Comparison of MnO activity calculated by the Modified Quasi-chemical model with measured data in $SiO_2-Al_2O_3-MnO-CaO$ melts at 1650 °C. Reference state: pure solid MnO . (after Li et al. 1998).....	80
Figure 21: Comparison of MnO activity calculated by the Cell model with measured data in $SiO_2-Al_2O_3-MnO-CaO$ melts at 1650 °C. Reference state: pure solid MnO . (after Li et al. 1998).....	81

Figure 22: The functional structure of ChemSage, after Klaus Hack, ChemSage Handbook 84

Figure 23: FactSage Timeline 98

Figure 24: FeO – TiO₂ phase diagram as calculated by the cell model 103

Figure 25: FeO – TiO₂ phase diagram as calculated by the modified quasi chemical model (after Eriksson and Pelton, 1993) 104

Figure 26: TiO₂ – Ti₂O₃ phase diagram as calculated by the modified quasi chemical model..... 105

Figure 27: TiO₂ – Ti₂O₃ phase diagram as calculated by the cell model 106

Figure 28: The liquidus isotherm at 1500 °C for the TiO₂ - TiO_{1.5} - FeO ternary after Pesl and Eric (1997)..... 107

Figure 29: Data points of the 1500 isothermal section using Ti₂O₃ in stead of TiO_{1.5} 108

Figure 30: The liquidus isotherm at 1500 °C for the TiO₂ - Ti₂O₃ - FeO ternary as calculated using the MQC model combined with the measured data points by Pesl (1997) 109

Figure 31: The liquidus isotherm at 1500 °C for the TiO₂ - Ti₂O₃ - FeO ternary as calculated using the Cell model combined with the measured data points by Pesl (1997)..... 110

Figure 32: Liquidus projection of the TiO₂ - Ti₂O₃ - FeO ternary system using the Cell model to describe the liquid slag phase. 111

Figure 33: Liquidus projection of the TiO₂ - Ti₂O₃ - FeO system using the Modified Quasi-chemical model to describe the liquid slag phase. 112

LIST OF TABLES

Table 1: World titanium production in thousand metric tons 3

Table 2: Type of bonding and attraction forces between cations and O²⁻ anions (After Tranell, 1999). 10

Table 3: Summarised interaction parameters. 114

1 INTRODUCTION

1.1 Titanium products

Titanium metal became famous during the Cold War as a space-age metal. Its very high strength-to-weight ratio and resistance to corrosion made it ideal for lightweight, high-performance jet engines. Today the main demand for titanium metal comes from the commercial aerospace industry. New applications for lightweight metals arise daily in leisure consumer products (such as golf clubs) and in medical implants. The demand for titanium is expected to increase as the economies of the world expand their commercial and military aerospace and consumer product markets.

However, only about 5 % of titanium is consumed in the form of metal alloys. The rest, 95 % of the total yearly consumption, is in the form of titanium dioxide (TiO_2) pigment (US Geological Survey, 2003). Titanium dioxide is a white pigment in paints, paper and plastics. This pigment is characterized by its purity, refractive index, particle size and surface properties. For optimum pigment properties, its particle size is controlled to be half the wavelength of visible light (about 0.3 microns). TiO_2 is a superior white pigment due to its high refractive index and light scattering ability. Titanium dioxide is produced as two major types: rutile and anatase, which are chemically similar, but have different crystal structures. The rutile-type pigment is less reactive than anatase when exposed to sunlight and is preferred for use in outdoor paints. Anatase has a bluer tone and is less abrasive than rutile and is used mainly in indoor paints and paper. Titanium pigments can exhibit a range of properties such as opacity, durability, dispersion and tinting, depending on the production route and finishing of the product.

1.2 Titanium feedstock

Titanium is the ninth most abundant element in the earth's crust and occurs primarily in the minerals: anatase, brookite, ilmenite, leucoxene, perovskite, rutile and sphene. Only ilmenite, leucoxene and rutile contain enough titanium to be of economic importance. Naturally occurring anatase and rutile are more or less pure TiO_2 , but cannot be used as white pigment due to discolouration caused by impurities. Of all the titanium bearing minerals, ilmenite and leucoxene are the most abundant, accounting for almost 90 % of the titanium feedstock with rutile and anatase making up the balance. Theoretically ilmenite contains 52.65 wt% TiO_2 , but this number can be increased due to weathering and the removal of iron oxide. Leucoxene is weathered ilmenite that can contain up to 90 % TiO_2 (Pesl, 1997).

Australia is currently the world's largest producer of titanium concentrates, consisting of rutile, ilmenite and synthetic rutile, with South Africa second and Canada third. Most of the high-titania slag currently produced derives from South Africa (~54%) and Canada (~46%) as a result of upgrading local ilmenite feedstock. The world titanium mineral production figures are summarized in Table 1 as published on the Internet by the United States government (2003).

Table 1: World titanium production in thousand metric tons

	Mine production		Reserves	Reserve base
	<u>2001</u>	<u>2002</u> [°]		
Ilmenite:				
United States	300	300	7 000	59 000
Australia	1 150	1 100	200 000	250 000
Canada	950	950	31 000	36 000
India	232	250	30 000	38 000
Norway	338	350	40 000	40 000
South Africa	960	950	63 000	220 000
Ukraine	252	250	5 900	13 000
Other countries	391	390	49 000	84 000
World total (ilmenite, rounded)	4 600	4 500	420 000	730 000
Rutile:				
United States	¹	¹	400	1 800
Australia	225	220	22 000	34 000
India	16	15	6 600	7 700
South Africa	110	105	8 300	24 000
Ukraine	56	56	2 500	2 500
Other countries	4	4	8 000	17 000
World total (rutile, rounded)	410	400	48 000	87 000
World total (ilmenite and rutile, rounded)	5 000	4 900	470 000	820 000

[°] Estimated

¹ Included with ilmenite to avoid revealing company proprietary data

1.3 Production of titanium dioxide pigment

Titanium dioxide pigment is produced via one of two routes: either the chloride process or the sulphate process. Either process may be used to produce rutile or anatase type pigment. The process chosen is dependent on a number of factors including raw material availability, freight and waste disposal cost.

In the chloride process, rutile is carbo-chlorinated at 850 – 950 °C to form TiCl_4 . Titanium tetrachloride is then oxidized in air at 1000 °C to form TiO_2 . Aluminium oxide can be added to ensure that all the TiO_2 formed, are in the rutile structure. The chloride route is used on feed with high titanium content. Feed with lower titanium content consumes much more chlorine and produces large quantities of ferric and other chlorides that have to be disposed of (Pesl, 1997).

Slag produced from hard rock titanium deposits are not suitable for the chloride process and are treated via the sulphate route. In the sulphate process, ilmenite or high titanium slag is reacted with sulphuric acid and some of the iron sulphate formed, is crystallized and removed. Titanium hydroxide is precipitated, filtered and calcined. This process produces large quantities of hydrated ferrous sulphate and diluted sulphuric acid.

Strict environmental laws and the high cost of waste disposal, makes the chlorine route the more desirable option. The chlorine route demands a feed high in titanium and only a small percentage of the world reserves are in the form of rutile, which has the highest titanium content. Therefore an ever increasing quantity of ilmenite will have to be upgraded to synthetic rutile or high-titania slag. Plants utilising the sulphate route, have also moved towards the use of high-titania feedstock to reduce the amount of waste and increase plant throughput (Pesl, 1997).

Objectives and motivation of this project

In sections 1.1 – 1.3, the importance of the upgrading of ilmenite ore to high-titania slag has been highlighted. The growing demand for high-titania feedstock and more stringent environmental laws will lead to an increase in the demand for high-titania slag. South Africa is a major exporter of high-titania slag and ilmenite smelting is expected to become a huge industry in the future. At the moment two major role-players in the South African titanium industry are Namakwa Sands and Richard Bay Minerals, who have ilmenite smelters in the Western Cape and Kwazulu Natal respectively. South Africa's third producer, Ticor-SA, started hot commissioning of their first smelter in March 2003 and their second smelter started up at the end of 2003. In a more competitive market, it will be the metallurgist's job to optimize and control the process in such a way to minimize production cost and maximize investors' returns. Important data needed to characterize and control the reactions in the furnace, are the phase equilibrium and fundamental thermodynamic data at high temperatures. Such data cannot be measured online and it would be beneficial to have a solution model to describe the process.

The objectives of this study were:

- To collect and critically evaluate all the experimental data available in the literature.
- To investigate the applicability of various slag solution models to high titanium slags.
- To calculate solution model parameters from the experimental data points.
- To calculate the phase diagram of the TiO_2 - Ti_2O_3 - FeO ternary system and compare it with published data. This ternary system has not been found to be optimised in open literature, at the date of compiling this thesis.

2 LITERATURE REVIEW

2.1 *General considerations*

Reliable information on the thermodynamic properties and activities of titanium oxides in high-titania slag, are very limited and sometimes contradictory. A number of investigators (De Vries and Roy (1952), Wahlbeck and Gilles (1966), Brauer and Littke (1960), Murray and Wriedt (1987), Waldner and Eriksson (1999), Eriksson and Pelton (1993), Grieve and White (1939), MacChesney and Muan (1961), Smith and Bell (1970)) studied the $\text{FeO} - \text{TiO}_2$ and $\text{TiO}_2 - \text{Ti}_2\text{O}_3$ binary systems and the commonly accepted phase diagrams have been improved over the years. Other researchers (Sevinç, 1989; Taylor, 1963) determined the $\text{FeO} - \text{TiO}_2 - \text{Fe}_2\text{O}_3$ ternary phase diagram at more oxidizing conditions. This phase equilibrium is more applicable to the weathering of ilmenite, solid state reduction of the ilmenite family of minerals and to steel production. Conditions during ilmenite smelting are far more reducing and the reactions take place at much higher temperatures than most of the work done up to date. Most of the fundamental work on the reduction of ilmenite encountered in the literature, were carried out at temperatures below 1300 °C and thus in the solid state. The only data found in the literature for the $\text{TiO}_2 - \text{Ti}_2\text{O}_3 - \text{FeO}$ ternary systems are activities measured by Pesl (1997) at 1500 and 1600 °C. Due to the lack of relevant data, all the data at lower temperatures were also studied to achieve a better understanding of the system. Information from different sources was evaluated and combined to form a complete and thermodynamically consistent database for the system under consideration.

The structure of high-titania slag as well as all the solid solutions of the system was also investigated. This had great importance in the application of the right type of solution model.

Thermodynamic models are very powerful tools in relating thermodynamic properties of solutions to the composition and temperature of the solution. A number of models are available for different types of slags, metallic- and solid solutions. Some of the relevant models were studied in detail and results of two powerful solution models

were compared directly. Both of the melt solution models are semi-empirical, that is they both have variables whose interrelationship can be explained through fundamental chemistry, but whose parameters have to be derived empirically.

2.2 Structure of high titanium slags

Since the thermodynamics of slags are directly related to their structure (Tranell, 1999), it is necessary to discuss the structure and physical properties of these melts in order to understand their thermodynamics.

2.2.1 General considerations

Slag is a generic term for non-metallic liquid oxide solutions, which may contain some halides or sulphides. In pyrometallurgical processes, slag usually forms a separate liquid phase that floats on top of the metal / matte phase because of its immiscibility and lower density. An exception to this rule is the high temperature aluminium process where alumina (Al_2O_3) has a higher density than aluminium metal and the metal floats on top of the slag. However, in this case halide salts are added which lowers the slag density. In most practical cases, the metal phase contains the valuable product. The slag phase then serves as a receiver of all the unwanted constituents such as gangue or impurities present in the feed materials. The physical properties of the slags are controlled by adjusting its composition through the addition of fluxes such as silica, lime and alumina or through reduction of some of its oxides with carbonaceous reductant. In electrical furnaces, the most important properties of the slag are viscosity, liquidus temperature and electrical conductivity. Liquid slag viscosity is dependent on slag composition and temperature. The effective viscosity is dependent on the degree of sub-cooling below the liquidus temperature, as crystal increases the slag viscosity.

High-titania slags are different from other slags, because in the case of ilmenite smelting, slag is the main valuable product. The metal phase, which is pig iron, is a by-product of much lesser value. Fluxing the slag to adjust its liquidus temperature and electrical conductivity increases the amount of impurities present and may cause problems in downstream processes or even render the slag useless as feed material for the sulphide and chloride processed of pigment production discussed earlier.

The liquidus temperature of high-titania slag is determined mainly by the FeO content of the slag and to some extent by the other impurity oxides. As these oxides are increasingly reduced during the ilmenite smelting process, the liquidus temperature of the slag rises steadily. When the FeO content of the slag drops below about 10-wt %, the liquidus temperature increases to above 1700 °C. At this elevated temperature, the slag is very corrosive and the process becomes costly due to repairs and downtime. The higher melting temperature also requires a higher energy input, resulting in an increase in energy costs.

The chemical composition of the $\text{Fe}_x\text{O} - \text{Ti}_x\text{O}$ system determines its liquidus temperature. The balance between energy input into the furnace and energy removal and the liquidus temperature determines the thickness of the freeze lining and the active volume of the melt.

Reaction kinetics also plays a role, as the reduction reaction becomes very slow at lower FeO values. To reduce the FeO to these low values will be very time consuming and therefore very costly (Fourie, 2003).

A third reason for not reducing all the FeO out of the system is the precipitation of Titanium carbide (TiC). At highly reducing conditions titanium carbides and titanium oxy-carbides will form. These compounds are very stable, with very high melting points and cause a very rapid increase in the slag viscosity. This will make it almost impossible to tap the slag from the furnace and might also cause foaming and furnace eruptions (Fourie, 2003). It is therefore of vital importance to be able to control the composition of the slag as well as the energy input into the melt.

2.2.2 The co-ordination of titanium ions

Titanium dioxide is generally classified as an amphoteric oxide although Ti^{4+} is regarded as a network-forming ion in traditional basic silicate slags. TiO_2 , however, weakens the silicate network (Tranell, 1999). It can therefore also act as a network breaker/modifier in acid silicate slags.

The ionic fraction of the bond between Ti^{4+} and O^{2-} is approximately 0.41. This indicates that the bond is covalent, but as can be seen in Table 2, titanium dioxide, like Fe_2O_3 and Al_2O_3 , is characterised as an amphoteric oxide. The Ti^{4+} ion is comparatively small and carries a large charge, leading to the Coulomb force between cation and anion being relatively large (Tranell, 1999). This means that the ionic bond is comparatively strong, giving TiO_2 the potential of tetrahedral co-ordination and therefore network forming ability.

Table 2: Type of bonding and attraction forces between cations and O^{2-} anions (After Tranell, 1999)

Oxide	$Z/(R_c+R_a)^2$ (\AA^{-2})	Ionic fraction of Bond	Co-ordination number		Character of oxide
			Solid	Liquid	
Na_2O	0.18	0.65	6	6 to 8	Network Breakers Or Basic Oxides
BaO	0.27	0.65	8	8 to 12	
SrO	0.32	0.61	8		
CaO	0.35	0.61	6		
MnO	0.42	0.47	6	6 to 8	
FeO	0.44	0.38	6	6	
ZnO	0.44	0.44	6		
MgO	0.48	0.54	6		
BeO	0.69	0.44	4		
Cr_2O_3	0.72	0.41	4		Amphoteric Oxides
Fe_2O_3	0.75	0.36	4		
Al_2O_3	0.83	0.44	6	4 to 6	
TiO_2	0.93	0.41	4		
SiO_2	1.22	0.36	4	4	Network Formers Or Acid Oxides
P_2O_5	1.66	0.28	4	4	

Z = cation charge, R_c = radius of cation, R_a = radius of anion

The co-ordination of Ti^{4+} in molten slags has been found to be strongly dependent on the slag composition and particularly the silica content. TiO_2 and SiO_2 behave similarly in terms of interaction with other components, but due to the large liquid miscibility gap in the $\text{TiO}_2 - \text{SiO}_2$ system, it is clear that these similarities do not

imply structural similarity. De Vries and co-workers (1954), who first confirmed the existence of the miscibility gap, concluded that Ti^{4+} probably has six-fold coordination. In high silica slags, for TiO_2 concentrations under 9 wt%, the titanium is in fourfold coordination and can substitute the Si^{4+} ions in the network. Somerville and Bell (1982) found that TiO_2 prefers octahedral co-ordination and simple ions unlike SiO_2 that prefers tetrahedral co-ordination and large polymerised ions. TiO_2 thus acts as a network breaker.

It is clear that, due to its amphoteric nature and opposing Coulomb and covalent forces, TiO_2 can behave as either a network former or a network modifier, depending on the slag composition. It is also accepted that, in high-titania, low-silica slags, Ti^{4+} will have an octahedral co-ordination and will prefer not to form polymerised structures. Very little work has been done on the co-ordination of the reduced oxides (Ti_2O_3 ; Ti_3O_5 ; etc.), but because Ti^{3+} ions are bigger (lower charge density) it is widely accepted that Ti^{3+} behaves as a network breaker.

2.2.3 Physical properties of titanium containing melts related to their structure

2.2.3.1 The viscosity of titanium containing slags

Single phase metallurgical slags are generally Newtonian liquids and their viscosities can be described by the Arrhenius – Guzman equation:

$$\mu = A \exp(E_{\mu} / RT) \quad 2.1$$

Where A is the Arrhenius constant, E_{μ} is the energy of activation for viscous flow, R the gas constant and T the absolute temperature (Tranell, 1999).

The activation energy for viscous flow is a function of the slag composition and is, for a particular temperature, directly related to its structure. A higher degree of polymerization promotes higher melt viscosity. Liquid oxide slags are considered to be dissociated into metal cations M^{x+} and oxygen anions O^{2-} . This model is very simple and only suitable for very basic oxides above their liquidus temperatures. The size of the different metal cations plays a crucial role in its co-ordination with the oxygen anions. Pesl (1997) showed that liquid viscosity is directly related to the size of the structural units in the liquid for high titanium slags. Pure molten oxides such as SiO_2 , P_2O_5 , As_2O_3 and B_2O_3 have low co-ordination numbers (3 or 4) for the central atom. The viscosities of these melts are quite high compared to pure ionic melts because of the presence of three-dimensional covalent metal-oxide bonds in the liquid structure. These liquids are strongly polymerised and their viscosities decrease exponentially with temperature if the degree of polymerisation remains constant. Oxides with high co-ordination numbers (6 or more), on the other hand, have very low viscosities. FeO , MnO , CaO and MgO all have viscosities in the order of 50 cp near their melting points.

Several investigators (Tranell, 1999) measured the viscosity of high-titania slags containing different minor constituents. These investigators showed that TiO_2

addition increases fluidity in the $\text{CaO} - \text{Al}_2\text{O}_3 - \text{TiO}_2$, $\text{Al}_2\text{O}_3 - \text{SiO}_2 - \text{TiO}_2$, $\text{CaO} - \text{SiO}_2 - \text{TiO}_2$ and $\text{CaO} - \text{Al}_2\text{O}_3 - \text{SiO}_2 - \text{TiO}_2$ systems. These slags were very fluid once molten, regardless of the FeO and Ti_2O_3 content. This indicates that the decrease in FeO is counterbalanced by the increase in Ti_2O_3 and this in turn implies that FeO and Ti_2O_3 have a similar effect on the viscosity of the slag. The viscosity remained constant with increase in temperature, which indicates that the structure in the liquid did not change (Tranell, 1999).

The effect of reduction on the viscosity of slags containing TiO_2 is very complex. The viscosity of a slag depends on the difference between actual and liquidus temperatures (i.e. superheat), the precipitation of solid insoluble particles and on the structure of the slag. High-titania slags have a very low viscosity, but after some reduction, slag thickening occurs. This is firstly due to the formation of high melting sub-oxides (Ti_2O_3 , Ti_3O_5 , etc.) increasing the liquidus temperature of the slag and therefore decreasing the amount of superheat (Handfield et al., 1971). If the amount of superheat is kept constant, the viscosity of the slag is still very low, because the reduced titanium ions (Ti^{3+} , Ti^{2+}) act as network breakers. After further reduction the rate of thickening increases rapidly. This is due to the formation of insoluble solid Titanium carbide and Titanium Oxy-carbide precipitates (Handfield et al., 1971).

2.2.3.2 The electrical conductivity of titanium containing slags

The mechanism of electrical conductivity in slags is predominantly ionic (Tranell, 1999) and follows the Arrhenius equation for electrical conductivity:

$$\kappa = A \exp(E_{\kappa} / RT) \quad 2.2$$

Where A is the Arrhenius constant, E_{κ} is the energy of activation for viscous flow, R the gas constant and T the absolute temperature.

The electrical conductivity in liquid slags is greater than in solid slags. In slags containing high concentrations of oxides such as FeO and MnO, electronic conductivity can dominate. Since the current is carried by the cations in the molten slag, their mobility will be crucial to the conductivity of the slag. Therefore, in a slag with a higher degree of polymerisation or larger cations, the conductivity will be lower.

Very high conductivities for high-titania slags have been measured. Such high values cannot correspond to purely ionic conductivity and a predominant electronic nature is the most probable type of conduction in these slags. This is supported by the fact that titanium exists in mixed valence states in the slag. Other systems where an element occurs in mixed valence show similar conductivity values (Tranell, 1999).

2.3 Thermodynamic models

Most pyrometallurgical processes consist of at least three phases, a gas phase, a liquid slag phase and a liquid alloy phase (Li et al., 1998). In most cases the gas phase has a very high temperature and a pressure close to atmospheric pressure and can therefore be treated as an ideal gas. The liquid slag phase usually consists of a non-ideal solution of various metal oxides and the alloy can also be treated as a non-ideal solution. It is therefore very important to choose appropriate solution models to calculate activities of components in the liquid slag and the liquid alloy phases. In the high-titania system the accurate estimation of the slag liquidus temperature is critical for the control of the furnace. Below the liquidus temperature, the slag viscosity increases dramatically and foaming can occur. Consequently, it is important to operate the furnace close to the slag liquidus.

Due to the corrosiveness of high-titania slag, the furnace is operated with a freeze lining to protect the refractory against attack from the liquid slag. Keeping most of the bath above the slag liquidus and stabilising a freeze lining, requires efficient control and a proficient estimation of the slag liquidus. In addition to the liquidus temperature, the distribution of contaminant species between the slag and alloy phases can also be calculated by means of solution models.

It is clear that thermochemical models can be a very effective tool to predict chemical properties of metallurgical systems and with the increasing calculation power of modern computers it can be very valuable in online control.

2.3.1 The basic approach to thermochemical modelling

Thermochemical modelling of a multiphase, multi-component system involves the following aspects:

1. Selection of possible pure components
2. Selection of optimized solution models for solid and liquid solutions (minerals, slags, alloys)
3. Minimizing the total Gibbs-free energy of the system using the solution models, thermodynamic laws and material balances and specified T,P or ΔH and P.

Good solution models are therefore critical for accurate modelling of the phase equilibria. According to Guochang et al. (1993) solution models can be divided into three categories:

1. Physical parameter models

The essence of this kind of model is an inference of slag microstructure from the measured physical properties. For example, the bonding energy of the Si – O bond is estimated according to the activation energy of viscous flow and based on the presumed relationship between microstructure and the physical properties.

2. Thermodynamic parameter models

The ultimate aim of these models is to deduce an equation group from the available thermodynamic data, and by means of this equation group to evaluate thermodynamic properties by interpolating and/or extrapolating. The foundation of these models is a set of presumed microstructural units. The relationship between these units and experimental data is stipulated to follow basic principle of thermodynamics.

3. Structural models

According to this approach the properties are related to the microstructure, which is either measured by some advanced instruments or determined along the theoretical

approach of chemical bonding. Of the three categories, the progression of this category is the fastest. The latest developed models of Gaye (1989) and Pelton (1993) belong to this category. These models will be explored in more depth in this thesis.

2.3.2 Raoult's law (ideal solution)

In an ideal solution there is no difference between the chemical interactions between like and unlike atoms. When considering the first nearest-neighbour interaction, the bond energy between the like atoms is the same as that between the unlike atoms. Raoult's law can be defined by the following relation:

$$a_i = X_i \quad 2.3$$

where a_i is the activity of component i and X_i the mole fraction of i .

Raoult found that for a limited number of binary solutions, the partial pressure of each constituent is equal to the product of the mole fraction and the vapour pressure of the pure component.

$$p_i = p_i^0 X_i \quad 2.4$$

where p_i^0 is the vapour pressure of the pure component i and p_i the partial pressure of component i in solution.

If the vapour behaves as an ideal gas, the partial pressure of a constituent is equal to its fugacity.

$$f_i = f_i^0 X_i \quad 2.5$$

where f_i^0 is the fugacity of the pure component i and f_i the fugacity of component i in solution.

The activity of a constituent of a liquid solution is defined as $a_i = f_i/f_i^0$ and equation 2.5 can thus be reduced to equation 2.3 if the vapour behaves ideally. The partial

molar Gibbs energy of component i in a solution can then be written as follows:

$$\Delta\bar{G}_i = RT \ln a_i = RT \ln X_i \quad 2.6$$

Although no real solution behaves like an ideal solution throughout its composition range, it was found that all solutions obey Raoult's law for the solvent at very low concentrations of the solute. Thus, for Raoult's law, as $X_i \rightarrow 1$, $a_i \rightarrow X_i$.

2.3.3 Henry's law (dilute solution)

In addition to Raoult's law for the solvent, there is another limiting law for the solute at infinite dilution. It was empirically found that if the concentration of the solute of any binary solution is sufficiently low, then the partial pressure of the solute is proportional to its mole fraction at constant temperature.

$$p_i = k'X_i \quad 2.7$$

This statement is referred to as Henry's law. For an ideal solution $k' = p_i^0$ and Raoult's law is obeyed. When the gas phase behaves ideally, then $p_i = f_i$ and equation 2.7 becomes

$$f_i = k'X_i \quad 2.8$$

Dividing through by f_i^0 and noting that $a_i = f_i/f_i^0$, we find that

$$a_i = \frac{k'}{f_i^0} X_i \quad 2.9$$

or

$$a_i = kX_i \quad 2.10$$

Equation 2.10 is regarded as the primary statement of Henry's law. As for Raoult's law, the partial molar Gibbs energy of component i (solute) in an infinitely dilute solution can then be written as follows:

$$\Delta \bar{G}_i = RT \ln a_i = RT \ln kX_i = RT \ln k + RT \ln X_i \quad 2.11$$

It can be derived, by means of Gibbs-Duhem integration, that Raoult's law will be obeyed for the solvent if Henry's law is obeyed by the solute. Thus, for Henry's law, as $X_i \rightarrow 0$, $a_i \rightarrow k$.

The difference between the laws of Raoult and Henry is illustrated in Figure 1.

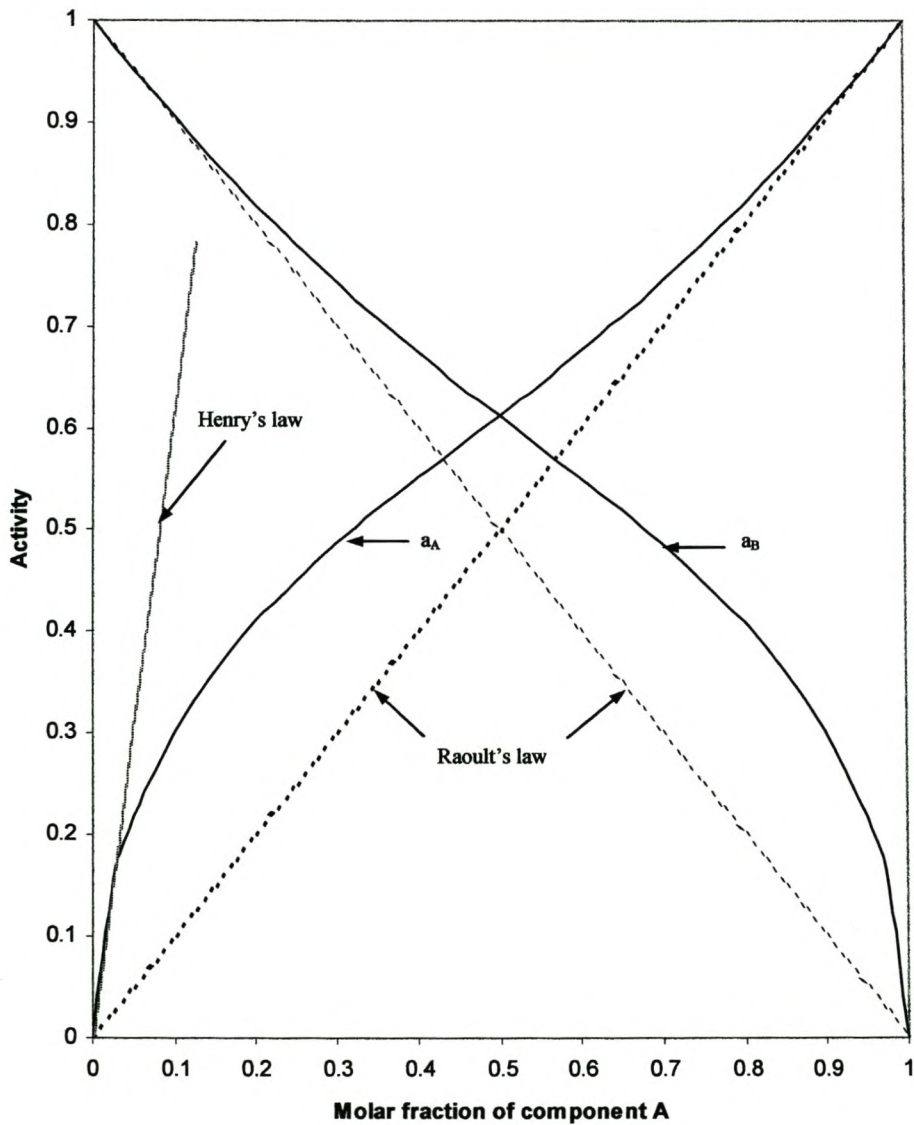


Figure 1: Activity - Composition diagram for a hypothetical binary solution *A - B*

2.3.4 The Regular solution model

During his extensive investigation of solutions and solubility, Hildebrand (1929) found that a significant portion of the solutions he studied were simple and predictable in their behaviour. He termed these solutions “regular” to distinguish them from other “irregular” solutions that behaved differently. He reasoned that the number of configurations possible should be independent of the ideality of the solution and therefore proposed that regular solutions had the same entropy of mixing as ideal solutions, but a non-zero enthalpy of mixing. This is better explained by looking at the following thermodynamic relationships for a system containing n components:

For ideal solutions:

$$\Delta H_{mix}^{id} = 0 \quad 2.12$$

$$\Delta G_{mix}^{id} = RT \sum_{i=1}^n X_i \ln X_i \quad 2.13$$

$$\Delta S_{mix}^{id} = -R \sum_{i=1}^n X_i \ln X_i \quad 2.14$$

and then for regular solutions:

$$\Delta S_{mix}^{reg} = -R \sum_{i=1}^n X_i \ln X_i \quad 2.15$$

$$\Delta G_{mix}^{reg} = RT \sum_{i=1}^n X_i \ln a_i \quad 2.16$$

$$\Delta H_{mix}^{reg} = RT \sum_{i=1}^n X_i \ln \left(\frac{a_i}{X_i} \right) = RT \sum_{i=1}^n X_i \ln \gamma_i = \Delta G_{mix}^E \quad 2.17$$

Margules (1895) noted that activities of components in a binary solution could be expressed as a series expansion in terms of X_A , the solute mole fraction:

$$\ln a_B = \ln X_B + \frac{1}{2} \beta'_B X_A^2 + \frac{1}{3} \beta''_B X_A^3 + \dots \quad 2.18$$

where β'_B and β''_B are constants. Then:

$$\ln a_B - \ln X_B = \frac{1}{2} \beta'_B X_A^2 + \frac{1}{3} \beta''_B X_A^3 + \dots \quad 2.19$$

then

$$\ln \frac{a_B}{X_B} = \alpha'_B X_A^2 + \alpha''_B X_A^3 + \dots \quad 2.20$$

and

$$\ln \gamma_B = \alpha'_B X_A^2 + \alpha''_B X_A^3 + \dots \quad 2.21$$

Any terms of the order higher than X^2 can usually be neglected and equation 2.21 can be truncated to:

$$\ln \gamma_B = \alpha'_B X_A^2 \quad 2.22$$

Substituting equation 2.22 into equation 2.17 yields for a binary solution:

$$\begin{aligned} \Delta H_{mix}^{reg} &= RT(X_B \alpha'_B X_A^2 + X_A \alpha'_A X_B^2) \\ &= RT \alpha'_B (X_B X_A^2 + X_A X_B^2) \\ &= \alpha (X_B X_A^2 + X_A X_B^2) \\ &= \alpha X_A X_B (X_A + X_B) = \alpha X_A X_B \end{aligned} \quad 2.23$$

Equation 2.23 forms the basis of Hildebrand's theory and regular solutions.

Therefore, for regular solutions:

$$\begin{aligned}\Delta G_{mix}^{reg} &= \Delta H_{mix}^{reg} - T\Delta S_{mix}^{reg} \\ &= \alpha X_A X_B + RT(X_A \ln X_A + X_B \ln X_B)\end{aligned}\tag{2.24}$$

and α can therefore be determined from the heat of mixing.

In recent times, the most contributions to the use of the regular solution model in slag are given by Ban-Ya et al. (1980,1982). He found that the model had an average error of $\pm 10\%$ over a wide range of slag compositions for the steel making slags. In this model O^{\ominus} anions compose of the main microscopic lattice in the slag and various cations distribute in the gaps between them to form different kinds of cells ($i - O - j$) where i and j denote cations. For regular solutions, α_{ij} represents the interaction between i and j cations, i.e. the number of ($i - O - j$) cells in the solution.

Major assumptions in the derivation of the model are the following:

- All kinds of cations are randomly distributed in a matrix of oxygen anions
- A constant co-ordination number
- Bonding energy is independent of slag composition

2.3.5 The Sub-regular solution model

This model allows the bonding energy to change to some extent with change in composition. It has been found that the excess properties of some simple binary solutions that appear “irregular” can often be adequately represented by expanding the enthalpy and excess Gibbs free energy as polynomials in the component mole fractions:

$$G^E = \alpha X_A X_B \quad 2.25$$

$$\alpha = {}^0L_{AB} + {}^1L_{AB}(X_A - X_B) + {}^2L_{AB}(X_A - X_B)^2 + \dots \quad 2.26$$

where ${}^kL_{ij}$ are empirical coefficients that are usually linear functions of T . If the series is truncated after the first term, the solution is regular. This sub-regular solution model can therefore be seen as an empirical extension of the regular solution theory where the fundamental assumptions are the same as for the regular solution model but the bonding energy is allowed to change with change in composition.

2.3.6 Temkin's theory

When a substance that does not disorder at elevated temperatures is finally melted, the possibility of long-range order disappears. It is impossible to tell whether two atoms, that are far enough apart, belong to the same or different sub-lattices. It is still possible that the tendency for chemical order is so large that each atom may periodically be surrounded by unlike atoms. This may be the case for purely ionic melts and is sometimes described by postulating the existence of two sub-lattices, one for the cations and another for the anions.

Temkin (1945) accepted this concept and suggested that the configurational entropy of a salt mixture could be estimated by assuming that all the cations mix randomly on one sub-lattice and all the anions mix randomly on another sub-lattice. Temkin's rule says that the activity of a component in a solution is the product of its ionic mole fractions. For a salt mixture $A_iL_j + B_pK_q$, where A and B are cations, L and K are anions and i, j, p and q are stoichiometric coefficients, the following equations can be derived:

$$a_{A_iL_j} = (X_{A^{i+}})^i (X_{L^{j-}})^j \quad 2.27$$

$$a_{B_pK_q} = (X_{B^{p+}})^p (X_{K^{q-}})^q \quad 2.28$$

where X is the ion fraction defined by:

$$X_{A^{i+}} = N_{A^{i+}} / \sum n_{cations} \quad 2.29$$

$$X_{L^{j-}} = N_{L^{j-}} / \sum n_{anions} \quad 2.30$$

Temkin's rule is a good approximation for highly basic slags. Since titanium oxides are known to dissociate into simple ions and are not inclined to polymerisation,

Temkin's theory is thought to be a good approximation for high-titania slags. It was furthermore found that FeO – TiO₂ melts behave fairly according to Temkin's rule (Smith and Bell, 1970; Sevinç, 1989). Temkin's rule assumes ideal mixing in both the cationic and anionic sub lattices.

2.3.6.1 Electrical equivalent ion fraction

The electrical equivalent ion fraction approach is used for slags containing ions of mixed valences like in the case of Ca²⁺ mixed into a Na⁺ lattice. In this case one lattice site must be kept vacant to maintain electrical neutrality. The number of sites is calculated with the following equations:

$$n = n_{Na^+} + n_{Ca^{2+}} + n_{Va} \quad 2.31$$

$$n_{Va} = n_{Ca^{2+}} \quad 2.32$$

$$n = n_{Na^+} + 2n_{Ca^{2+}} \quad 2.33$$

where n_{Va} is the number of vacant sites in the lattice.

In a mixture of A^+ , B^{2+} , C^{3+} and D^{4+} ions, the electrical equivalent ion fraction of B^{2+} is defined as:

$$X'_{B^{2+}} = \frac{2n_{B^{2+}}}{n_{A^+} + 2n_{B^{2+}} + 3n_{C^{3+}} + 4n_{D^{4+}}} \quad 2.34$$

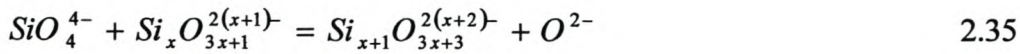
In this special case the activity of FeO and TiO₂ is expressed by the cation fraction of the species in the system (Temkin's rule).

The following assumptions were made by Temkin's theory and must be kept in mind when using this rule:

1. The slag is completely dissociated into ions,
2. The ideal solution for salts visualises random distribution of cations and anions on the sites of their respective sub-lattice,
3. There is no interaction between similarly charged ions,
4. All ion species in the slag are known.

2.3.7 The Polymerization model

The polymerization model follows on Temkin's model and also belongs to the ionic slag theories. Masson (1965) considered binary silicate melts to contain M^{2+} cations, O^{2-} anions and an array of linear chain silicate anions of the general formula $Si_x O_{3x+1}^{2(x+1)-}$. The equilibrium size distribution of the linear chain silicate anions is determined by assuming that the equilibrium constant, $k_{1,x}$ for the reaction:



is independent of x . This assumes that the free energy change for the reaction given by equation 2.35 is independent of the composition and degree of polymerization of the melt. By assuming Temkin type mixing of the anionic species, the following expression for $k_{1,x}$ is obtained:

$$k_{1,x} = \frac{X_{x+1} \cdot X_{O^{2-}}}{X_x \cdot X_1} \quad 2.36$$

where

$$X_{x+1} = Si_{x+1} O_{3x+3}^{2(x+2)-} \quad \text{anion fraction;}$$

$$X_x = Si_x O_{3x+1}^{2(x+1)-} \quad \text{anion fraction;}$$

$$X_1 = SiO_4^{4-} \quad \text{anion fraction and}$$

$$X_{O^{2-}} = O^{2-} \quad \text{anion fraction.}$$

From equation 2.36 the ion fractions can be written as:

$$\frac{X_{x+1}}{X_x} = \frac{k_{1,x} \cdot X_1}{X_{O^{2-}}} \quad \text{or} \quad X_x = \left(\frac{k_{1,x} \cdot X_1}{X_{O^{2-}}} \right)^{x-1} \cdot X_1 \quad 2.37$$

From mass balance considerations the following can be derived:

$$X_1 = \frac{X_{O^{2-}}(1 - X_{O^{2-}})}{(X_{O^{2-}} + k_{1,x} - k_{1,x} \cdot X_{O^{2-}})} \quad 2.38$$

and

$$X_{O^{2-}}^2(1 - k_{1,x})(1 - 2X) + X_{O^{2-}}[3X - 1 + 2k_{1,x}(1 - 2X)] - 2k_{1,x}(1 - 2X) = 0 \quad 2.39$$

as the variation of $X_{O^{2-}}$ with composition and $k_{1,x}$ in these theoretical melts. For Temkin mixing of anionic species, $a_{MO} = X_{O^{2-}}$ and therefore equation 2.39 is the variation of the activity of MO in the theoretical melts with $k_{1,x}$ and composition. Mason fitted equation 2.39 to experimental data and derived values of $k_{1,x}$ for several binary silicate systems (Gaskell, 1981).

An alternative approach, also developed by Masson is to consider that linear polysilicate ions are formed by polymerization of pseudo-bifunctional SiO_4^{4-} monomers. That is SiO_4^{4-} , where only two of the four O^- groups may react according to the following reaction:



X is the mole fraction of SiO_2 of the bulk slag analysis. That is, the completely depolymerised basic melt contains $X SiO_4^{4-}$ and $(1 - X) O^{2-}$ ions. The principle parameter is the degree of polymerization of the melt (α_{II}). This can be defined as the fraction of $2X O^-$ groups available for reaction on the $X SiO_4^{4-}$ pseudo-

bifunctional monomers which has reacted to form the polymerized system. From the stoichiometry of equation 2.40 the numbers of O^0 , O^{2-} and O^- groups in the polymerized melt are $\alpha_{II}X$, $(1-3X+\alpha_{II}X)$ and $2X(2-\alpha_{II})$ respectively. Each of the $X(1-\alpha_{II})$ silicate anions is started with an O^- group and the most probable distribution of these ions is determined as the most probable way in which the $\alpha_{II}X O^0$ groups and the remaining $X(1-\alpha_{II})$ reactive O^- groups are distributed among the silicate ions. The number of anions occurring as x -mers is calculated as $X(1-\alpha_{II})^2 \alpha_{II}^{x-1}$ and as there are $(1-2X)$ anions per mole of binary silicate the anion fraction of x -mers is:

$$X_x = \frac{X(1-\alpha_{II})^2 \alpha_{II}^{x-1}}{(1-2X)} \quad 2.41$$

and the anion fraction of the O^{2-} ions is:

$$X_{O^{2-}} = \frac{1-3X+\alpha_{II}X}{(1-2X)} \quad 2.42$$

The most probable size distribution is therefore:

$$\frac{X_{x+1}}{X_x} = \alpha_{II} \quad 2.43$$

where α_{II} has a value in the range $1 > \alpha_{II} \geq 0$.

Assuming Temkin mixing for the anions, the following expression for the equilibrium constant for equation 2.35 is obtained:

$$k_{1,x} = \frac{(1-3X+\alpha_{II}X)\alpha_{II}}{X(1-\alpha_{II})^2} \quad 2.44$$

which gives the variation of the equilibrium values of α_{II} with $k_{1,x}$ and melt composition.

Both these approaches uses Temkin mixing of anionic species and therefore assumes independence of ΔG_1^0 on melt composition and degree of polymerization, where ΔG_1^0 the standard free energy change for the reaction $MO(1) + \frac{1}{2}SiO_2(1) = \frac{1}{2}M_2SiO_4$ (1, completely depolymerised).

The Gibbs free energy of formation of these theoretical melts can be calculated as the sum of a ΔG_{chem} contribution due to the breaking of O^0 bonds and ΔG_{conf} contribution due to random mixing of the anions. The first contribution is obtained from:

$$\Delta G_{chem} = n_{O^-} \frac{\Delta G_1}{2} \quad 2.45$$

The number of moles of O^- groups formed per mole of $MO - SiO_2$ is

$$n_{O^-} = 4n_1 + 6n_2 + 8n_3 + \dots = 2 \sum (x+1)n_x \quad 2.46$$

One mole of binary silicate melt of $X < 0.5$ contains $(1 - 2X)$ moles of anions and therefore equation 2.46 can be rewritten as:

$$n_{O^-} = 2(1 - 2X) \left(\sum xX_x + \sum X_x \right) \quad 2.47$$

From equation 2.41

$$\sum xX_x = \frac{X}{1 - 2X} \quad \text{and} \quad \sum X_x = \frac{X(1 - \beta_{II})}{1 - 2X}$$

and therefore equation 2.45 becomes

$$\Delta G_{chem} = \Delta G_1 \cdot X(2 - \alpha_{II}) \quad 2.48$$

ΔG_{conf} is obtained as $-T\Delta S_{conf}$ where ΔS_{conf} per mole of binary silicate melt is given as:

$$\Delta S_{conf} = -(1-2X)R[X_{O^{2-}} \ln X_{O^{2-}} + \sum X_x \ln X_x] \quad 2.49$$

Configurational entropy (ΔS_{conf}) is defined as the entropy change at zero Kelvin and is associated solely with the configuration of the species in solution. The non-configurational entropy could then also be called the thermal entropy or the change in

entropy due to a change in temperature ($\Delta S_{nonconfig} = \int_0^T \frac{\Delta C_p}{T} dT$).

Substitution from equations 2.41 and 2.42 gives:

$$\frac{\Delta G_{conf}}{RT} = (1-3X + \alpha_{II}X) \ln \frac{(1-3X + \alpha_{II}X)}{1-2X} + X(1-\alpha_{II}) \ln \frac{X(1-\alpha_{II})^2}{1-2X} + X\alpha_{II} \ln \alpha_{II} \quad 2.50$$

and therefore:

$$\begin{aligned} \frac{\Delta G_{mix}}{RT} &= \frac{\Delta G_1^0}{RT} \cdot X(2 - \alpha_{II}) + (1-3X + \alpha_{II}X) \ln(1-3X + \alpha_{II}X) \\ &+ X(1-\alpha_{II}) \ln X(1-\alpha_{II})^2 + X\alpha_{II} \ln \alpha_{II} + (2X-1) \ln(1-2X) \end{aligned} \quad 2.51$$

Alternatively, substitution of equation 2.41 into equation 2.51 gives:

$$\begin{aligned} \frac{\Delta G_{mix}}{RT} = \frac{\Delta G_1^0}{RT} & \left[1 - X - X_{O^{2-}} \cdot (1 - 2X) \right] \\ & + (1 - 2X) \left[X_{O^{2-}} \cdot \ln X_{O^{2-}} + \frac{3X - 1 + X_{O^{2-}} \cdot (1 - 2X)}{1 - 2X} \ln \frac{3X - 1 + X_{O^{2-}} \cdot (1 - 2X)}{X} \right. \\ & \left. + (1 - X_{O^{2-}}) \ln \frac{(1 - X_{O^{2-}})^2 \cdot (1 - 2X)}{X} \right] \end{aligned} \quad 2.52$$

For Temkin mixing of anionic species, $a_{MO} = X_{O^{2-}}$ and therefore equation 2.52 expresses the total Gibbs free energy of mixing (ΔG_{mix}) in terms of the activity of MO (a_{MO}) and the total molar fraction of SiO_2 (X) in the melt. Both these values can be determined experimentally.

2.3.8 Two-Sub lattice Model

The basis of this model is the ionic nature of melts where ions of different charges are present. The ionic melts are described by postulating two sub lattices, one for cations and one for anions (Li et al., 1998). The two-sublattice model follows Temkin's theory, assuming that cations mix on one sublattice and anions on another (Sundman 1991). The two-sublattice model for oxide slags uses some artificial means, such as introducing neutral species into the sub lattices to represent the thermodynamic properties of melts (Hillert, 1985). Its authors have already noted that, although the assessment of some systems is successful by using this model, it does not imply the model is correct. It should primarily be regarded as a formal way of constructing a suitable mathematical expression for the Gibbs energy and it should not be implied that some species used to describe the system actually exist in the real melts. The model can be written as

$$(C_i^{z_i})_P (A_i^{z_i}, Va, B_i^0)_Q \quad 2.53$$

where each pair of parenthesis surrounds a sublattice. C represents cations, A anions, Va hypothetical vacancies and B neutrals. The charge of an ion is denoted z_i and the subscript i is used to denote a specific component. The number of sites on the sub lattices, P and Q , must vary with composition in order to maintain neutrality. The values of P and Q are calculated as follows:

$$P = \sum_i (-v_i) y_{A_i} + Q y_{Va} \quad 2.54$$

$$Q = \sum_i z_i y_{C_i} \quad 2.55$$

In these equations y denotes the site fraction of a constituent. P and Q are therefore merely the average charge on the opposite sub-lattice (Sundman, 1991) with the hypothetical vacancies having an induced charge equal to Q .

The ordinary mole fractions can be calculated from the site fractions in the following way:

$$X_{C_i} = \frac{P y_{C_i}}{P + Q(1 - y_{V_a})} \quad 2.56$$

for components which behave like cations, and

$$X_{D_i} = \frac{Q y_{D_i}}{P + Q(1 - y_{V_a})} \quad 2.57$$

for components behaving like anions or neutrals where D is used to denote any constituent on the anion sublattice. It is clear that equation 2.57 cannot be applied to vacancies, because the mole fraction of vacancies is zero.

2.3.9 The Quasi Chemical model

Another solution model was suggested by Guggenheim (1935). It is named the quasi-chemical model for short range ordering. It describes the thermodynamic properties of a system by taking structural ordering in account.

2.3.9.1 Basic Quasi Chemical theory

In a binary system with components A and B , the A and B particles are considered to mix substitutionally on a quasi-lattice. The relative amounts of the three types of nearest neighbour pairs ($A - A$, $B - B$ and $A - B$) are determined by the energy change associated with the formation of two $A - B$ pairs from an $A - A$ and a $B - B$ pair:



If this energy change is zero, then the solution is an ideal mixture. As the energy change becomes more negative, the formation of $A - B$ pairs is favoured. The result is then that the enthalpy of mixing tends to form a negative peak at the composition $X_A = X_B = \frac{1}{2}$, while the entropy of mixing have the shape of a letter m. (see Figure 2) This suggests that the maximum ordering of any binary system $A - B$ occur at 0.5 mole fraction.

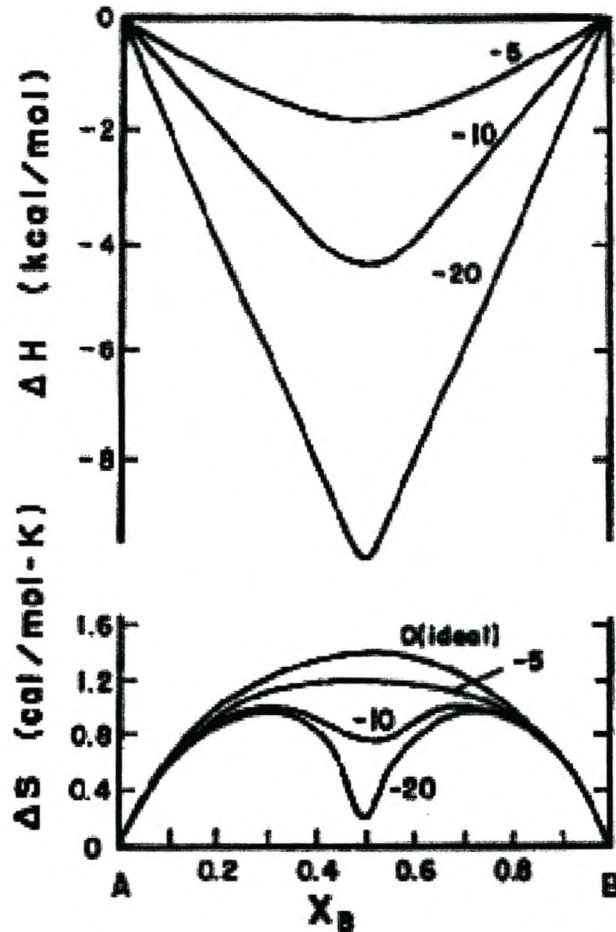


Figure 2: Enthalpy and entropy of mixing of a binary system for different degrees of ordering about $X_A = X_B = \frac{1}{2}$. Curves are calculated from the modified quasi-chemical theory at $T = 1000$ °C with $z = 2$ for the constant values of ω (kcal) and with $\eta = 0$. (Pelton and Blander, 1984)

Therefore the basic quasi-chemical theory cannot be used for silicate melts where the minimum enthalpies and entropies of mixing are not at a mole fraction of 0.5. Pelton and Blander (1984 and 1988) modified the basic theory in order to provide an expression for the entropy and enthalpy of a highly ordered system with minima in entropy and enthalpy at any desired composition. As a further modification, the energy change for reaction 2.58 was expressed as a function of composition with adjustable coefficients.

In the following sections, the general modified quasi-chemical theory will first be developed for binary systems and then extended to ternary systems.

2.3.9.2 The modified binary quasi chemical theory

Pelton and Blander (1984 and 1988) modified the basic quasi-chemical model. As in the basic quasi-chemical theory, a binary system with components A and B are considered where the A and B particles mix substitutionally on a quasi-lattice with a constant co-ordination number z . The three types of nearest neighbour pairs ($A - A$, $B - B$ and $A - B$) have “pair bond energies” ε_{ij} . The total number of such pairs per mole of solution is $N^0 z/2$ where N^0 is Avogadro’s number. The formation of two $A - B$ pairs from a $A - A$ and $B - B$ pair according to reaction 2.58 is considered. The enthalpy change for this reaction is then $(2\varepsilon_{AB} - \varepsilon_{AA} - \varepsilon_{BB})$ according to Hess’s law of addition of enthalpies. A molar enthalpy change ω is defined by multiplying with $N^0 z/2$:

$$\omega = \frac{N^0 z}{2} (2\varepsilon_{AB} - \varepsilon_{AA} - \varepsilon_{BB}) \quad 2.59$$

A molar non-configurational entropy change η , can also be defined:

$$\eta = \frac{N^0 z}{2} (2\sigma_{AB} - \sigma_{AA} - \sigma_{BB}) \quad 2.60$$

where σ_{ij} is the “pair bond non-configurational entropy”.

Let n_A and n_B be the number of moles of A and B particles. Then, for one mole of solution, $(n_A + n_B) = 1$, the mole fractions of A and B are defined as $X_A = n_A/(n_A + n_B) = 1 - X_B$. Now let n_{AA} , n_{BB} and n_{AB} be the number of moles of each type of pair in solution. The fraction of $i - j$ pairs are defined as:

$$X_{ij} = n_{ij} / (n_{AA} + n_{BB} + n_{AB}) \quad 2.61$$

from the mass balance it follows that:

$$zn_A = 2n_{AA} + n_{AB} \quad 2.62$$

$$zn_B = 2n_{BB} + n_{AB} \quad 2.63$$

and that

$$2X_A = 2X_{AA} + X_{AB} \quad 2.64$$

$$2X_B = 2X_{BB} + X_{AB} \quad 2.65$$

When components A and B are mixed, $A - B$ pairs are formed at the expense of $A - A$ and $B - B$ pairs. The enthalpy of mixing, ΔH_{mix} , is given in the model by the summation of the pair bond energies:

$$\Delta H_{mix} = (X_{AB}/2)\omega \quad 2.66$$

The non-configurational excess entropy of the solution is then given by:

$$\Delta S_{nonconfig}^E = (X_{AB}/2)\eta \quad 2.67$$

The approximate configurational entropy of mixing as proposed by Guggenheim (1935), is:

$$\begin{aligned} \Delta S_{config} = & -R(X_A \ln X_A + X_B \ln X_B) \\ & - \frac{Rz}{2} \left(X_{AA} \ln \frac{X_{AA}}{X_A^2} + X_{BB} \ln \frac{X_{BB}}{X_B^2} + X_{AB} \ln \frac{X_{AB}}{2X_A X_B} \right) \end{aligned} \quad 2.68$$

Therefore, the total molar excess entropy (configurational plus non-configurational entropy) of the solution is given from equations 2.67 and 2.68 as:

$$\Delta S_{mix}^E = -\frac{Rz}{2} \left(X_{AA} \ln \frac{X_{AA}}{X_A^2} + X_{BB} \ln \frac{X_{BB}}{X_B^2} + X_{AB} \ln \frac{X_{AB}}{2X_A X_B} \right) + (X_{AB}/2)\eta \quad 2.69$$

The equilibrium concentrations are given by minimizing the Gibbs energy at constant composition:

$$\partial(\Delta H_{mix}^E - T\Delta S_{mix}^E)/\partial X_{AB} = 0 \quad 2.70$$

Substituting equations 2.66 and 2.69 into equation 2.70 yields:

$$\partial\left((X_{AB}/2)\omega - T\left(-\frac{Rz}{2}\left(X_{AA}\ln\frac{X_{AA}}{X_A^2} + X_{BB}\ln\frac{X_{BB}}{X_B^2} + X_{AB}\ln\frac{X_{AB}}{2X_AX_B}\right) + (X_{AB}/2)\eta\right)\right)/\partial X_{AB} = 0 \quad 2.71$$

then

$$\partial\left(\frac{TRz}{2}\left(X_{AA}\ln\frac{X_{AA}}{X_A^2} + X_{BB}\ln\frac{X_{BB}}{X_B^2} + X_{AB}\ln\frac{X_{AB}}{2X_AX_B}\right) + (X_{AB}/2)\omega - (X_{AB}/2)\eta T\right)/\partial X_{AB} = 0 \quad 2.72$$

and

$$\partial\left(\frac{TRz}{2}\left(X_{AA}\ln\frac{X_{AA}}{X_A^2} + X_{BB}\ln\frac{X_{BB}}{X_B^2} + X_{AB}\ln\frac{X_{AB}}{2X_AX_B}\right) + (X_{AB}/2)(\omega - \eta T)\right)/\partial X_{AB} = 0 \quad 2.73$$

Doing the differentiation then gives:

$$\frac{X_{AB}^2}{X_{AA}X_{BB}} = 4e^{-2(\omega - \eta T)/zRT} \quad 2.74$$

Equation 2.74 resembles an equilibrium constant for reaction 2.58 and therefore the model is called “quasi chemical”.

Substitute equations 2.64 and 2.65 into equation 2.74:

$$X_{AB} = 4X_AX_B/(1 + \xi) \quad 2.75$$

where

$$\xi = \left[1 + 4 X_A X_B \left(e^{2(\omega - \eta T)/zRT} - 1 \right) \right]^{1/2} \quad 2.76$$

For a given value of $(\omega - \eta T)$ at a given composition X_A , equations 2.75 and 2.76 give X_{AB} and equations 2.64 and 2.65 then give X_{AA} and X_{BB} . Substituting these values into equations 2.66 and 2.69 gives ΔH_{mix} and S^E .

In the case when, $\omega = 0$ and $\eta = 0$ it follows that $\Delta H_{mix} = 0$ and $S^E = 0$ and the solution is ideal. When ω and η are very small, $S^E \approx 0$ and $X_{AB} \approx 2X_A X_B$. Then equation 2.66 becomes: $\Delta H_{mix} = X_A X_B \omega$. In this case the solution is regular. As $(\omega - \eta T)$ is made progressively more negative, ΔH_{mix} assumes a negative peaked form as in Figure 2, and ΔS assumes the “m-shaped” form of Figure 2. The configurational ΔS as calculated by equation 2.68 assumes large negative values around $X_A = X_B = 1/2$ for large negative values of $(\omega - \eta T)$. This is clearly incorrect since when $(\omega - \eta T) \rightarrow -\infty$, perfect ordering will result at the composition $X_A = X_B = 1/2$ with all A particles having only B particles as nearest neighbours and vice-versa. Therefore, the configurational ΔS should be zero at this composition. The fact that the calculated configurational ΔS is not zero is a result of the approximate nature of the entropy equation 2.68. If we solve the preceding equations for $(\omega - \eta T) = -\infty$, we obtain for the configurational entropy of mixing at $X_A = X_B = 1/2$:

$$\Delta S_{mix} = R \left(\frac{z}{2} - 1 \right) \ln \frac{1}{2} \quad 2.77$$

This will only be equal to zero when $z = 2$.

For highly ordered systems, the model therefore gives the correct entropy expression only when $z = 2$. This can be more fully understood if it is realised that equation 2.68 with $z = 2$ is, in fact, the solution of the one-dimensional Ising model. For the Ising

model, consider a one-dimensional “necklace” of n_A particles of type A and n_B particles of type B with n_{AA} , n_{BB} and n_{AB} being the numbers of $A - A$, $B - B$ and $A - B$ pairs. Now place the n_A particles of type A in a ring and choose at random $(n_A - n_{AA})$ of the n_A spaces between them. This choice can be made in $\Omega_A = n_A! / (n_{AA}!(n_A - n_{AA})!)$ ways. We now place one particle of type B in each of these chosen spaces. This leaves $n_B - (n_A - n_{AA}) = n_{BB}$ particles of type B . These are all placed into the $(n_A - n_{AA})$ chosen spaces with no restriction on the number in each space. This can be done in $\Omega_B = n_B! / (n_{BB}!(n_B - n_{BB})!)$ ways since $(n_A - n_{AA}) = (n_B - n_{BB})$. The entropy is then given by:

$$\Delta S = -k_b \ln \Omega_A \Omega_B \quad 2.78$$

where k_b is Boltzmann’s constant.

Solving for one mole of particles gives an expression for ΔS identical to that of equation 2.68 with $z = 2$.

Hence, the model as presented is exact in one-dimension ($z = 2$). Thus, for highly ordered systems, the correct entropy is only approached by the model when $z = 2$. For solutions that are only slightly ordered ($S^E \approx 0$), it may be argued that the approximate three-dimensional expression is superior to the exact one-dimensional expression and so a larger value of z should be used.

2.3.9.3 Fixing the composition of maximum ordering

The next modification to the model concerns the composition of maximum ordering. As presented above, the model always gives maximum ordering at $X_A = X_B = 1/2$. In order to make the model general, we must be able to choose the composition of maximum ordering to correspond to that which is observed. For instance in the binary system $\text{MgO} - \text{SiO}_2$, this composition is observed near $X_{\text{MgO}} = 2/3$, $X_{\text{SiO}_2} = 1/3$ (i.e. the composition of the intermediate compound: $(\text{MgO})_2\text{SiO}_2$ or Mg_2SiO_4).

The simplest means of accomplishing this is to replace the mole fractions X_A and X_B in the preceding equations by equivalent fractions, Y_A and Y_B defined by :

$$Y_A = \frac{aX_A}{aX_A + bX_B} \quad 2.79$$

$$Y_B = \frac{bX_B}{aX_A + bX_B} \quad 2.80$$

Where a and b are numbers chosen so that $Y_A = Y_B = 1/2$ at the composition of maximum ordering. For example, in the MgO – SiO₂ system, by choosing a and b such that $a/(a + b) = 1/3$ (for example, by choosing $a = 1, b = 2$) we obtain $Y_A = Y_B = 1/2$ when $X_A = 2/3$ and $X_B = 1/3$. Formally, in the model, we let the coordination numbers of A and B particles be (az) and (bz) respectively. Equations 2.62 to 2.65 then become:

$$zan_A = 2n_{AA} + n_{AB} \quad 2.81$$

$$zbn_B = 2n_{BB} + n_{AB} \quad 2.82$$

and

$$2Y_A = 2X_{AA} + X_{AB} \quad 2.83$$

$$2Y_B = 2X_{BB} + X_{AB} \quad 2.84$$

The molar enthalpy of mixing and molar excess entropy (per mole of components A and B) become:

$$\Delta H_{mix} = (aX_A + bX_B)(X_{AB}/2)\omega \quad 2.85$$

$$\Delta S_{mix}^E = -\frac{Rz}{2}(aX_A + bX_B) \left(X_{AA} \ln \frac{X_{AA}}{Y_A^2} + X_{BB} \ln \frac{X_{BB}}{Y_B^2} + X_{AB} \ln \frac{X_{AB}}{2Y_A Y_B} \right) \\ + (aX_A + bX_B)(X_{AB}/2)\eta \quad 2.86$$

In the ideal entropy term however, we do not replace X_A and X_B by Y_A and Y_B , but we retain the expression:

$$\Delta S^{ideal} = -R(X_A \ln X_A + X_B \ln X_B)$$

2.87

that when $(\omega - T\eta) \rightarrow 0$ the equations reduce to the ideal solution equations.

Equations 2.75 and 2.76 are now rewritten as:

$$X_{AB} = 4Y_A Y_B / (1 + \xi) \quad 2.88$$

and

$$\xi = \left[1 + 4Y_A Y_B \left(e^{2(\omega - \eta T)/zRT} - 1 \right) \right]^{1/2} \quad 2.89$$

while equation 2.74 stays the same as before. The total excess Gibbs free energy can now be expressed as:

$$G^E = \frac{RTz}{2} (aX_A + bX_B) \left[Y_A \ln \left(\frac{\xi - 1 + 2Y_A}{Y_A(\xi + 1)} \right) + Y_B \ln \left(\frac{\xi - 1 + 2Y_B}{Y_B(\xi + 1)} \right) \right] \quad 2.90$$

In order to choose the composition of maximum ordering, it is only the ratio $a/(a + b)$ which must be fixed. For example, the choice $a = 2, b = 4$ or the choice $a = 1, b = 2$ will both give $Y_A = Y_B = 1/2$ at $X_A \approx 2/3$. As before, however, we may apply the additional condition that $\Delta S = 0$ when $\omega = -\infty$ at the composition of maximum ordering ($Y_1 = Y_2 = 1/2$). This condition is satisfied when:

$$bz = - \left[\ln(r) + \left(\frac{1-r}{r} \right) \ln(1-r) \right] / \ln 2 \quad 2.91$$

$$a = br / (1 - r) \quad 2.92$$

Where $r = a/(a + b)$ is the ratio required to fix the composition of maximum ordering.

2.3.9.4 Composition dependence of ω and η

The final modification to the quasi-chemical model concerns the composition dependence of ω and η . Constant values may be sufficient to represent the main features of the curves of ΔH and ΔS for ordered systems, but for a quantitative representation of the thermodynamic properties of real systems it is necessary to introduce an empirical composition dependence. Pelton and Blander chose simple polynomial expansions in the equivalent fraction Y_B :

$$\eta = \eta_0 + \eta_1 Y_B + \eta_2 Y_B^2 + \eta_3 Y_B^3 + \dots \quad 2.93$$

$$\omega = \omega_0 + \omega_1 Y_B + \omega_2 Y_B^2 + \omega_3 Y_B^3 + \dots \quad 2.94$$

where the temperature- and composition-independent coefficients ω_i and η_i are chosen empirically to give the best representation of the available experimental data for a system.

When $(\omega - \eta T)$ is small, then the excess configurational entropy is also small and $X_{AB} \approx 2X_A X_B$. (For simplicity, let $a = b = 1$ so that $X_A = Y_A$ and $X_B = Y_B$). In this case:

$$\Delta H_{mix} \approx X_A X_B (\omega_0 + \omega_1 X_B + \omega_2 X_B^2 + \dots) \quad 2.95$$

$$S_{mix}^E \approx X_A X_B (\eta_0 + \eta_1 X_B + \eta_2 X_B^2 + \dots) \quad 2.96$$

These equations are identical to the enthalpy of mixing and the excess entropy expressed as polynomial expansions in the mole fractions of the components.

Therefore, as the solution approaches ideality, the present model approaches the simple and common representation of excess properties by polynomial expansions and the coefficients ω_i and η_i become numerically equal to the coefficients of these expansions.

2.3.9.5 Partial molar properties

Expressions for the partial molar Gibbs energies of the components are obtained by differentiation:

$$\Delta \bar{G}_A = RT \ln a_A = RT \ln X_A + \frac{az}{2} RT \ln \frac{X_{AA}}{Y_A^2} - a \left(\frac{X_{AB}}{2} \right) Y_B \frac{\partial(\omega - \eta T)}{\partial Y_B} \quad 2.97$$

$$\Delta \bar{G}_B = RT \ln a_B = RT \ln X_B + \frac{bz}{2} RT \ln \frac{X_{BB}}{Y_B^2} - b \left(\frac{X_{BB}}{2} \right) Y_A \frac{\partial(\omega - \eta T)}{\partial Y_B} \quad 2.98$$

Where a_A and a_B are the activities of the components.

2.3.9.6 The modified quasi-chemical theory for ternary solutions

The modified quasi-chemical equations may be extended to multi component systems in a straightforward manner. Consider a ternary solution with mole fractions X_A , X_B , X_C . Equivalent fractions Y_A , Y_B , Y_C may be defined as:

$$Y_A = \frac{aX_A}{aX_A + bX_B + cX_C} \quad 2.99$$

$$Y_B = \frac{bX_B}{aX_A + bX_B + cX_C} \quad 2.100$$

$$Y_C = \frac{cX_C}{aX_A + bX_B + cX_C} \quad 2.101$$

For the various nearest-neighbour pairs $i - j$ we defined pair mole fractions X_{ij} as before. Mass balance considerations then give, by extension of equations 2.83 and 2.84:

$$2Y_A = 2X_{AA} + X_{AB} + X_{CA} \quad 2.102$$

$$2Y_B = 2X_{BB} + X_{AB} + X_{BC} \quad 2.103$$

$$2Y_C = 2X_{CC} + X_{CA} + X_{BC} \quad 2.104$$

The functions ω_{AB} , ω_{BC} , ω_{CA} and η_{AB} , η_{BC} , η_{CA} are the molar enthalpy and nonconfigurational entropy changes for the three pair exchange reactions as in equation 2.58.

The ternary enthalpy of mixing and excess entropy is then given by:

$$\Delta H_{mix} = (aX_A + bX_B + cX_C)(X_{AB}\omega_{AB} + X_{BC}\omega_{BC} + X_{CA}\omega_{CA})/2 \quad 2.105$$

$$\begin{aligned} \Delta S_{mix}^E = & -\frac{Rz}{2}(aX_A + bX_B + cX_C) \cdot \\ & \left(X_{AA} \ln \frac{X_{AA}}{Y_A^2} + X_{BB} \ln \frac{X_{BB}}{Y_B^2} + X_{CC} \ln \frac{X_{CC}}{Y_C^2} + X_{AB} \ln \frac{X_{AB}}{2Y_A Y_B} + X_{BC} \ln \frac{X_{BC}}{2Y_B Y_C} + X_{CA} \ln \frac{X_{CA}}{2Y_C Y_A} \right) \\ & + (aX_A + bX_B + cX_C)(X_{AB}\eta_{AB} + X_{BC}\eta_{BC} + X_{CA}\eta_{CA})/2 \quad 2.106 \end{aligned}$$

By minimising the total Gibbs energy at constant composition, three equations similar to equation 2.74 are generated:

$$\frac{X_{ij}^2}{X_{ii}X_{jj}} = 4e^{-2(\omega_{ij}-\eta_{ij}T)/zRT} \quad 2.107$$

The functions ω_{ij} and η_{ij} are the polynomial expansions in the three binary subsystems which can be obtained by analysis of the measured binary data. In order to be able to estimate the thermodynamic properties of the ternary from the binary data, it is necessary to approximate ω_{ij} and η_{ij} in the ternary system from their values in the binaries.

Two methods that suggest themselves are illustrated in Figure 3. In the “symmetric approximation”, ω_{ij} and η_{ij} are assumed to be constant along lines of constant molar ratio Y_i/Y_j , while in the “asymmetric approximation” ω_{AB} and ω_{CA} (and η_{AB} and η_{CA}) are constant at constant Y_A , while ω_{CA} (and η_{CA}) are constant at constant Y_B/Y_C .

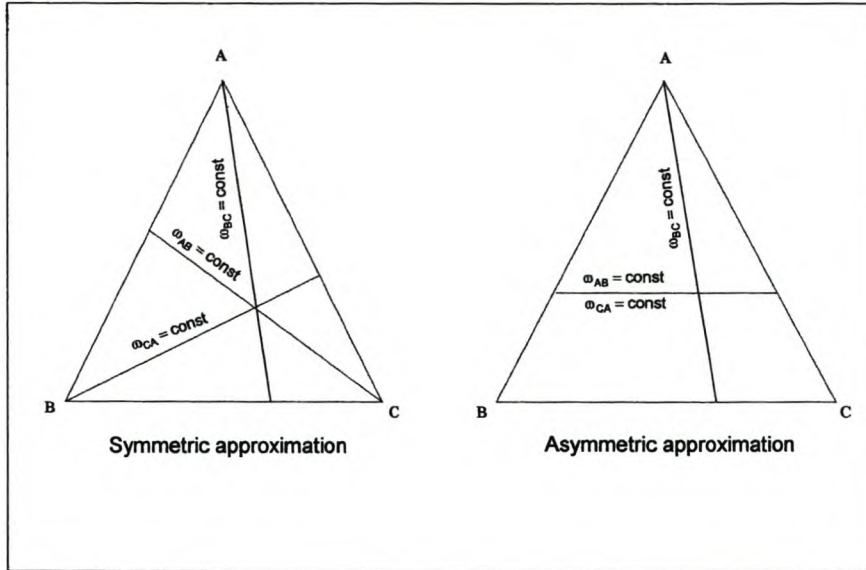


Figure 3: Two methods to approximate ω_{ij} and η_{ij} in the ternary system from their values in the binaries

With values of ω_{ij} and η_{ij} in the ternary obtained by one of these approximation techniques, the three equations 2.107 can be solved simultaneously with equations 2.102 through 2.104 to give the six bond fractions X_{ij} which can then be substituted into equations 2.105 and 2.106 to give ΔH and S^E . The calculation is similar to a simultaneous complex chemical equilibrium calculation and can be solved by similar computer algorithms.

The properties of ternary systems may be approximated from the assessed parameters of the binary subsystems in this manner. If experimental ternary data are available, then the approximations may be refined by the addition of “ternary terms” to the Gibbs energy expression such as $\phi_{ijk}X_A^iX_B^jX_C^k$ where i, j, k are all positive non-zero integers and where ϕ_{ijk} are adjustable ternary parameters. Ideally the model should be good enough so that such ternary terms should be small, or not necessary at all.

Extension of the equations of this section to systems with more than 3 components is straightforward. The solution of the resultant set of equations for the “complex quasi-chemical equilibria” can be solved by computer algorithms such as the Solgasmix

Gibbs – free energy minimisation package developed by GTT. Alternative techniques such as genetic algorithms may also be used.

2.3.9.7 Partial molar properties

Expressions for ternary partial molar properties of the components may be obtained by differentiation. In the symmetric approximation:

$$\begin{aligned}\Delta\bar{G}_A &= RT \ln a_A \\ &= RT \ln X_A + \frac{az}{2} RT \ln \frac{X_{AA}}{X_A^2} - a \left(\frac{X_{AB}}{2} \right) \frac{Y_B}{(Y_A + Y_B)^2} \frac{\partial(\omega_{AB} - \eta_{AB}T)}{\partial[Y_B/(Y_A + Y_B)]}\end{aligned}\quad 2.108$$

and similarly for $\Delta\bar{G}_B$ and $\Delta\bar{G}_C$.

In the asymmetric approximation equation 2.108 becomes:

$$\begin{aligned}\Delta\bar{G}_A &= RT \ln a_A \\ &= RT \ln X_A + \frac{az}{2} RT \ln \frac{X_{AA}}{Y_A^2} + \frac{a(1-Y_A)}{2} \left(X_{AB} \frac{\partial(\omega_{AB} - \eta_{AB}T)}{\partial Y_A} + X_{CA} \frac{\partial(\omega_{CA} - \eta_{CA}T)}{\partial Y_A} \right)\end{aligned}\quad 2.109$$

$$\begin{aligned}\Delta\bar{G}_B &= RT \ln a_B \\ &= RT \ln X_B + \frac{bz}{2} RT \ln \frac{X_{BB}}{Y_B^2} + \frac{bY_A}{2} \left(X_{AB} \frac{\partial(\omega_{AB} - \eta_{AB}T)}{\partial Y_A} + X_{CA} \frac{\partial(\omega_{CA} - \eta_{CA}T)}{\partial Y_A} \right) \\ &= b \frac{X_{BC}}{2} \frac{Y_C}{(Y_B + Y_C)^2} \frac{\partial(\omega_{BC} - \eta_{BC}T)}{\partial[Y_C/(Y_B + Y_C)]}\end{aligned}\quad 2.110$$

And similarly for $\Delta\bar{G}_C$.

2.3.10 The Cell Model

2.3.10.1 Background

Yokokawa and Niwa (1969) first developed a cell model using the concept of Oxygen and Cation sub-lattices. Later Kapoor and Froberg developed a similar model, but it had no applications beyond a few ternary systems. This model was then extended by Gaye and co-workers (1989) to represent the properties of multi component systems in terms of only binary parameters. Hongjie Li (1995) extended this model further to accommodate not only oxygen, but any number of anionic species such as S^{2-} and F_2^{2-} .

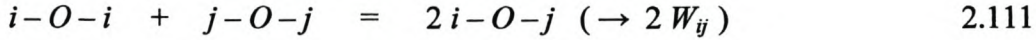
Up to date, the model was primarily applied to slags in the composition range of steel-making slag. It has been successful in predicting the distribution ratios of sulfur and phosphorus between metal and slag and it proved very reliable in multi-component systems (Li and Morris, 1997).

2.3.10.2 Basic Hypotheses

The cell model uses a concept of oxygen and cation sub-lattices. The cation sub-lattice is filled in decreasing order of cation charge. A liquid mixture of m oxides in which X_i represents the mole fraction of oxide $(M_i)_{u_i} \cdot O_{v_i}$ ($i = 1$ to m) is considered. The structure is described in terms of symmetric ($i - O - i$) and asymmetric ($i - O - j$) cells. This oversimplified picture has no claim at representing the actual polymeric structure of the melt. However, on the example of the CaO-SiO₂ system, a ($Si - O - Si$) cell represents a double bonded (O°) oxygen, a ($Si - O - Ca$) cell represents a singly bonded oxygen (O^-) and a ($Ca - O - Ca$) cell represents a free oxygen ion (O^{2-}). The computed numbers R_{Si-Si} and $2R_{Si-Ca}$ of ($Si - O - Si$) and ($Si - O - Ca$) cells will reflect the degree of polymerisation. This model, although being developed for ionic melts, is still able to predict the degree of polymerisation of the melt.

2.3.10.3 Energy of cells formation

To each asymmetric cell is associated its energy of formation, W_{ij} , from the symmetric cells constituting the limiting pure liquid oxides.



It was necessary to consider a linear variation of W_{ij} with composition:

$$W_{ij} = (W_{ij})_1 + (W_{ij})_2 \cdot X_i \quad 2.112$$

where i is the cation of highest charge.

2.3.10.4 Energy of cells interaction

The various cells are assumed to be distributed randomly and interaction energies between them are considered (e.g. E_{ij-kl} to represent interaction energy between cells $i-O-j$ and $k-O-l$). Further assumptions are made which allow the consideration of only binary interaction parameters:

Interaction between like cells is neglected and “addition rules” are assumed, such as:

$$E_{ii-ij} = 2 E_{ii-ij} \quad 2.113$$

$$E_{ij-kk} = E_{ik-kk} + E_{jk-kk} \quad 2.114$$

The only remaining type of interaction parameter (E_{ij-ii}) will be called E_{ij} . As with the energy of formation, a linear relationship was considered:

$$E_{ij} = (E_{ij})_1 + (E_{ij})_2 \cdot X_i \quad 2.115$$

Thus, the model was designed with the objective to describe multi-component systems only in terms of a few binary parameters. These parameters were taken as temperature independent. No ternary interactions are taken into account and the interaction and formation energies are functions of a simple linear model with only two parameters.

While the cell model interaction parameters W_{ij} and E_{ij} represent the energy change of two different cell reactions (cells formation and cells interaction) the modified quasi-chemical model parameters ω and η represent the enthalpy and entropy changes of all cells reactions respectively. The linear variation of W_{ij} and E_{ij} with composition in equations 2.112 and 2.115 can be compared to the polynomial expansions of quasi-chemical model parameters, ω and η in equations 2.93 and 2.94, with parameters $\omega_0, \omega_1, \omega_2 \dots \omega_n$ and $\eta_0, \eta_1, \eta_2 \dots \eta_m$.

2.3.10.5 Expression of the thermodynamic functions of the liquid mixture of oxides

2.3.10.5.1 Free energy of mixing

The free energy of mixing is expressed by the following equation:

$$G_{mix} = 2 \sum_{i=1}^{m-1} \sum_{j=i+1}^m \left[R_{ij} W_{ij} + R_{ij} \frac{v_j \cdot X_j}{D_1} E_{ij} \right] - RT \sum_{i=1}^{m-1} \frac{u_i}{v_i} \left[D_i \ln \left(\frac{D_i}{v_i X_i} \right) - D_{i+1} \ln \left(\frac{D_{i+1}}{v_i X_i} \right) \right] - RT \sum_{i=1}^m \sum_{j=1}^m \left[R_{ij}^* \ln R_{ij}^* - R_{ij} \ln R_{ij} \right] \quad 2.116$$

where the fraction of $(i - O - j)$ cells for a random distribution of cations on their sublattice, R_{ij}^* satisfy a system of $m(m+1)/2$ constraints ($i = 1$ to m).

$$\sum_{j=1}^m R_{ij} = v_i X_i \quad 2.117$$

$$R_{ii} \cdot R_{jj} - \frac{R_{ij}^2}{P_{ij}^2} = 0 \quad (j = i + 1 \text{ to } m) \quad 2.118$$

The linear equations 2.117 are material balances and the quadratic equations 2.118 are derived from the maximisation of the partition function.

2.3.10.5.2 Enthalpy and entropy of mixing

The enthalpy and entropy of mixing are obtained using GIBBS-HELMHOLTZ's equation.

$$H_{mix} = \frac{\partial \left(\frac{G_{mix}}{T} \right)}{\partial \left(\frac{1}{T} \right)} \quad 2.119$$

$$S_{mix} = \frac{(H_{mix} - G_{mix})}{T} \quad 2.120$$

When E_{ij} and W_{ij} are assumed temperature independent, the mixing entropy is identical to the configurational entropy.

The component activities are calculated with the following equation which follows from the definition of partial molar properties.

$$RT \ln a_i = G_{mix} + \sum_{j=2}^m (\delta_{ij} - X_j) \frac{\partial G_{mix}}{\partial X_j} \quad (i = 1 \text{ to } m) \quad 2.121$$

where δ_{ij} represents KRONECKER's delta with $\delta_{ij} = \begin{cases} 0 & \text{when } i \neq j \\ 1 & \text{when } i = j \end{cases}$.

The derivatives of the free energy of mixing, can be calculated numerically:

$$\frac{\partial G_{mix}}{\partial X_j} = \frac{[G_{mix}(X_k, X_j + \Delta X_j) - G_{mix}(X_k, X_j - \Delta X_j)]}{2\Delta X_j} \quad 2.122$$

Changes of the reference state can then be made to express the activities with respect

to the classically used reference state, e.g.

$$\frac{(a_{MO_s})}{(a_{MO_l})} = \exp\left(\frac{\Delta H_m - T\Delta S_m}{RT}\right) \quad 2.123$$

ΔH_m and ΔS_m in this equation are the enthalpy and entropy of melting of the pure component.

The cell model has been successfully applied to steel making slags and has been used by Gaye et al. (1992) as a standard modelling method. To estimate E_{ij} and W_{ij} (also ω and η for the quasi chemical model), data from literature is required. It is very important that a positive number of degrees of freedom are maintained by having more datasets than model parameters.

2.3.11 Unified interaction parameter formalism

The interaction parameter formalism for infinitely dilute solutions was first proposed by Wagner (1962). This formalism is limited to infinite dilution and is thermodynamically inconsistent at finite concentrations. Darken (1967) proposed a “quadratic formalism” for ternary systems, which reduces to the first-order interaction parameter formalism at infinite dilution, but this formalism has not been used extensively. Pelton and Bale (1986) proposed a slight modification to the interaction parameter formalism to overcome the thermodynamic inconsistency at finite solute concentrations. This modified formalism reduces to the standard formalism at infinite dilution and preserves the notation and numerical values of the parameters. In the following section, the thermodynamic inconsistency of the standard formalism will be discussed as well as Pelton and Bale’s modification that they called the Unified Interaction Parameter Formalism (UIPM) (Bale and Pelton, 1990).

2.3.11.1 The standard interaction parameter formalism

Consider a system containing N solutes (1, 2, 3, ... N) and a solvent for a total of $(N + 1)$ components. Let X_i denote the mole fractions, ε_{ij} the coefficients (parameters), γ_i the activity coefficients, and γ_i° the activity coefficients at infinite dilution ($X_{\text{solvent}} = 1$).

2.3.11.1.1 First-order interaction parameters

In the standard formalism, $\ln \gamma_i / \gamma_i^\circ$ ($i = 1, 2, 3, \dots, N$) for each solute can be expanded as:

$$\ln \gamma_i / \gamma_i^\circ = \varepsilon_{i1} X_1 + \varepsilon_{i2} X_2 + \varepsilon_{i3} X_3 + \dots + \varepsilon_{iN} X_N \quad (i = 1, 2, 3, \dots, N) \quad 2.124$$

where ε_{ij} are “first-order interaction parameters” given by:

$$\varepsilon_{ij} = \left(\frac{\partial \ln \gamma_i}{\partial X_i} \right)_{X_{\text{solvent}}=1} \quad 2.125$$

For thermodynamic consistency the following thermodynamic expression must always be respected:

$$\frac{\partial}{\partial n_i} \left(\frac{\partial G}{\partial n_j} \right) = \frac{\partial}{\partial n_j} \left(\frac{\partial G}{\partial n_i} \right) \quad 2.126$$

from which follows that:

$$\left(\frac{\partial \ln \gamma_j}{\partial n_i} \right) = \left(\frac{\partial \ln \gamma_i}{\partial n_j} \right) \quad 2.127$$

where G = Gibbs free energy and n_i = number of moles of component i and X_i = mole fraction of component i defined as:

$$X_i = n_i / (n_{\text{solvent}} + n_1 + n_2 + n_3 + \dots + n_N) \quad 2.128$$

If equation 2.124 is substituted into equation 2.127, it yields:

$$\varepsilon_{ij} - \varepsilon_{ji} = \ln(\gamma_i/\gamma_i^0) / (\gamma_j/\gamma_j^0) \quad 2.129$$

When $X_{\text{solvent}} = 1$, then $\gamma_i/\gamma_i^0 = \gamma_j/\gamma_j^0 = 1$ and equation 2.129 gives the following coefficient relationship:

$$\varepsilon_{ij} = \varepsilon_{ji} \quad 2.130$$

In the general case, at finite concentrations, it can be seen from equation 2.129 that the coefficients ε_{ij} cannot be constant. Therefore the formalism (equation 2.124) is inconsistent with the thermodynamic relationship in equation 2.127 except at infinite dilution.

From the Gibbs-Duhem equation:

$$(1 - X_1 - X_2 - \dots - X_N)d \ln \gamma_{solvent} + X_1 d \ln \gamma_1 + X_2 d \ln \gamma_2 + \dots + X_N d \ln \gamma_N = 0 \quad 2.131$$

the following expression for the activity coefficient of the solvent is obtained:

$$\ln \gamma_{solvent} = -\frac{1}{2} \sum_{j=1}^N \sum_{k=1}^N \varepsilon_{jk} X_j X_k \quad 2.132$$

It can be seen by substitution of equations 2.124 and 2.132 into equation 2.131 that the Gibbs-Duhem equation is only satisfied when $X_{solvent} = 1$. The consequence is that this formalism can only be used when $X_{solvent} \rightarrow 1$ or at infinite dilution.

This problem of thermodynamic inconsistency at finite solute concentrations was overcome by Pelton and Bale (1986) by adding $\ln \gamma_{solvent}$ to the right-hand side of equation 2.124. In the UIPM equation 2.124 now becomes:

$$\ln \gamma_i / \gamma_i^0 = \ln \gamma_{solvent} + \varepsilon_{i1} X_1 + \varepsilon_{i2} X_2 + \varepsilon_{i3} X_3 + \dots + \varepsilon_{iN} X_N \quad 2.133$$

Substitution of equations 2.132 and 2.133 into equation 2.131 shows that the UIPM is consistent with the Gibbs-Duhem equation at all concentrations. Equation 2.127 is also satisfied and the coefficient relationship, equation 2.130, still applies. Equation 2.132 for $\ln \gamma_{solvent}$ contains only quadratic terms in concentration and in very dilute solutions these terms become much smaller than the linear terms in equation 2.133 and can be ignored. Therefore, when $X_{solvent} \rightarrow 1$, equation 2.133 reduces to the standard formalism in equation 2.3.11.1. Equation 2.125 still applies and therefore the first-order ε_{ij} parameters of the UIPM are identical to the parameters of the standard formalism.

2.3.11.1.2 Higher-order interaction parameters

This modified formalism can be generalized to contain higher-order terms and equation 2.133 becomes:

$$\ln \gamma_i / \gamma_i^0 = \ln \gamma_{\text{solvent}} + \sum_{j=1}^N \varepsilon_{ij} X_j + \sum_{j=1}^N \sum_{k=1}^N \varepsilon_{ijk} X_j X_k + \sum_{j=1}^N \sum_{k=1}^N \sum_{l=1}^N \varepsilon_{ijkl} X_j X_k X_l + \dots \quad 2.134$$

where $\ln \gamma_{\text{solvent}}$ for the solvent is given by:

$$\ln \gamma_{\text{solvent}} = -\frac{1}{2} \sum_{j=1}^N \sum_{k=1}^N \varepsilon_{jk} X_j X_k - \frac{2}{3} \sum_{j=1}^N \sum_{k=1}^N \sum_{l=1}^N \varepsilon_{jkl} X_j X_k X_l - \frac{3}{4} \sum_{j=1}^N \sum_{k=1}^N \sum_{l=1}^N \sum_{m=1}^N \varepsilon_{jklm} X_j X_k X_l X_m - \dots \quad 2.135$$

where the parameters ε_{ij} , ε_{ijk} , ε_{ijkl} , ... may be called first-order, second-order, third-order, etc. interaction parameters. It can be shown that equation 2.134 and equation 2.135 satisfy the relationship of equation 2.127. It can also be shown that the Gibbs-Duhem equation is satisfied by substituting equations 2.134 and 2.135 into equation 2.131. The following relationships exist among the higher-order parameters:

$$\varepsilon_{ijk} = \varepsilon_{ikj} = \varepsilon_{jik} = \varepsilon_{jki} = \varepsilon_{kji} = \varepsilon_{kij} \quad 2.136$$

and

$$\varepsilon_{ijkl} = \varepsilon_{ikjl} = \varepsilon_{jikl} = \varepsilon_{jkil} = \varepsilon_{kjil} = \varepsilon_{kijl} = \dots \quad 2.137$$

The same relationships are true when two or more of the subscripts are identical:

$$\varepsilon_{ijj} = \varepsilon_{jij} = \varepsilon_{jji} \quad 2.138$$

This is analogous to the relationship between first-order interaction parameters described in equation 2.130.

The UIPM can therefore be extended to non-dilute solutions without losing thermodynamic consistency and without changing existing parameters or their values. This model has its main application in the modelling of metal systems (which may be in equilibrium with liquid slag and solid solution phases modelled by other solution models) as it is a non-ionic, non-polymer type of solution model.

3 THERMODYNAMICS/PHASE DIAGRAM DATA

3.1 *Relating thermodynamics and phase diagrams*

Consider components *A* and *B* that are completely miscible over the entire composition range in both the liquid and solid phases (Figure 4).

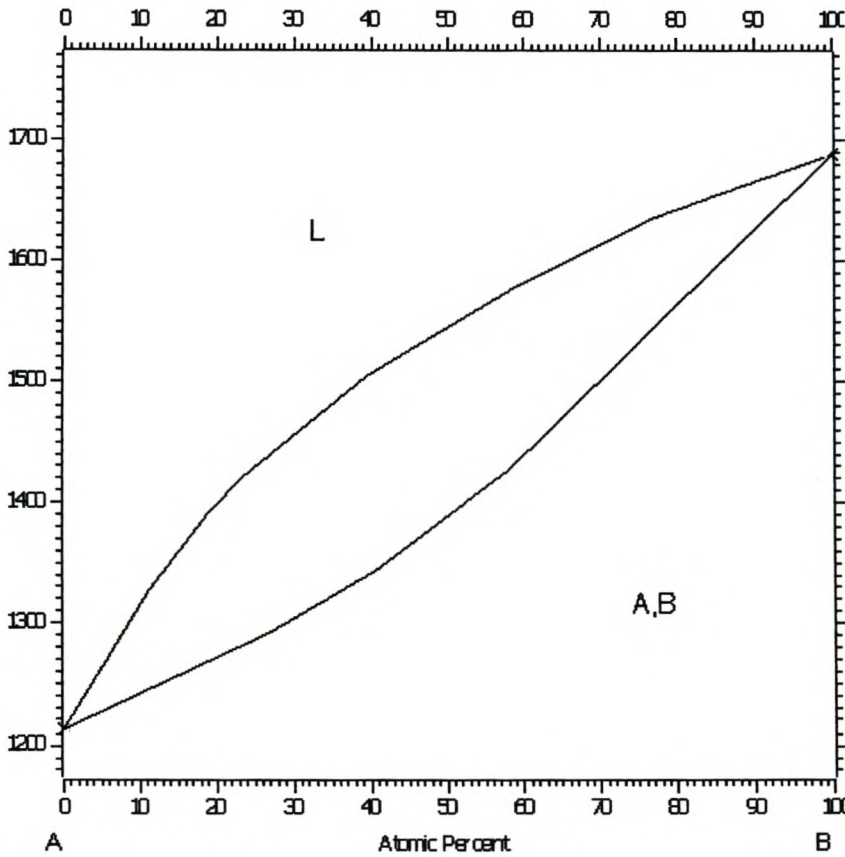


Figure 4 The binary phase diagram for components *A* and *B* that are completely miscible over the entire composition range

At chemical equilibrium, the partial molar Gibbs free energy (chemical potential) of any component in one phase must be equal to the chemical potential of the same component in all the other phases.

$$\bar{G}_B(l, X_B^l) = \bar{G}_B(s, X_B^s) \quad 3.1$$

$$\bar{G}_A(l, X_A^l) = \bar{G}_A(s, X_A^s) \quad 3.2$$

At temperature T, for component A :

$$\bar{G}_A(l) = \bar{G}_A^\circ(l) + RT \ln a_A(l) \quad 3.3$$

$$\bar{G}_A(s) = \bar{G}_A^\circ(s) + RT \ln a_A(s) \quad 3.4$$

where:

$$a_A(s) = \gamma_A^s \cdot X_A^s \quad 3.5$$

$$a_A(l) = \gamma_A^l \cdot X_A^l \quad 3.6$$

then:

$$RT \ln[a_A(s) / a_A(l)] = \bar{G}_{A(l)}^\circ - \bar{G}_{A(s)}^\circ = \Delta G_{s \rightarrow l(A)}^\circ \quad 3.7$$

$$\Delta G_{s \rightarrow l(A)}^\circ = \Delta H_{mA}^\circ - T \Delta S_{mA}^\circ = \Delta H_{mA}^\circ (1 - T / T_{mA}) \quad 3.8$$

$$\gamma_i^\alpha = f(x_i, \text{parameters}) \quad 3.9$$

$$\ln[a_A(s) / a_A(l)] = (\Delta H_{mA}^\circ / R)(1/T - 1/T_{mA}) \quad 3.10$$

The activity coefficients (γ) can be calculated using a solution model and the liquidus curve can thus be generated using the equations derived above. It is clear that, given the liquidus curve, the activity coefficients can be calculated as a function of composition, and model parameters can be regressed.

3.2 Thermodynamics and phase equilibrium in the Ti – O system

3.2.1 The Ti – TiO₂ system

De Vries and Roy (1952) first established the phase diagram for the Ti – TiO₂ system (Figure 5). They observed that rutile was reduced in air and darkened on heating above 1500 °C. They also found that the oxygen : titanium ratio of the rutile phase varied between 1.99 : 1 and 1.95 : 1. They concluded that rutile was a solid solution phase between TiO₂ and Ti₃O₅ with a eutectic reaction at 1830 °C.

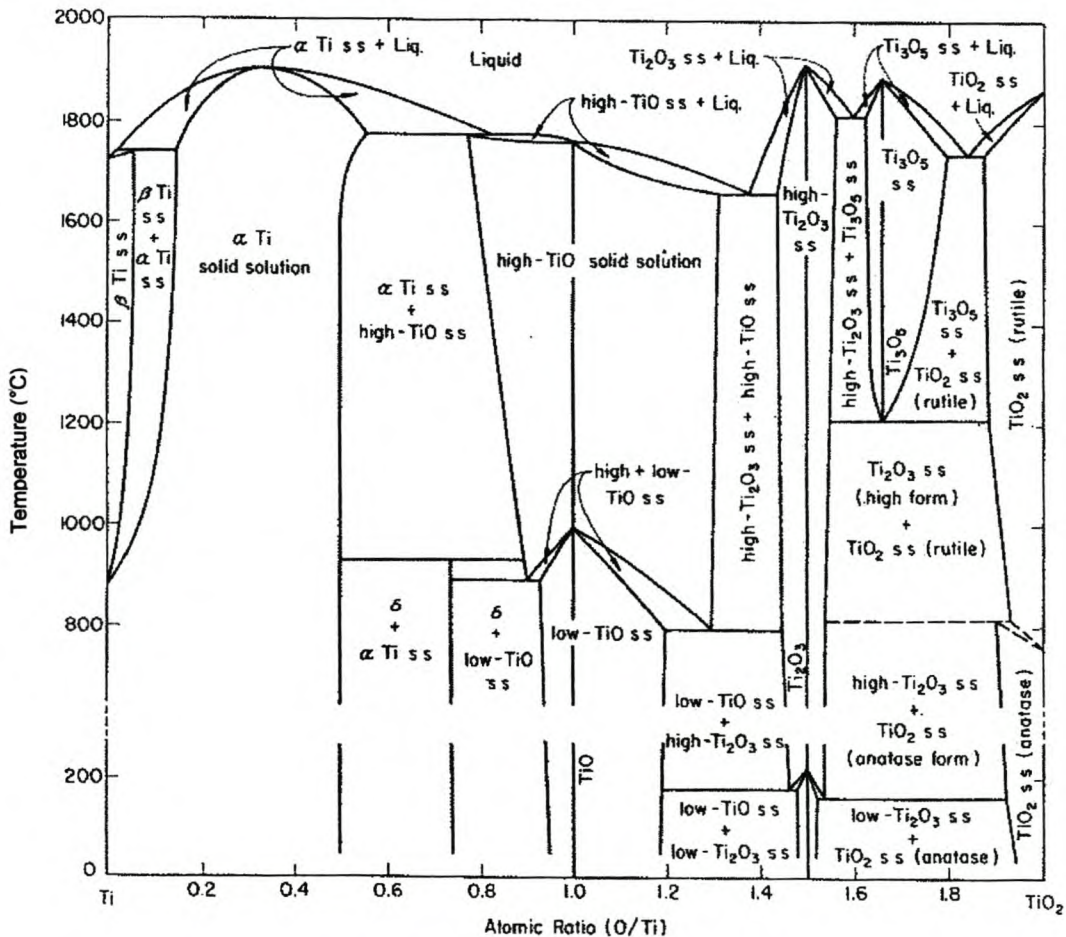


Figure 5 Binary phase diagram for the system Ti-TiO₂ summarizing various data in the literature (after De Vries and Roy (1952))

Wahlbeck and Gilles (1966) reinvestigated the Ti – TiO₂ system, incorporating data that were more recent. They also measured chemical equilibrium data in the Titanium

monoxide region. When compared with the proposed phase diagram of de Vries and Roy (Figure 5), it can be seen that Wahlbeck and Gilles (1966) accepted a much smaller homogeneity range for Ti_2O_3 and an even smaller one for Ti_3O_5 (Figure 6).

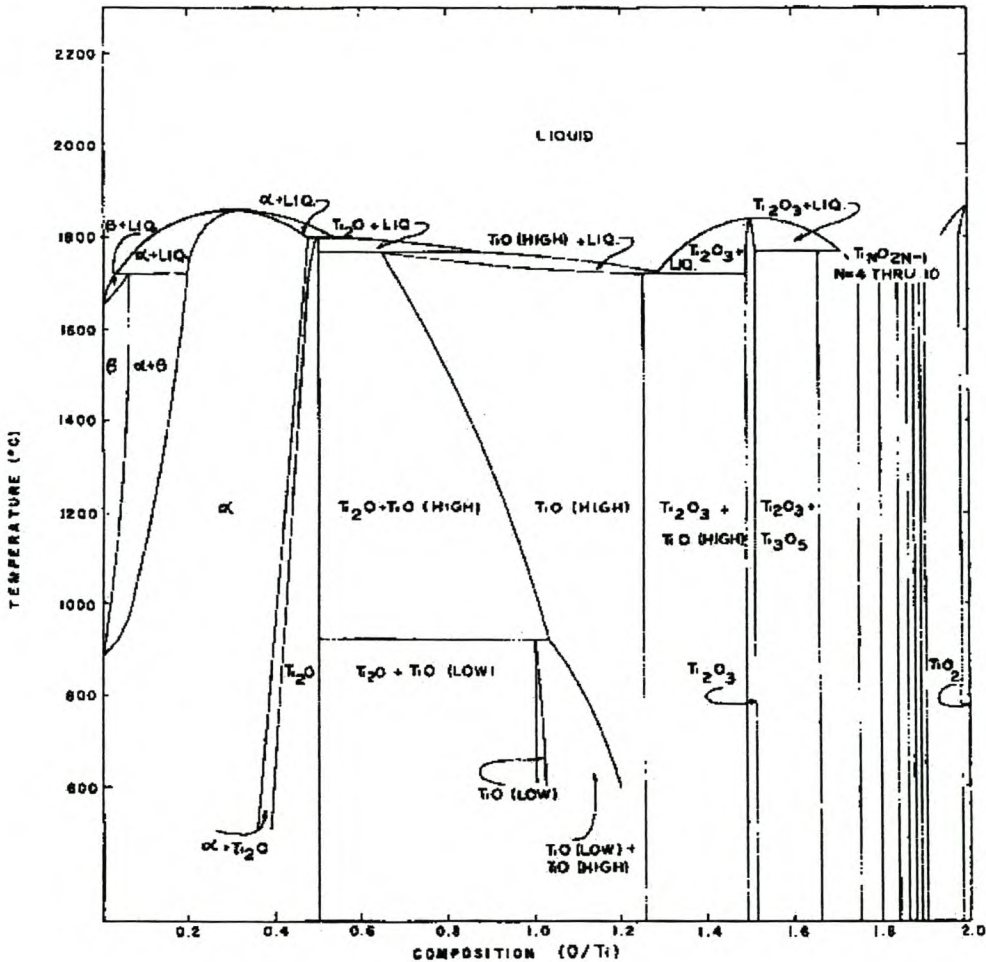


Figure 6: Titanium-oxygen phase diagram (after Wahlbeck and Gilles, 1966).

Wahlbeck and Gilles (1966) also included the Magnéli phases between Ti_3O_5 and TiO_2 where de Vries and Roy (1952) assumed a eutectic reaction. The so-called Magnéli phases are represented by the general formula Ti_nO_{2n-1} with the value of n ranging from 4 to 10. The melting point of TiO_2 was taken to be 1870 °C from Brauer and Littke (1960).

In 1987 a more recent critical review of the system was done by Murray and Wriedt. The Ti-O phase diagram published by Murray and Wriedt (1987) can be seen in Figure 7.

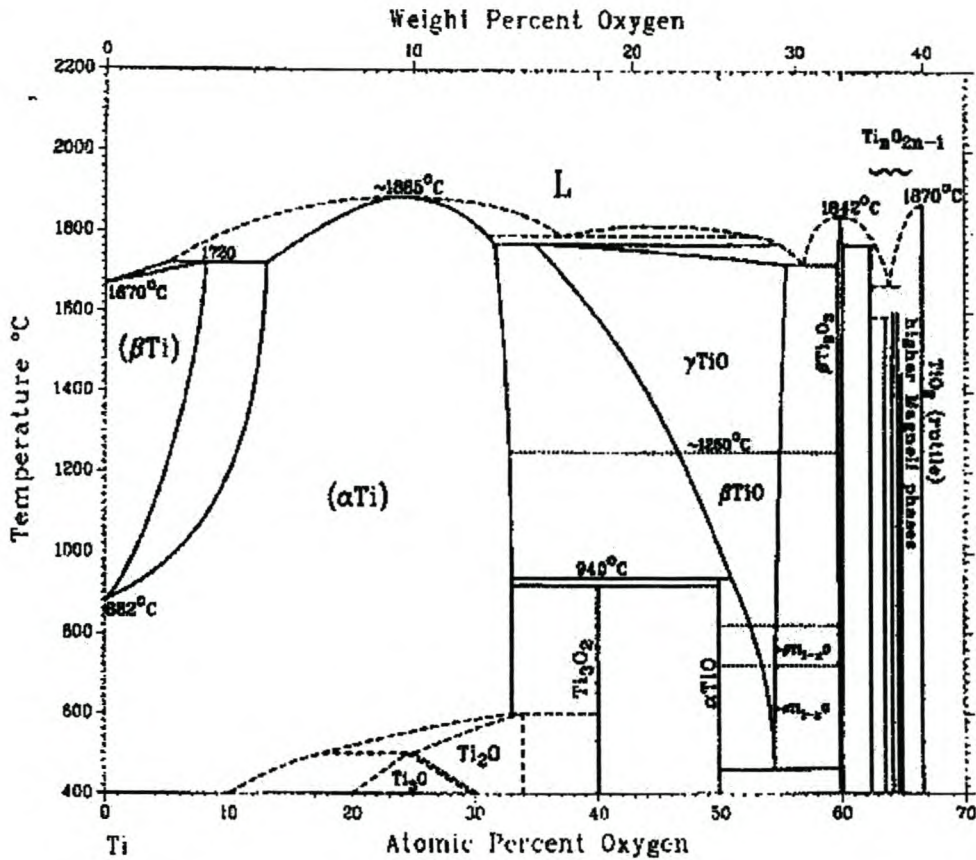


Figure 7: Assessed Ti-O phase diagram (after Murray and Wriedt (1987)).

Waldner and Eriksson (1999) used all available T-X phase diagrams and thermodynamic data (about 600 points) to calculate the Gibbs free energies of 18 phases. Twelve of these phases were treated as line components. The complete Ti-O system was calculated, including gaseous oxygen and Magnéli phases, between 298 K and the liquidus temperature and at a pressure of 1 bar. The TiO_x solid solution was described using a sublattice model based on bond-energy formalism which enables short and long range interactions to be distinguished. The liquid phase was described using the ionic two-sublattice approach and the gas phase was considered an ideal solution. The model parameters for all the different phases were obtained by an optimisation procedure for finding the best fit to the experimental information.

These calculations were carried out with the Gibbs energy minimization program ChemSage and produced the optimised phase diagram in Figure 8.

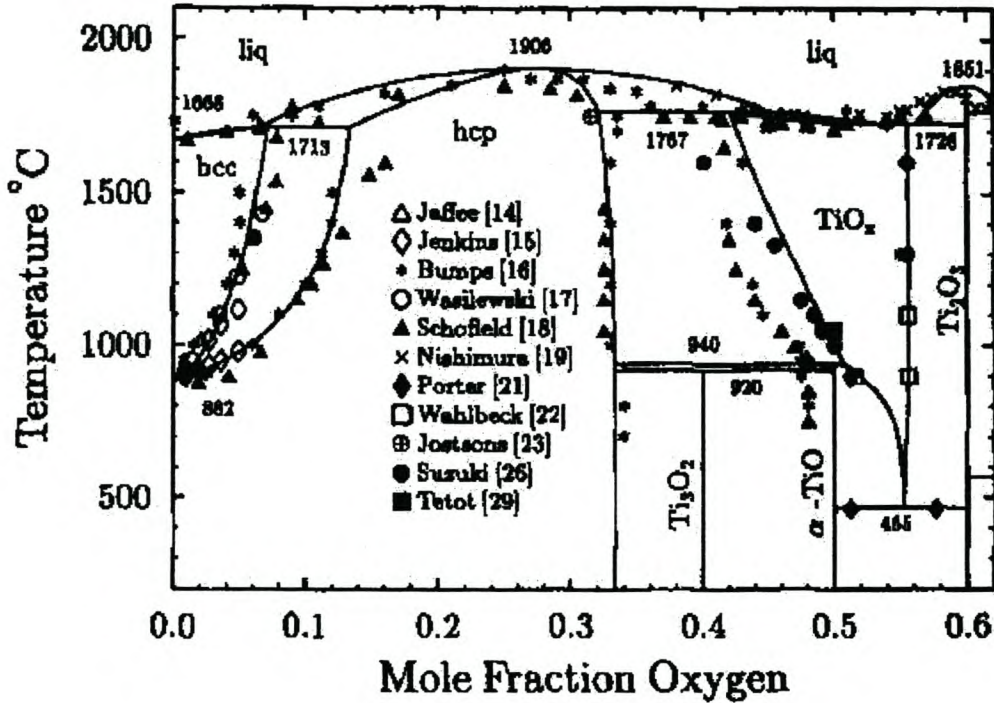


Figure 8: Calculated T-X phase diagram of Ti-O and experimental data up to 0.62 mole fraction oxygen (after Waldner and Eriksson, 1999).

Waldner and Eriksson (1999) found some regions of the phase diagram difficult to interpret, e.g. the liquidus above the TiO_x solid solution and the phase boundary between $TiO_x(s)$ and the hcp phase. Since the whole phase diagram could be calculated using optimised Gibbs free energy functions, they found that their work could give some information on uncertain phase boundaries within the predictive capacity of the applied models.

Figure 9 shows the complete Ti-O system including the liquid/gas equilibrium as predicted by Waldner and Eriksson (1999).

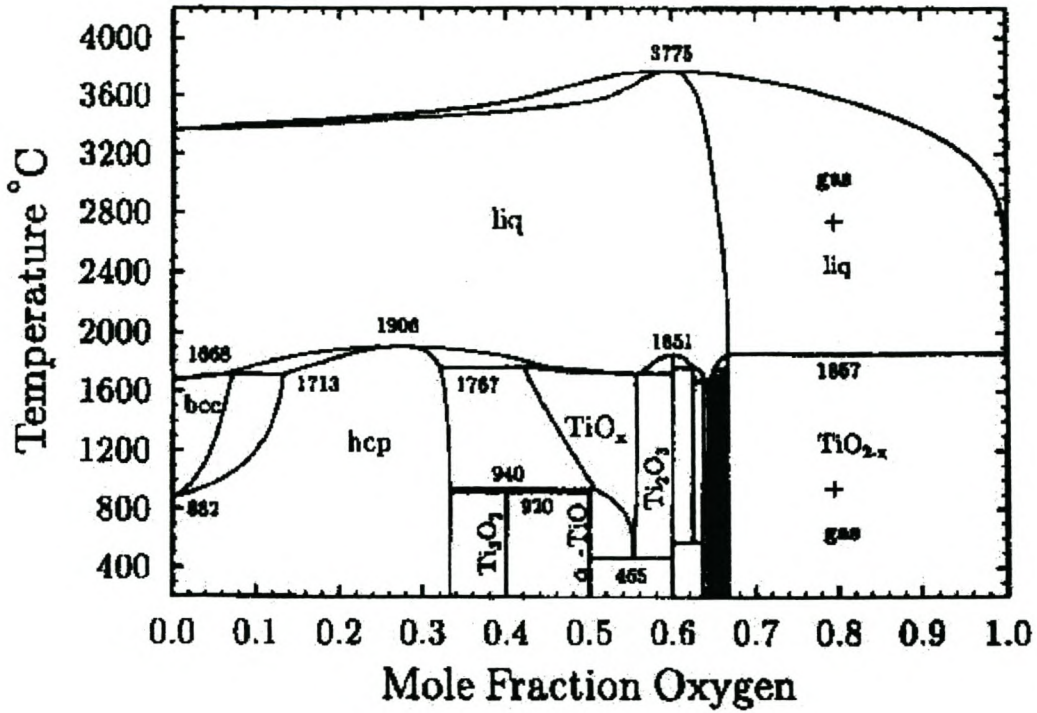


Figure 9: Calculated T-X phase diagram of the system Ti-O for $0 \leq x_o \leq 1$ and 1 bar total pressure. Predicted gas/liquid equilibria are also shown (after Waldner and Eriksson, 1999).

3.2.2 The $\text{TiO}_2 - \text{Ti}_2\text{O}_3$ system

Although this system forms part of the $\text{Ti} - \text{TiO}_2$ system discussed above (3.2.1), it is still poorly characterised. The most complete and reliable liquidus data were obtained by Brauer and Littke (1960) by optical techniques. Their liquidus points are shown in Figure 10.

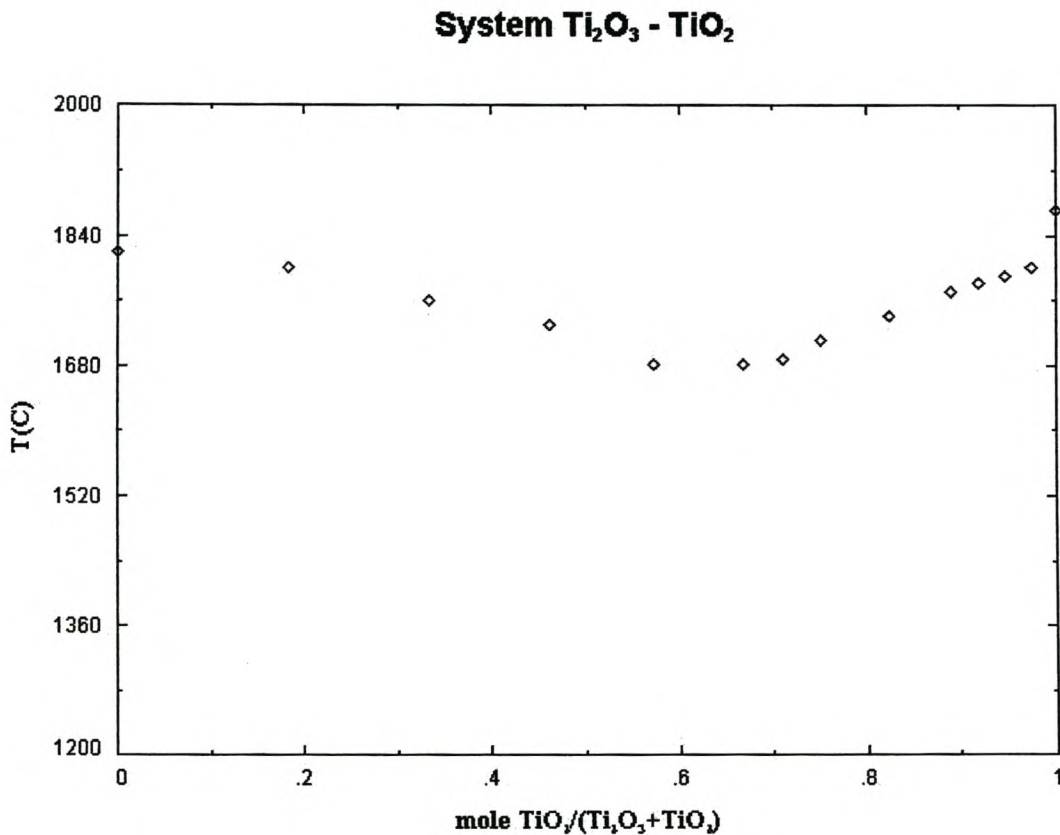


Figure 10: $\text{TiO}_2 - \text{Ti}_2\text{O}_3$ phase diagram determined by Brauer and Littke (1960)

Eriksson and Pelton (1993) did a full assessment of the $\text{TiO}_2 - \text{Ti}_2\text{O}_3$ binary system using all the available thermodynamic and phase diagram data for all the phases at 1 bar pressure from 298 K to above the liquidus temperature. All reliable data were simultaneously optimised using the modified quasi-chemical model for the liquid slag phase.

The phase diagram optimised by Eriksson and Pelton (1993) is shown in Figure 11.

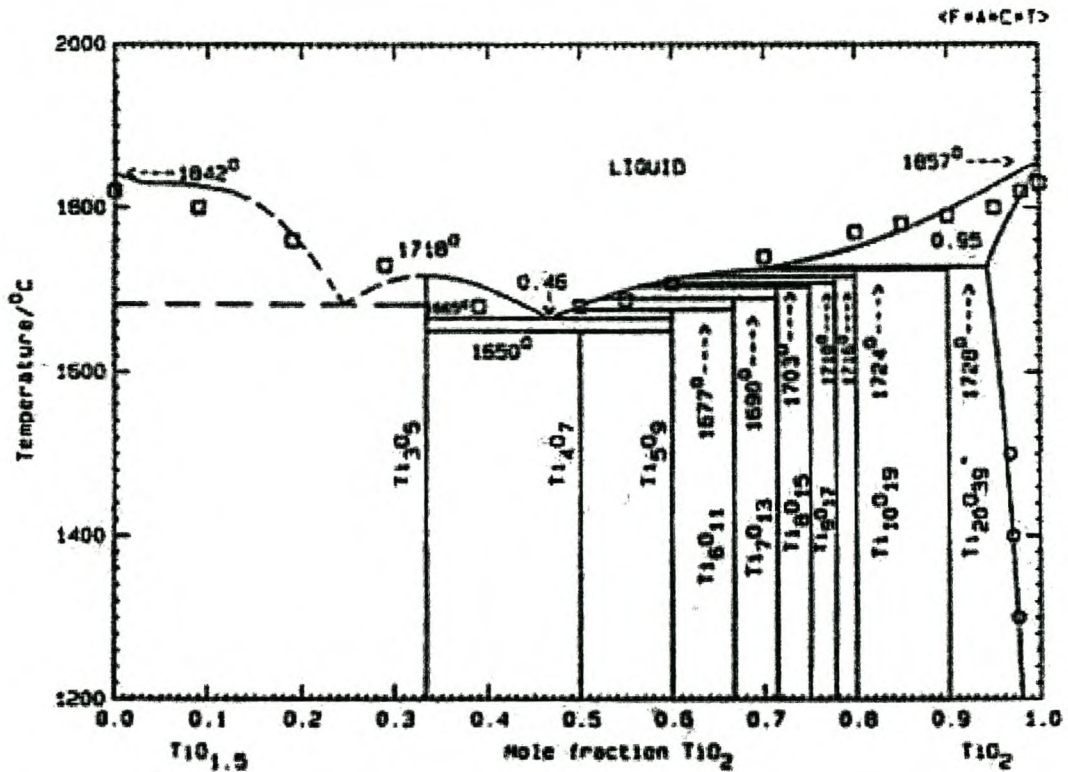


Figure 11: Optimised Ti₂O₃ - TiO₂ phase diagram. Composition in terms of components TiO_{1.5} - TiO₂ (after Eriksson and Pelton, 1993)

All the Magnéli phases (Ti_nO_{2n-1}) with n > 10 were grouped together and n was arbitrarily set equal to 20. In Eriksson and Pelton's (1993) assessment, all higher order Magnéli phases were therefore represented by Ti₂₀O₃₉. The rutile phase was taken as a Henrian solution of TiO_{1.5} in TiO₂ with:

$$RT \ln \gamma_{TiO_{1.5}} = 17786 \text{ J/mol} \quad 3.11$$

The quasi-chemical parameters determined by the optimisation of the liquidus points of Brauer and Littke (1960) are:

$$\omega = 18913 - 175126 Y_{TiO_2} + 338410 Y_{TiO_2}^2 - 177916 Y_{TiO_2}^3 \quad 3.12$$

$$\eta = 0 \quad 3.13$$

3.3 Thermodynamics and phase equilibrium in the Ti – Fe – O system

3.3.1 The FeO – TiO₂ system

The first attempt to measure liquidus points in the FeO – TiO₂ binary system was made by Grieve and White (1939). They measured the heating and cooling curves of FeO – TiO₂ mixtures of different compositions by means of the differential thermocouple method. The phase diagram they derived from thermal and microscopic studies is shown in Figure 12. They proposed two inter-oxide compounds, 2FeO·TiO₂ (pseudo brookite) and FeO·TiO₂ (ilmenite) both melting at approximately 1470 °C. They indicated high uncertainty in the high TiO₂ region.

Fe–Ti–O

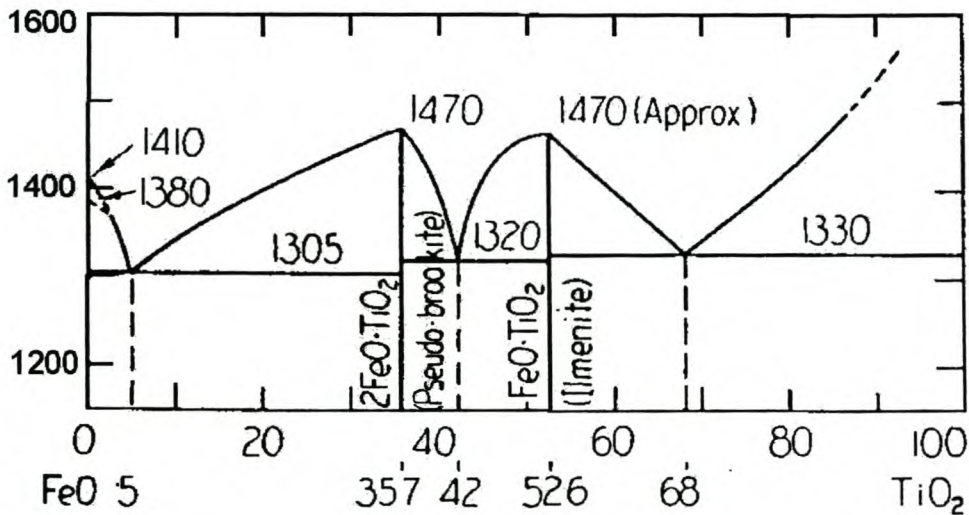


Figure 12: FeO - TiO₂ phase diagram as postulated by Grieve and White (1939)

MacChesney and Muan (1961) determined phase relations in the Fe – Ti – O system using the quenching technique combined with microscopic and x-ray examination. Mixtures of iron oxide and titanium dioxide were equilibrated under carefully controlled atmospheres and then quenched rapidly to room temperature. The composition of mixtures were determined by chemical analysis of the quenched samples. They used an iron – wüstite buffer to control the oxygen partial pressure of

the system and constructed the phase diagram in Figure 13.

Their diagram shows three congruently melting compounds: $\text{FeO}\cdot\text{TiO}_2$ (ilmenite), $2\text{FeO}\cdot\text{TiO}_2$ and $\text{FeO}\cdot 2\text{TiO}_2$. They suggested that $2\text{FeO}\cdot\text{TiO}_2$ has been wrongly named pseudo brookite by Grieve and White (1939) and they named it ulvospinel. They called $\text{FeO}\cdot 2\text{TiO}_2$ pseudo brookite.

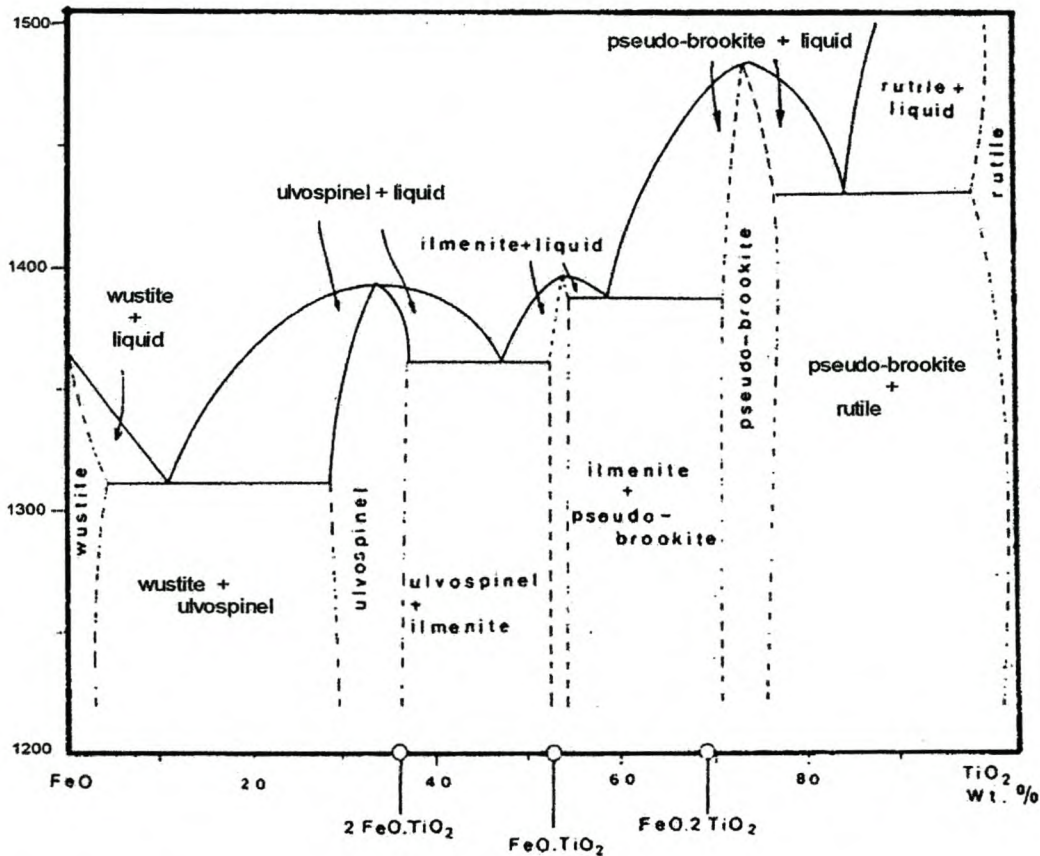


Figure 13: FeO - TiO₂ phase diagram after MacChesney and Muan (1961)

They attributed the disagreements between their study and that of Grieve and White (1939) to poorly defined atmospheres in the latter case.

The phase diagram proposed by MacChesney and Muan (1961) was accepted as being accurate until Grau (1979) performed cooling curve experiments in the high titanium region (Figure 14).

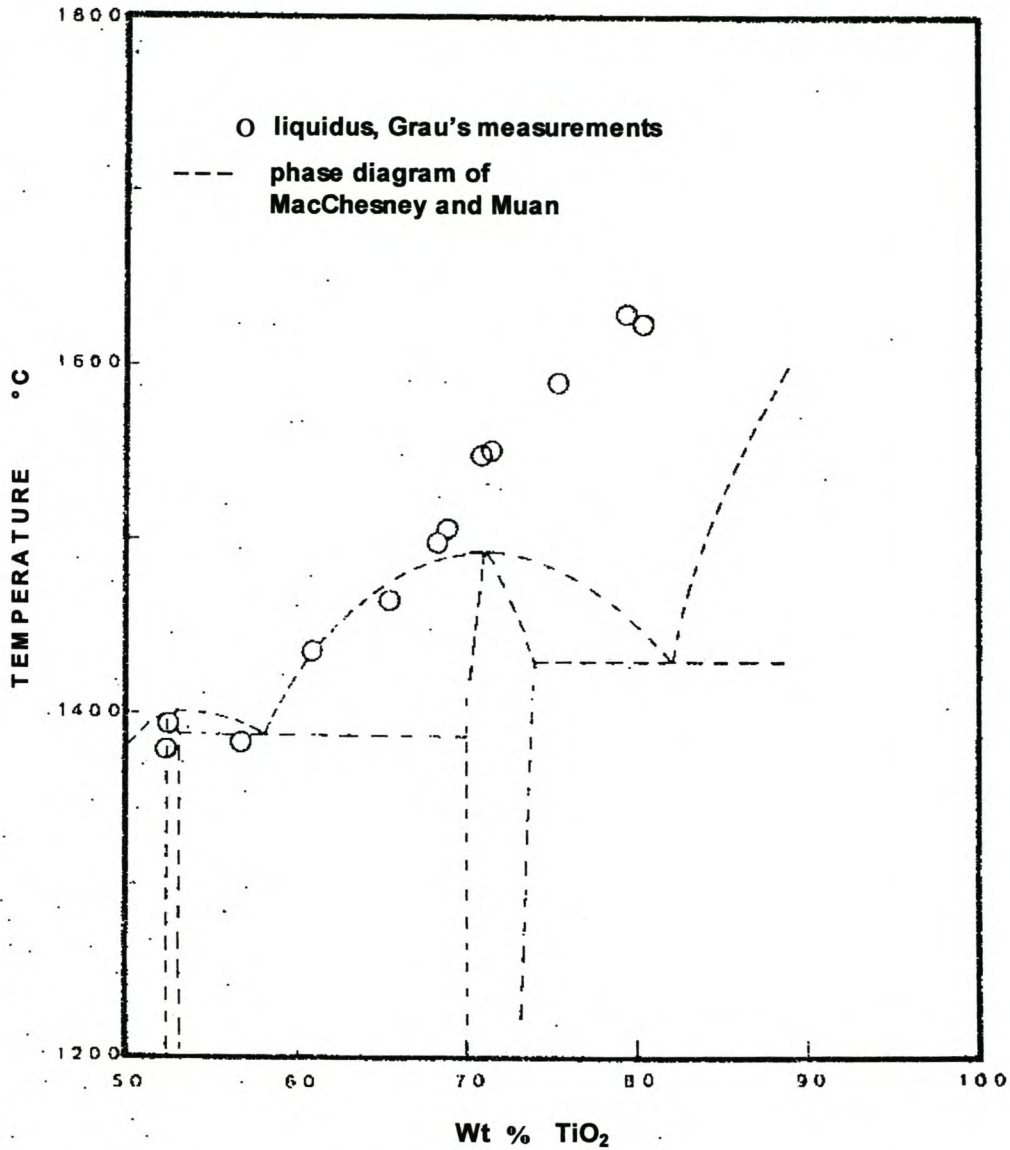


Figure 14: Liquidus points in the high titanium region of the FeO - TiO₂ binary, after Grau (1979)

In the technique Grau (1979) used, the slag temperature is continuously recorded during a cooling cycle and the liquidus temperature is determined from the arrest in the time-temperature curve, which indicates the beginning of crystallization. FeO - TiO₂ slags crystallize rapidly and only occasionally show a weak tendency to super cool. The relatively high heats of fusion of titania and titanates should result in clear changes in the cooling curve patterns at the beginning of the solidification (Figure 15).

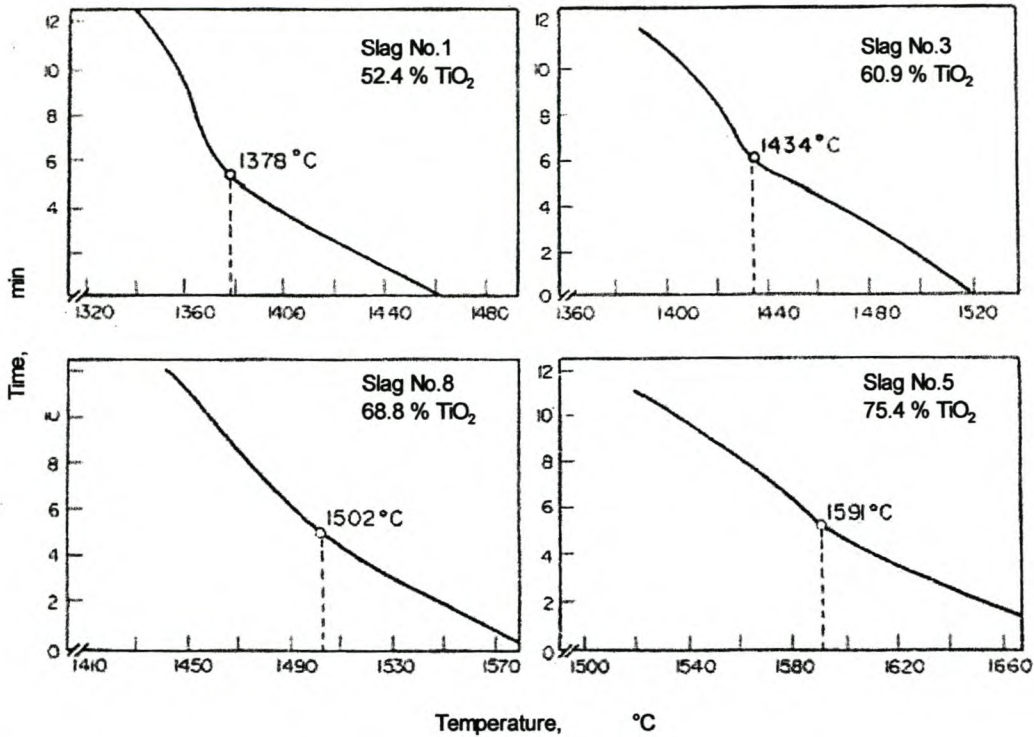


Figure 15: Examples of cooling curves after Grau (1979)

Grau (1979) thoroughly mixed synthetic ilmenite with reagent grade TiO₂ (in the form of anatase) in the proportions corresponding to the desired slag composition. The synthetic ilmenite was prepared by mixing pure iron powder and reagent grade Fe₂O₃ and TiO₂ in the amounts required to satisfy the stoichiometry of the reaction:



His results showed that pseudo brookite melts incongruently, forming rutile and liquid in a peritectic reaction. The eutectic point which MacChesney and Muan (1961) located at about 80 % TiO₂ was eliminated. This corresponded with an earlier suggestion by Smith and Bell (1970) that rutile should be the primary phase precipitating upon solidification of FeO – TiO₂ slags containing more than 62 % TiO₂. The high titanium side of the FeO – TiO₂ phase diagram was amended accordingly (Figure 16).

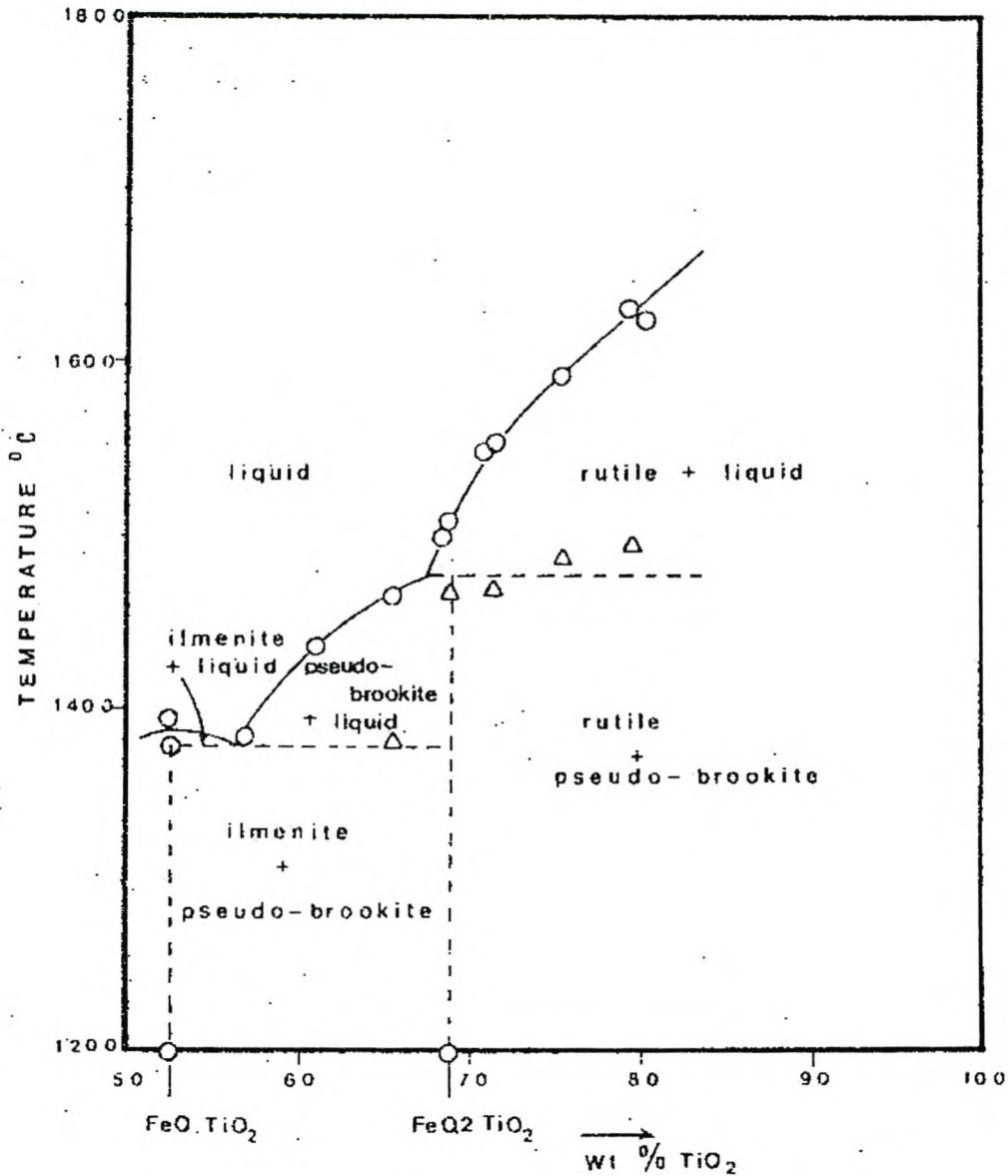


Figure 16: High titanium region of the FeO - TiO₂ binary, after Grau (1979)

Berman and Brown (1985) calculated the heat capacity equations for several minerals including Ilmenite and Pseudobrookite using the low temperature data of Shomate (1947) and the high temperature data from Naylor (1946).

A full thermodynamic assessment was again later done by Eriksson and Pelton (1993), using their modified quasi-chemical model for the liquid phase. Their assessed diagram agrees very well with the FeO rich data of MacChesney and Muan (1961) and on the TiO₂ rich side with the data of Grau (1979). Their model predicts a

melting point of 1857 °C for TiO_2 and requires only two quasi-chemical parameters:

$\omega = -12405 - 10227 Y_{\text{TiO}_2}^2 \text{ J/mol}$ and $\eta = 0$. The TiO_2 solid solution was treated as

Henrian with: $RT \ln \gamma_{\text{TiO}_{1.5}} = 6171 \text{ J/mol}$.

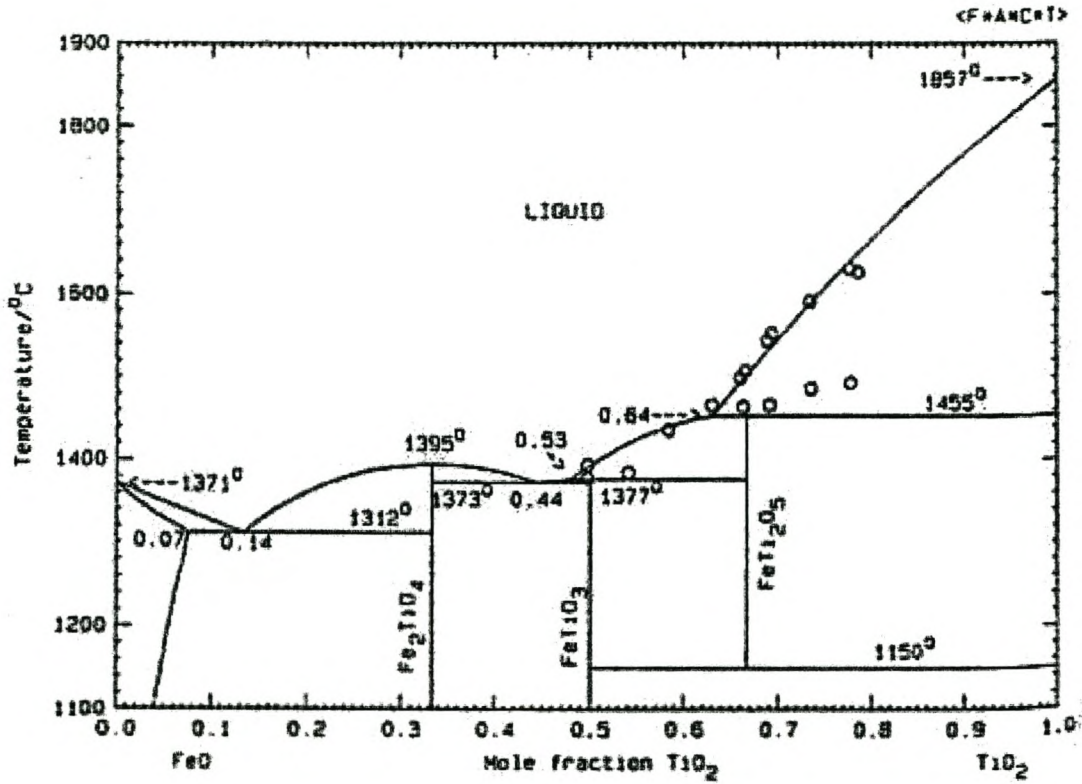


Figure 17: Optimised FeO - TiO_2 phase diagram, after Eriksson and Pelton (1993). Experimental points from Grau (1979)

3.3.2 The FeO – Ti₂O₃ system

In this binary system there is believed to exist a reaction-equilibrium rather than a phase-equilibrium. This equilibrium can be described by the following reactions:



Reaction 3.16 is highly spontaneous and will go to completion. Therefore Fe³⁺ and Ti³⁺ cannot co-exist.

From this equation it is clear that FeO and Ti₂O₃ cannot co-exist without the formation of TiO₂ and therefore the Ti₂O₃ – FeO binary only exists as part of the TiO₂ – Ti₂O₃ – FeO ternary.

4 MODELLING TECHNIQUE AND PROCEDURE

4.1 Choosing a model

It is apparent that a number of solution models exist to model the slag phase and the performance of the methods therefore have to be evaluated and a comparison of the strengths and weaknesses have to be made with respect to modelling the FeO – TiO₂ – Ti₂O₃ system. Hongjie Li et al (1998) compared the Cell model with the Modified Quasi-chemical model and published the following results.

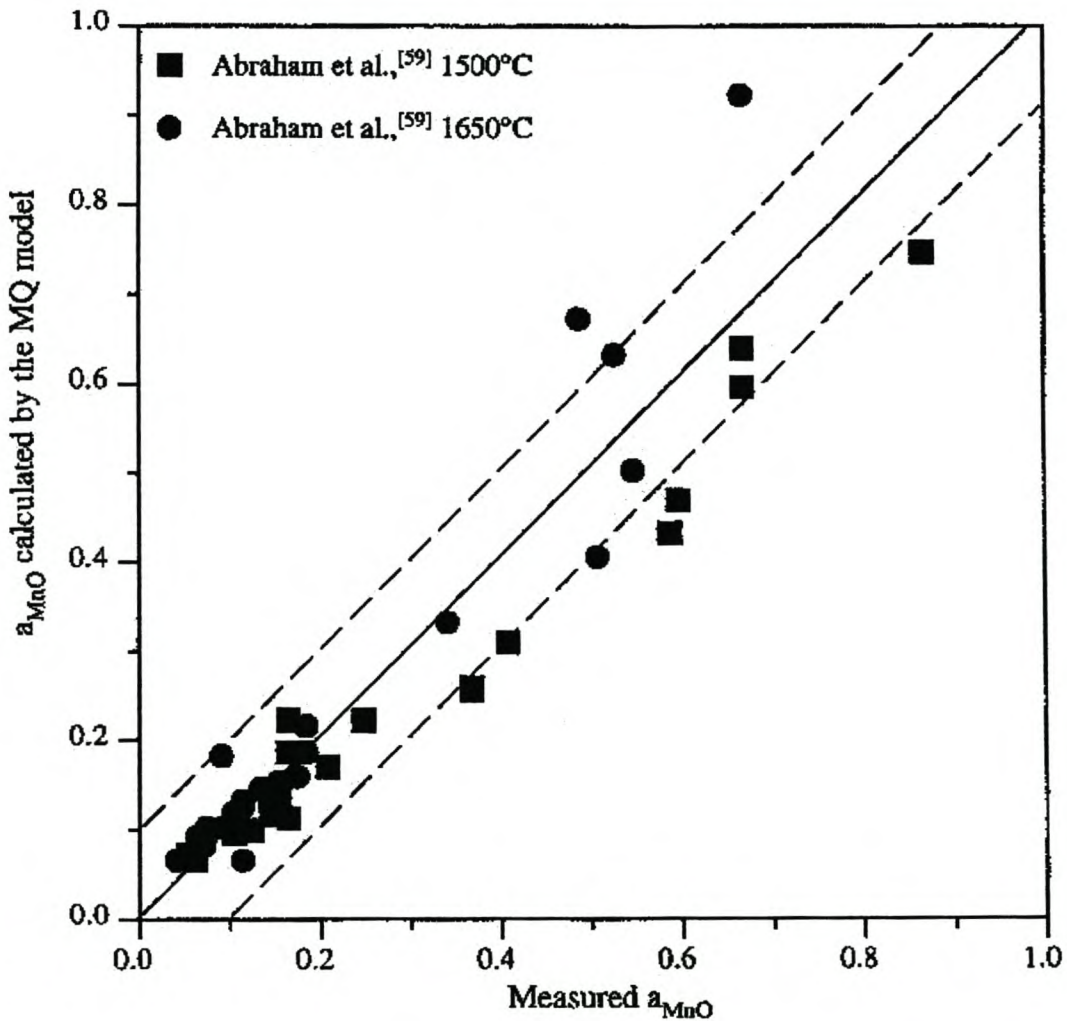


Figure 18: Comparison of MnO activity calculated by the Modified Quasi-chemical model with measured data in SiO₂-MnO-CaO melts at 1500 °C and 1650 °C. Reference state: pure solid MnO. (after Li et al. 1998)

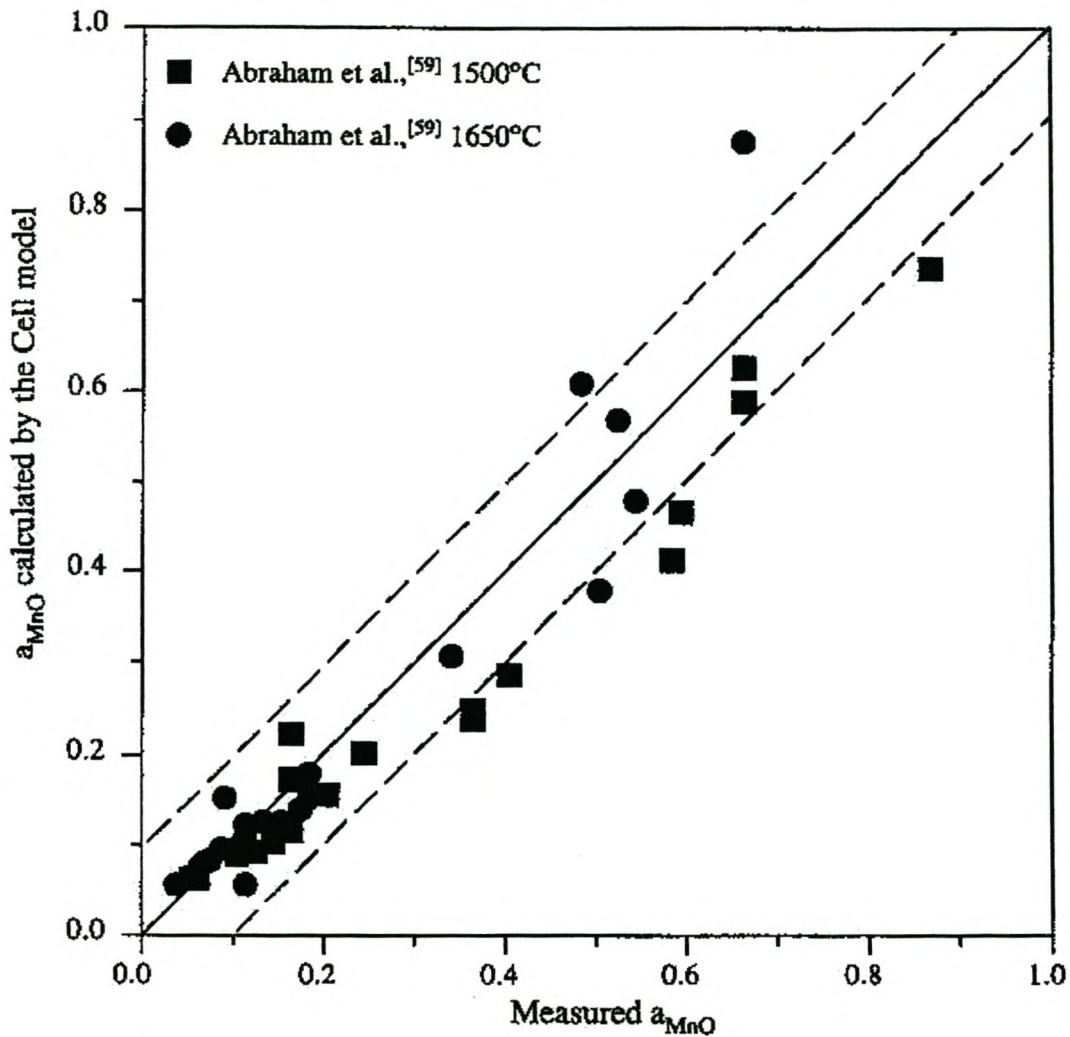


Figure 19: Comparison of MnO activity calculated by the Cell model with measured data in SiO₂-MnO-CaO melts at 1500 °C and 1650 °C. Reference state: pure solid MnO. (after Li et al. 1998)

The first comparison (Figure 18) and (Figure 19) was done on the SiO₂-MnO-CaO ternary system. There were hardly any difference between the Modified Quasi-chemical and the Cell model over the entire measured range. Over 95 % of all the datapoints fell within a tolerance of ± 0.1 and showed a good fit with the measured data.

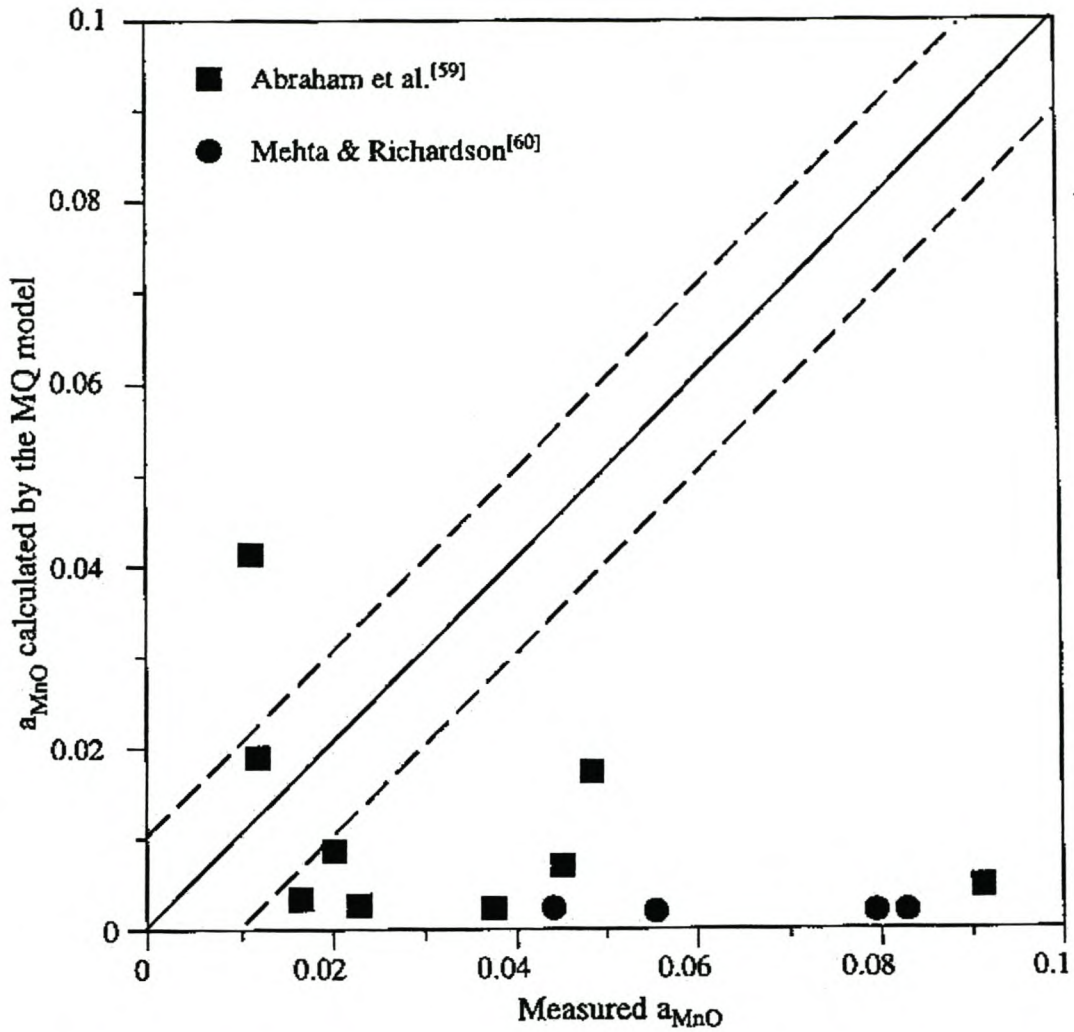


Figure 20: Comparison of MnO activity calculated by the Modified Quasi-chemical model with measured data in $\text{SiO}_2\text{-Al}_2\text{O}_3\text{-MnO-CaO}$ melts at 1650 °C. Reference state: pure solid MnO. (after Li et al. 1998)

The comparison was repeated for the $\text{SiO}_2\text{-Al}_2\text{O}_3\text{-MnO-CaO}$ ($\text{MnO} < 10\%$) quaternary system (Figure 20) and (Figure 21). From figure 20 it can be seen that the activities of MnO calculated by the Modified Quasi-chemical model are about one order of magnitude smaller than the measured data. For the Cell model (Figure 21), the difference between the measured and calculated MnO activities was less than ± 0.01 for most of the data points.

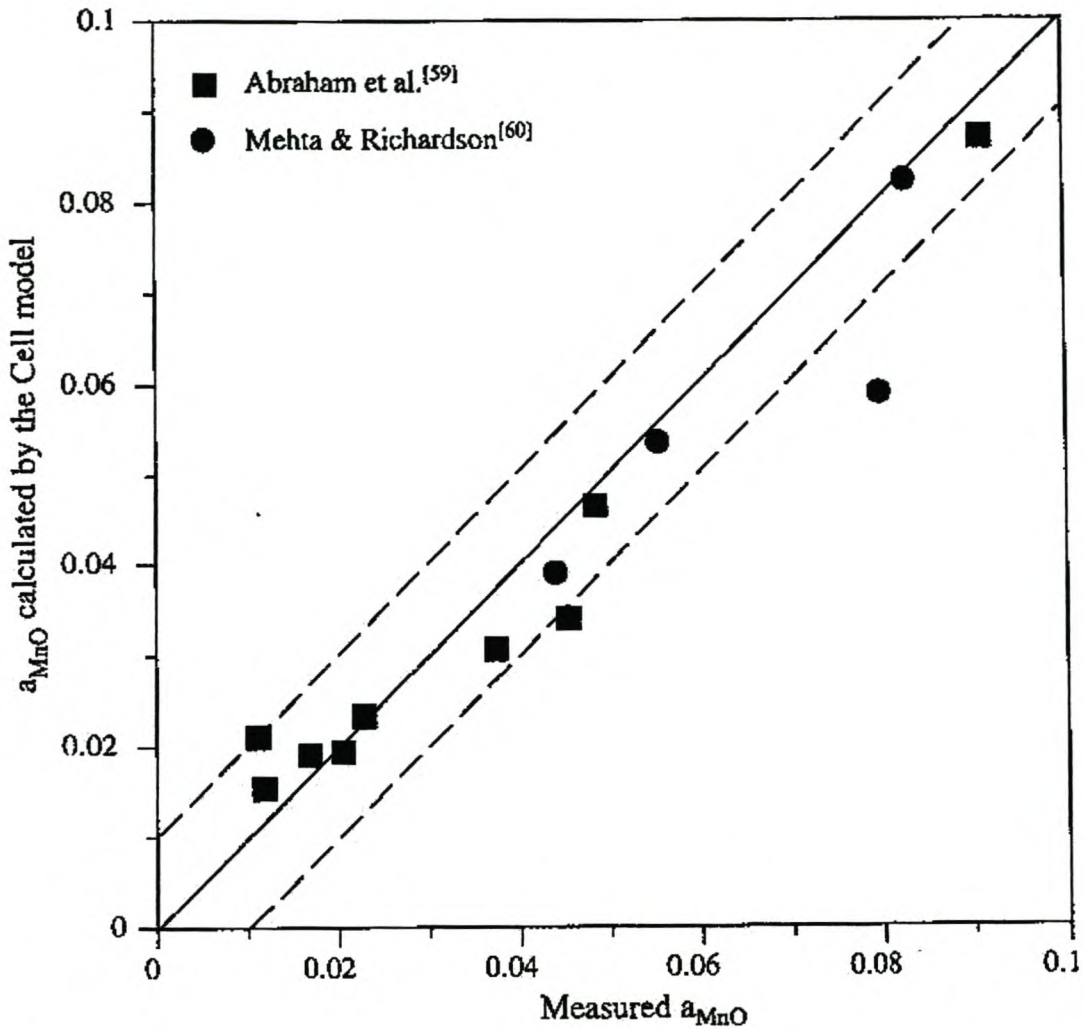


Figure 21: Comparison of MnO activity calculated by the Cell model with measured data in $\text{SiO}_2\text{-Al}_2\text{O}_3\text{-MnO-CaO}$ melts at 1650 °C. Reference state: pure solid MnO. (after Li et al. 1998)

While the Cell model still predicts the activity satisfactorily, the MQ model becomes inaccurate for higher-order systems. The Cell model has been successfully used on systems containing up to six different components (Gaye et al., 2000). The Cell model was developed for the steelmaking industry and is therefore very powerful in predicting the properties of ionic slags. It was therefore expected that it would work equally well with high-titania slags for these slags are also ionic in nature, especially in the highly reducing conditions of ilmenite smelters.

4.2 Model implementation on computers

The following sections contain a discussion of the thermochemical software used to model the FeO – TiO₂ – Ti₂O₃ system.

Over the past 20 to 30 years a number of different computer packages have been developed for the calculation of phase equilibria. These different packages have been developed separately, using different component databases and solution models. In 2001 two of the biggest role-players (GTT Technologies and Thermfact Ltd) joined forces to produce one of the most complete computational thermodynamics packages available, FactSage.

4.2.1 ChemSAGE

ChemSAGE is a direct descendant of the widely used SOLGASMIX Gibbs energy minimizer program developed by Dr. Gunnar Eriksson (Eriksson, 1975).

The early versions of SOLGASMIX could calculate equilibria in multi-component non-ideal solution phases. The user at that time needed programming skills since the first code only provided the necessary subroutines for the inclusion of non-ideal Gibbs energy models. The first interactive program (SOLGASALLOY) was released in 1984 after some co-operation between G. Eriksson and K Hack. This program incorporated non-ideal Gibbs energy models e.g. polynomials for substitutional metallic solutions. Later, more solution models were added, for example the Gaye – Kapoor – Frohberg cell formalism for non-ideal liquid oxides and the models developed by the F*A*C*T group (e.g. Modified Quasi-chemical model). SOLGASMIX was further enhanced by adding modules for the calculation of thermodynamic properties of phases and a reactor module for the calculation of co- and counter flow reactors. A SOLGASMIX – based Advanced Gibbs Energy minimizer (SAGE) was developed and released in 1988. These computational capabilities combined with the full access to thermodynamic databases of SGTE

(Scientific Group Thermodata Europe) led to ChemSage initially running under DOS. The programs were continually improved by the development of e.g. a thermodynamic assessment module, by the addition of an optimisation routine and finally by the development of a module for two-dimensional phase mapping. Two-dimensional phase mapping is used for the generation of generalized phase diagrams. ChemSage is used worldwide in universities, governmental and non-governmental research laboratories and in industry.

4.2.1.1 The general structure of ChemSage (Bale et al., 2002)

ChemSAGE is a menu-driven DOS program. The program has a modular structure as illustrated in Figure 22. New users are guided through menu option lists, on-line help and error messages, while more experienced users can proceed quickly, using simple commands in response to screen prompts. ChemSAGE has a multi-level structure of menus and feature displays. This structure contributes to the ease of learning and use of the program. There are four levels in the structure, each of which is entered from the one above it. The four levels are: the MAIN MENU; the calculation module menus; lower level menus; and the feature displays.

ChemSAGE contains 6 calculation modules, which are:

- the THERMODYNAMIC FUNCTIONS MODULE for the calculation of thermodynamic function values,
- the STOICHIOMETRIC REACTION MODULE for the calculation of thermodynamic properties of reactions,
- the PHASE EQUILIBRIUM MODULE for the calculation of complex heterogeneous phase equilibria,
- the TWO DIMENSIONAL PHASE MAPPING MODULE for phase diagram calculations,
- the REACTOR MODEL MODULE for the calculation of materials flow in simple multi-stage reactors and
- the PARAMETER OPTIMIZATION MODULE for the assessment of experimental thermochemical data

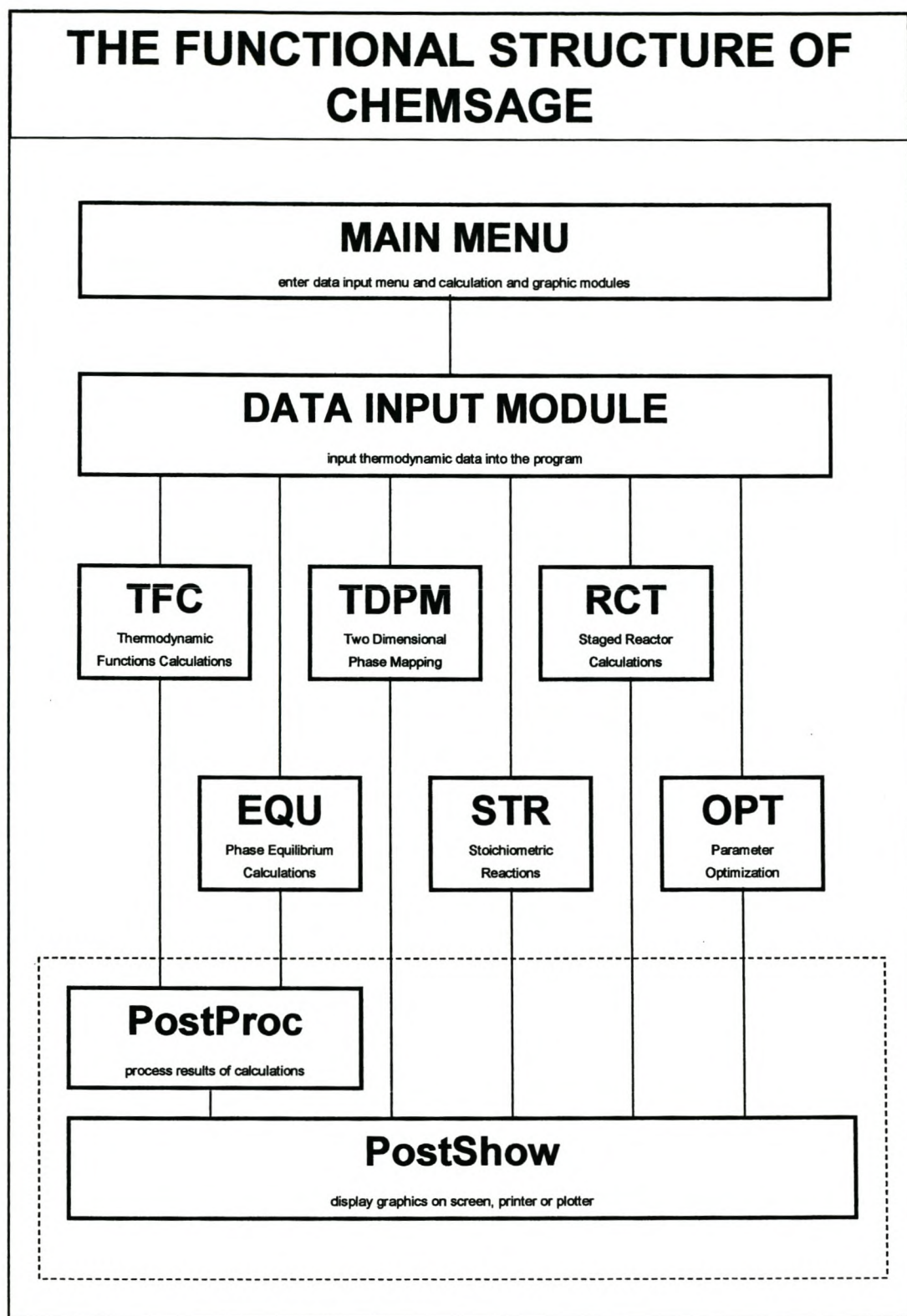


Figure 22: The functional structure of ChemSage, after Klaus Hack, ChemSage Handbook

4.2.1.1.1 *The THERMODYNAMIC FUNCTIONS module*

Many thermodynamic properties of solutions can be derived from the Gibbs energy. The following quantities can be calculated with respect to a chosen reference state, using ChemSAGE routines for thermodynamic function calculations:

- for single solution phases:
 - integral and partial values of heat capacity
 - total or excess entropy
 - enthalpy
 - Gibbs energy
 - Activity (a) or activity coefficient (γ)
 - Partial and total molar volume

- for stoichiometric condensed phases:
 - heat capacity
 - entropy
 - enthalpy
 - Gibbs energy

4.2.1.1.2 *The STOICHIOMETRIC REACTION module*

Stoichiometric reactions and related equilibrium constants are classically used in equilibrium thermo chemistry calculations. Electrochemical calculations are based on mass balance equations and the number of electrons transferred through the cell. The following quantities can be derived from stoichiometric reaction calculations:

- ΔC_p^0 , ΔS^0 , ΔG^0 , ΔV^0 and K as well as $\ln K$ and $\log K$
- The standard Nernst potential: $E^0 = \frac{\Delta G^0}{\nu_e} \cdot F$
- Change in: density, thermal expansion, bulk-modulus, heat capacity at constant volume and Grüneisen-Parameter.

4.2.1.1.3 The PHASE EQUILIBRIUM module

The phase equilibrium routines can be used to predict the chemical equilibrium state of a system. This system has to be uniquely defined with respect to temperature, pressure (or volume) and total amounts and/or equilibrium activities of independent system components. A calculation can also be controlled by:

- the change of an extensive property of the system, e.g. enthalpy to calculate adiabatic flame temperature or volume to calculate vapour pressure
- the selection of a phase target e.g. to calculate a liquidus temperature
- one dimensional phase mapping; the automatic variation of temperature, pressure, volume of composition through a selected interval to determine all phase boundaries lying within the interval

4.2.1.1.4 The TWO DIMENSIONAL PHASE MAPPING module

This module calculates two dimensional phase diagrams with any of the following axes combinations:

- temperature vs. total pressure at constant composition, T – P
- temperature vs. composition at constant total pressure, T – X, T – W
- total pressure vs. composition at constant temperature, P – X, P – W
- composition vs. composition at constant total pressure and temperature, $X_A - X_B$, $W_A - W_B$ (X = mol fraction, W = mass fraction)

After completion of the calculations, the phase diagram is automatically displayed and the actual coordinate pairs are stored in a *.PLO file.

4.2.1.1.5 The REACTOR MODEL module

The set of routines contained in this module enable steady-state calculations for dynamic chemical reactors.

4.2.1.1.6 *The PARAMETER OPTIMIZATION module*

This module permits the simultaneous assessment of a user-defined set of Gibbs energy parameters based on experimental input data. The Gibbs energy parameters can be:

- H_{298} , S_{298} , C_p – coefficients, compressibility coefficients or coefficients of the pressure derivative of the bulk modulus for pure substances or constituents of solution phases
- Coefficients of any of the excess Gibbs energy modules included in the ChemSAGE library of Excess Models.

The experimental input data could be any of the following:

- Phase boundary information (temperature, pressure, composition)
- Calorimetric data (enthalpies of formation, transformation, mixing)
- Gibbs energy data (components activities or partial pressures)

After the experimental data has been set up in an *.OPT file and the known thermochemical data has been combined with the unknown parameters in an *.DAT file, the actual assessment starts. The user enters ‘a priory’ errors for the values of the parameters to be optimised. The Bayesian parameter optimisation routine uses these errors to keep the changes to the parameters between iterations within certain limits. In the results file all the experimental values are compared with the calculated values (using the optimized parameters) in a table. This module does not provide a direct means for a graphical check of the quality of the assessment. This can be done by setting up and *.PLO file with the experimental data and using the overlay feature to compare it with the graphical output from either the TWO DIMENSIONAL PHASE MAPPING, the THERMODYNAMIC FUNCTIONS or the PHASE EQUILIBRIUM modules.

In this work ChemSAGE was used for the optimisation of the model parameters and FACTSage for the graphical representation due to the latter's user-friendly Windows interface and ease of reproduction. As yet, FACTSage does not allow optimization of said models while ChemSAGE does.

4.2.1.2 Gibbs free energy minimization

The total Gibbs free energy for a system at constant temperature, pressure and composition can be represented as:

$$G = \sum_i n_i \mu_i \quad 4.1$$

where n is the number of moles of component i , μ is the chemical potential and the sum extends over all species in the system. The equation can be misinterpreted, as it is easy to confuse the chemical potential of a species with that of an independent system component. To clarify this potential confusion, the expression can be written as:

$$G = \sum_{\phi} N^{\phi} G_m^{\phi} \quad 4.2$$

where ϕ is a phase index, N^{ϕ} is the number of moles and G_m^{ϕ} is the integral molar Gibbs free energy of phase ϕ . G in equation 4.2 is minimized with the constraints of the mass balance equations in terms of k independent system components. These may be written as:

$$\sum_{\phi} \sum_i n_i^{\phi} a_i^{\phi} = b_j \quad (j=1,2,\dots,k) \quad 4.3$$

where n_i^{ϕ} is the amount of the i^{th} constituent of phase ϕ , a_i^{ϕ} is a coefficient of the stoichiometry matrix composed of the constituents of phase ϕ and b_j is the total amount of the j^{th} system component. At equilibrium, the following equation is true:

$$G = \sum_j b_j \mu_j \quad 4.4$$

Integral and partial molar Gibbs free energy equations are required in the equilibrium calculations. The integral expression is written as:

$$G_{mix} = G_{mix}^0 + G_{mix}^{id} + G_{mix}^E + G_{mix}^{mo} + G_{mix}^P \quad 4.5$$

where G_{mix}^0 and G_{mix}^{id} are the Gibbs energy contributions from the pure phase components and the ideal entropy term respectively and G_{mix}^E is the excess Gibbs energy. The excess Gibbs energy contribution is often very small or even negligible if a proper ideal state has been chosen. Certain effects like chemical ordering and immiscibility can however not be modelled without this excess term. The G_m^E (Excess Gibbs free energy) term is therefore sometimes called the chemical interaction term. The Gibbs free energy contributions from magnetic ordering, G_{mix}^{mo} , and from changes in the molar volume, G_{mix}^p , are non-chemical and are normally neglected. The partial molar Gibbs energies can be derived from equation 4.5 according to generalized relationships.

In the Gibbs free energy minimization, the equations of an ideal system algorithm are used, with the chemical potentials replaced by their non-ideal values. Therefore, in this approximation, the ideal solution values are used for the compositional derivatives of the chemical potentials and the non-ideal values for the chemical potentials themselves. This cancels out when a minimum of the Gibbs energy surface is reached. The minimization algorithm is therefore independent of the solution model used and the convergence criteria are the same for ideal and non-ideal systems.

The shape of the Gibbs free energy surface and the existence and uniqueness of a solution are very important considerations in calculating the global minimum. Systems containing only ideal liquid and solid phases have convex Gibbs free energy surfaces and have no local minima. In these systems, the computed equilibrium composition corresponds to a global minimum. For non-ideal systems, uniqueness cannot be guaranteed, as many local minima may exist. Newer, more advanced optimization techniques are required to ensure the finding of the global minimum.

4.2.1.3 Least squares parameter estimation

The least squares method is one of the most popular techniques of regression analysis for calculating an expression that fits experimental data smoothly and as close as possible. In the following section, only the basic principles will be reviewed, as this method is well documented.

If one has a variable y which is a linear function of the independent variables x_1, x_2, \dots, x_m (i.e. $y; x_1, x_2, x_3, \dots, x_m$):

$$y = c_1x_1 + c_2x_2 + c_3x_3 + c_4x_4 + \dots + c_mx_m = \sum c_jx_j \quad 4.6$$

and n experimental points $y_i; x_{i1}, x_{i2}, x_{i3}, \dots, x_{im}$ (where $i = 1, n$), then the “best” values of c_1, c_2, \dots, c_m are determined by minimising the function below by a linear least-squares method.

$$S = \sum_{i=1}^n \left(y_i - \sum_{j=1}^m c_j x_{ij} \right)^2 \quad 4.7$$

S is minimized by setting $dS/dc_j = 0$ for $j = 1, m$. This gives m linear equations that may be solved simultaneously by a standard numerical method to obtain the coefficients $c_j (j = 1, m)$.

Suppose that one has, for example, two independent variables, z and t , and n data points $y_i; z_i, t_i$ (where $i = 1, n$), and the best fit to the following expression has to be found:

$$y = c_1 + c_2t + c_3z^2 + c_4z^2t + c_5 \exp(z) \quad 4.8$$

The same linear method as for equation 4.6 can be utilised, if the following identifications are made:

$$x_{i1} = 1.0$$

$$x_{i2} = t_i$$

$$x_{i3} = z_i^2$$

$$x_{i4} = z_i^2 t$$

$$x_{i5} = \exp(z_i)$$

In general, if $y = \sum c_j f_j(z, t)$, then one can use a linear least-squares method by letting $x_{ij} = f_j(z_i, t_i)$.

In a standard linear least-squares optimisation procedure for the excess thermodynamic properties of a binary system expressed as a power series one has:

$$\begin{aligned} G^E &= X_B (1 - X_B) (c_1 + c_2 X_B + c_3 X_B^2 + \dots) \\ &= X_B (1 - X_B) \sum_{j=1} c_j X_B^{j-1} \end{aligned} \quad 4.9$$

where X_B is the mole fraction of component B . If there are n experimental isothermal points for the total molar excess free energy G^E [G^E_i ; X_{Bi} ($i = 1, n$)] we could write $y = \sum c_j f_j(X_B)$ with $y_i = G^E_i$ and $f_j(X_{Bi}) = (1 - X_{Bi}) X_{Bi}^j$. If, in addition, one also has k isothermal experimental values of the partial molar excess free energy G^E_B [G^E_{Bi} ; X_{2i} ($i = (n + 1), (n + k)$)], one can calculate an expression for G^E_B from equation 4.9 by proper differentiation:

$$G^E_B = (1 - X_B) \sum_{j=1} j c_j X_B^{j-1} \quad 4.10$$

where the written coefficients c_j in equations 4.9 and 4.10 are the same. Equation 4.10 can be written in the form $y = \sum c_j f_j(X_B)$ if $y_i = G^E_{Bi}$ and $f_j(X_{Bi}) = (1 - X_{Bi})^2 j X_{Bi}^{j-1}$. Consequently, all n data points for G^E and all k data points for G^E_B can be simultaneously fitted in one least-squares procedure by setting $y = \sum c_j f_j(X_B)$ and letting $y_i = G^E_i$ when $i = 1, n$; $y_i = G^E_{Bi}$ when $i = (n + 1), (n + k)$; $f_j(X_B) = (1 - X_B) X_B^j$ when $i = 1, n$; and $f_j(X_B) = (1 - X_B)^2 j X_B^{j-1}$ when $i = (n + 1), (n + k)$. Data for G^E_A , the

partial molar excess free energy of mixing of component A , and other thermodynamic properties can also all be simultaneously optimised.

If experimental data points are measured at different temperatures T_i , as well as at different composition X_{Bi} , then G^E can be written as:

$$G^E = X_B (1 - X_B) \sum_{j=1} (\Delta H_j^E - T \Delta S_j^E) X_B^{j-1} \quad 4.11$$

where ΔH_j^E and ΔS_j^E are enthalpy and excess entropy coefficients respectively. The above optimisation procedure can then be used if we set $y_i = G_i^E$ and $f_j(X_B, T) = (1 - X_B)X_B^j$ for the ΔH_j^E terms and $f_j(X_B, T) = -T(1 - X_B)X_B^j$ for the ΔS_j^E terms. It is now clear that data sets $G_{Bi}^E; X_{Bi}, T_i$ and $G_{Ai}^E; X_{Bi}, T_i$ can also be simultaneously optimised.

In the case of the modified quasi-chemical theory, direct application of this standard optimisation procedure is not possible, because of the non-linear nature of the equations (Pelton and Blander, 1988). For example, equation 2.90 for G^E cannot be written in the form $G^E = \sum c_j f_j(X_B, T)$ because ξ is a function of $(\omega - \eta T)$ which is a function of Y_B . However, if one has an experimental point G_i^E at (Y_{Bi}, T_i) , then one can find the value of $(\omega - \eta T)$ at this composition which, when substituted into equation 2.90, will give G_i^E . Since G^E varies monotonically with $(\omega - \eta T)$ at any given composition and temperature, this can easily be done by trail and error. Hence, experimental data points $G_i^E; Y_{2i}, T_i$ can be converted into “experimental” points $(\omega - \eta T)_i; Y_{2i}, T_i$ which can then be optimised by the standard linear optimisation procedure to give the coefficients of equations 2.90 and 2.91.

The problem becomes more difficult in the case of experimental partial molar excess Gibbs energies which are given by equation 2.97 and 2.98. In this case, one cannot convert experimental data points $G_{Ai}^E; Y_{Bi}, T_i$ into $(\omega - \eta T)_i; Y_{Bi}, T_i$ points because G_{Ai}^E depends not only on $(\omega - \eta T)$ but also on $\partial(\omega - \eta T)/\partial Y_B$. To overcome this problem, equation 2.97 can be written as:

$$G_A^E = F(\omega - \eta T) - C(\omega - \eta T) \left(\frac{\partial(\omega - \eta T)}{\partial Y_B} \right) \quad 4.12$$

$F(\omega - \eta T)$ is a relatively strong function of $(\omega - \eta T)$. However, $C(\omega - \eta T)$ depends only weakly on $(\omega - \eta T)$ through the factor $(1 + \xi)$ which can vary only between the limits $1 < (1 + \xi) < 2$.

Let ω^* and η^* be initial guesses for ω and η as a function of Y_B :

$$\omega^* = \sum_{j=0} \omega_j^* Y_B^j \quad 4.13$$

$$\eta^* = \sum_{j=0} \eta_j^* Y_B^j \quad 4.14$$

and then expand $F(\omega - \eta T)$ as a Taylor expansion about $(\omega^* - \eta^* T)$ up to the first order term and replace $C(\omega - \eta T)$ by $C(\omega^* - \eta^* T)$:

$$G_A^E = F(\omega^* - \eta^* T) + F'(\omega^* - \eta^* T) \left[(\omega - \omega^*) - (\eta - \eta^*) T \right] - C(\omega^* - \eta^* T) \left(\frac{\partial(\omega - \eta T)}{\partial Y_B} \right) \quad 4.15$$

Upon performing the differentiations and substitutions and rearranging, one obtains:

$$\begin{aligned} & \frac{[G_A^E - F(\omega^* - \eta^* T)](1 + \xi^*)}{2\alpha Y_A Y_B^2} + \frac{(\xi^* - 1 + 2Y_B)(\omega^* - \eta^* T)}{2\xi^* Y_A Y_B} \\ & = \frac{\xi^* - 1 + 2Y_B}{2\xi^* Y_A Y_B} \sum (\omega_j - \eta_j T) Y_B^j - \sum j(\omega_j - \eta_j T) Y_B^{j-1} \end{aligned} \quad 4.16$$

where $\xi^* \equiv \xi^*(\omega^* - \eta^* T)$. Equation 4.16 is linear, so we can simultaneously optimise G_A^E , G_B^E and G^E . The procedure is as follows. First, a suitable guess for $(\omega^* - \eta^* T)$ is made and a linear optimisation is performed. The resulting expression for $(\omega - \eta T)$ can be taken as a second guess for $(\omega^* - \eta^* T)$ and so on. Pelton and Blander (1988) found that any guess for $(\omega^* - \eta^* T)$ that was of the right order led to an

expression for $(\omega - \eta T)$ which changed negligibly with the second iteration. This Taylor expansion technique thus appears to work very well unless $(\omega^* - \eta^* T)$ is very far from the final result.

The optimisation procedure may also be applied to miscibility gap data. If X_B and Y_B are molar and equivalent fractions on one side of the gap in equilibrium with compositions x_B, y_B on the other side, then if we equate $(G_A - G_A^\circ)$ on the two sides and use the notation of equation 4.15 we can arrive at a linear expression:

$$\begin{aligned}
 & RT \ln(X_A/x_A) + F(\omega^* - \eta^* T, Y_B) - F(\omega^* - \eta^* T, y_B) \\
 & - F'(\omega^* - \eta^* T, Y_B) [\omega^*(Y_B) - \eta^*(Y_B)T] + F'(\omega^* - \eta^* T, y_B) [\omega^*(y_B) - \eta^*(y_B)T] \\
 & = \sum (\omega_j - \eta_j T) [F'(\omega^* - \eta^* T, y_B) y_B^j - F'(\omega^* - \eta^* T, Y_B) Y_B^j \\
 & + C(\omega^* - \eta^* T, Y_B) j Y_B^{j-1} - C(\omega^* - \eta^* T, y_B) j y_B^{j-1}] \quad 4.17
 \end{aligned}$$

A similar equation can be written by equating $(G_B - G_B^\circ)$ on the two sides of the miscibility gap. Consequently, miscibility gap information can be simultaneously optimised along with G^E , G_A^E and G_B^E data.

Experimental enthalpy of mixing data can also be included in the simultaneous optimisation. From equation 2.85, ΔH depends on ω and also on $(\omega - \eta T)$, since X_{AB} is a function of $(\omega - \eta T)$. If η is held constant at a fixed value, then ΔH varies monotonically with ω . A procedure similar to that used for G^E data can then be employed. Let η^* be an initial estimate of η obtained, for example, by optimising data other than enthalpy of mixing data. With η^* constant, experimental points $\Delta H_i; X_{2i}, T_i$ are then converted into "experimental" points $\omega_i; X_{2i}, T_i$ by trial and error, and an expression for ω is obtained by simultaneous optimisation of all data. Additional iterations can then be performed.

With these techniques, all available data for a binary solution can be optimised. This includes all phase diagram data, Gibbs energies of formation of compounds, enthalpies of fusion, enthalpies of mixing, activities, and other related data.

4.2.2 F*A*C*T

The facility for the Analysis of Chemical Thermodynamics (F*A*C*T) started in 1976 as a joint research project between two universities. Professors Christopher W. Bale and Arthur D. Pelton from École Polytechnique and prof. William T Thompson from McGill University worked together on this project for treating thermodynamic properties and calculations in chemical metallurgy. The first programs were written in FORTRAN and performed chemical thermodynamic calculations involving pure substances and ideal gases. In 1979 F*A*C*T On-line was offered as an interactive program. It could be accessed through the McGill University MUSIC system via Datapac and Telenet telephone links, but was mainly used as a teaching tool. Solution programs and databases were added, as well as POTCOMP and TERNFIG algorithms for optimizing, calculating and plotting of binary and ternary phase diagrams. In the 1990's, F*A*C*T started to incorporate the Gibbs Energy Minimizer, SOLGASMIX, developed by Dr. Gunnar Eriksson (GTT) and evolved into a PC-based program. FACT-DOS was released in 1994 and offered unlimited access to the software databases. The research centre CRCT (Centre for Research in Computational Thermochemistry) was founded in 1984 by professors Arthur D Pelton and Christopher W Bale at the École Polytechnique. In 1996, FACT-Web provided demonstration modules through the Internet at the CRCT. The Windows® version of F*A*C*T, FACT-win, was released in 1999. This offered a fully integrated thermochemical database system that combined proven software with critically assessed thermodynamic data.

4.2.3 FactSage

In 2001 FACTwin and ChemSage were merged into one common product called FactSage 5.0. This was a combined effort of the F*A*C*T Group (Thermfact Ltd./CRCT, Montreal) and the ChemSage/ChemApp Group (GTT-Technologies, Germany). It offers most of the features available in the FACTwin 3.05 and ChemSage 4.0 packages in a Windows® environment. The modules in FactSage include View Data, View Figure, Compound, Solution, Reaction, Predom, EpH, Equilib, Phase Diagram, Mixture and Results. The Optimize module is not yet functional in FactSage and this function of ChemSage was used in this investigation. Due to the user friendliness of the Windows® environment, all the phase diagram calculations and figures were done using FactSage.

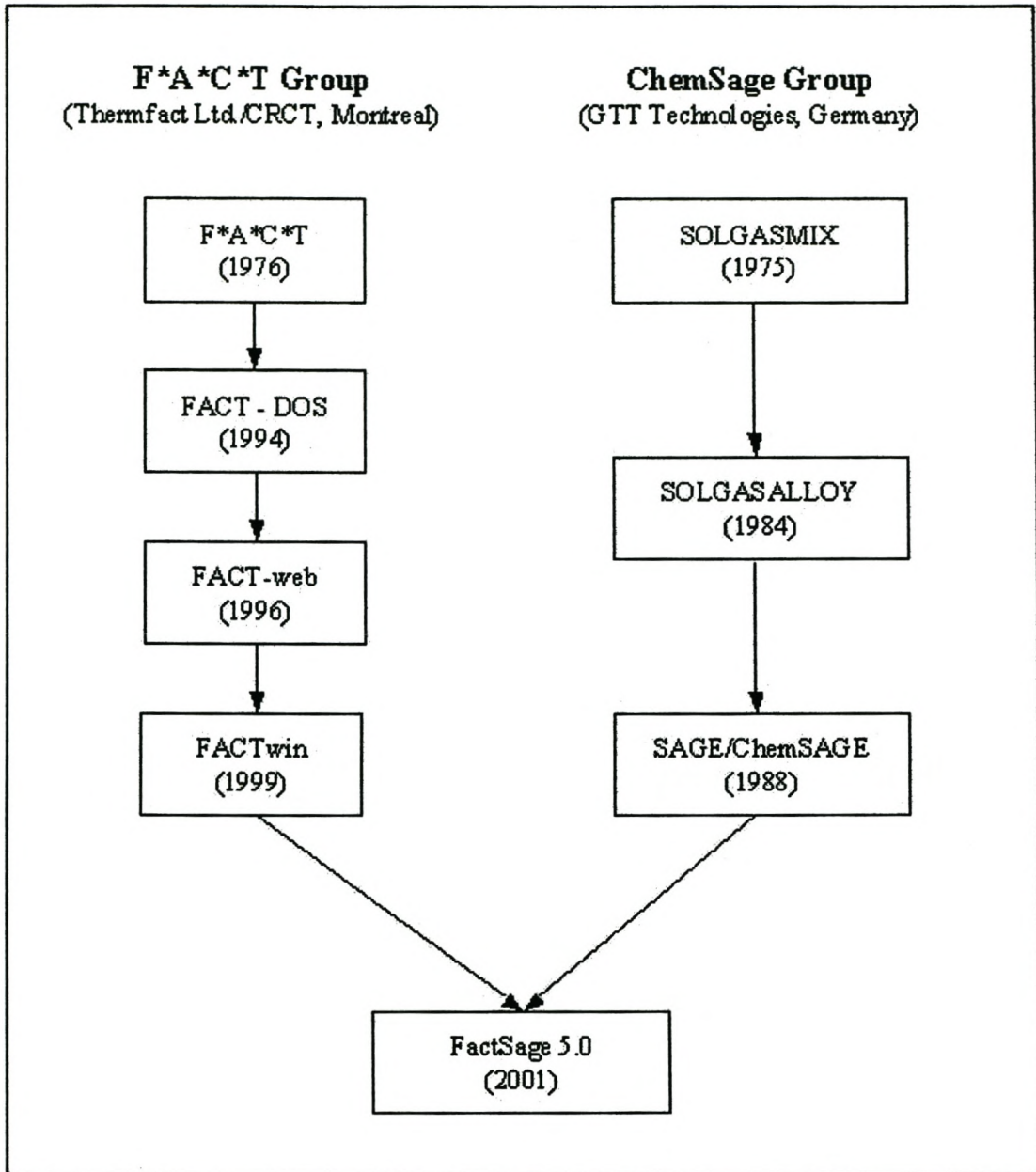


Figure 23: FactSage Timeline

4.2.4 Optimization procedure

The following general procedure was followed in using ChemSage for the optimization of the model parameters from experimental data.

- Choose the data points to be used in the optimization.

An extensive literature search was carried out for all applicable equilibrium data available. All the different datasets were critically evaluated and only the most reliable and consistent data was used. A summary of the data used and the different sources is discussed in Chapter 5.

- Enter the data points.

The data points are entered via the keyboard. ChemSage is a DOS-based program and the user is prompted for each input that is necessary to define a particular experiment/dataset. The basic information for each experiment/dataset comprises:

1. A short descriptive text
2. The number and type of independent and dependent variables
3. The phases involved and
4. The actual set of experimental values (for example the compositions and temperatures of a phase boundary)

- Set up a thermochemical data file.

This file (Newdat.dat) contains all the thermochemical data for the system, including number of phases, number of solutions, Cp equations for all phases, solution models for all solution phases and initial model parameters. The data files for this work can be found in Appendix A.

- Create a ChemSage file.

Once the experimental data input is complete, ChemSage automatically stores the data in a file (Newopt.opt) for further use.

- Run the optimization.

During this step, initial estimates as well as errors are entered for all the parameters to be optimized. During the execution of the optimization ChemSage gives intermediate output so that the user can see for which data point of which experiment the calculations are being performed at that stage. When the maximum number of iterations (also set interactively by the user) has been reached, or the solution has converged, an output table is generated which shows a direct comparison between the calculated result and the experimental input for each of the data points entered. The Newdat.dat file is also automatically modified to contain the new optimized parameters.

- Graphical inspection of the optimization.

The optimized parameters can now be used to calculate a phase diagram for easier comparison with experimental data points. This can be done in the TWO DIMENSIONAL PHASE MAPPING MODULE of ChemSage. At this point it was decided to use the graphical output of FACTSage for this purpose. The Newdat.dat file is imported into FACTSage and added to the list of databases. In the phase diagram module of FACTSage, this custom database is then used to calculate the phase diagram. FACTSage (being a Windows® based program) is much more user friendly and it is also easier to manipulate the final figure for use in a report.

5 A REVIEW OF THE DATA USED

No single source contains all the relevant data to the required degree of accuracy, consequently data from different sources were used in this optimisation.

The thermodynamic properties of TiO_2 , Ti_2O_3 and FeO (values of ΔH_{298}° , S_{298}° and $C_P(s)$) were taken from Eriksson and Pelton (1993). They performed a critical assessment of all available thermodynamic and phase diagram data and used the most accurate and reliable data in their optimisations.

TiO_2

The melting point of TiO_2 was taken to be 1857 °C from Brauer and Littke (1960). An expression for $C_P(l)$ was derived from data in the JANAF Thermochemical Tables by Eriksson and Pelton (1993) and used in this optimisation (APPENDIX C). Below 2130 K, $C_P(l)$ was set to be equal to $C_P(s)$.

Ti_2O_3

The melting temperature was taken from the JANAF Thermochemical Tables as 2115 ± 10 K. The values of ΔH_{298}° , S_{298}° , $\Delta H_{\text{fus}}^\circ$, S_{fus}° were also taken from the JANAF Thermochemical Tables. Expressions for C_P were fitted to the data in these tables by Eriksson and Pelton. Below 2115 K, $C_P(l)$ was set equal to $C_P(s)$.

FeO

The thermodynamic properties of 1 mol solid FeO were obtained from Eriksson and Pelton (1993) who added the values of the molar enthalpy, entropy and heat capacity of $\text{Fe}_{0.947}\text{O}$ to those of 0.053 mol of Fe . The melting point of 1644 K was adopted from the data of MacChesney and Muan (1961). Below 1644 K, $C_P(l)$ was set equal to $C_P(s)$.

$\text{TiO}_2 - \text{Ti}_2\text{O}_3$

The oxides from Ti_2O_3 to the 'last' of the Magnéli phases, " $\text{Ti}_{20}\text{O}_{39}$ ", were described

as line components, as was done by Waldner and Eriksson (1999). Magnéli phases are defined as Ti_nO_{2n-1} , where $n \geq 4$ and ranges to values above $n = 20$. These phases have a crystal structure derived from the rutile phase by crystallographic shear. The maximum value of n is not yet determined and therefore an arbitrary value of $n = 20$ were chosen to represent all the phases where $n > 10$. The most complete and consistent liquidus measurements are those of Brauer and Littke (1960).

TiO₂ – FeO

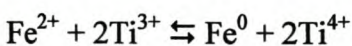
The data used in this optimisation, were the low titanium data from MacChesney and Muan (1961), which is the melting point of FeO, 1644 K and the melting point of Ulvospinel, 1670 K.

On the high titanium side, ten data points from Grau were used. Two points on the pseudo-brookite/liquid phase boundary and eight points on the Rutile/liquid boundary.

All the Cp equations from the JANAF thermochemical tables were also used.

Ti₂O₃ – FeO

In this binary system there is believed to exist a reaction-equilibrium rather than a phase-equilibrium. This equilibrium can be described by the following reaction:



From this equation it is clear that FeO and Ti₂O₃ cannot co-exist without the formation of TiO₂ and therefore the Ti₂O₃ – FeO binary only exists as part of the TiO₂ – Ti₂O₃ – FeO ternary.

TiO₂ – Ti₂O₃ – FeO

According to Nell (2000), no unique ternary compounds exist in this system.

6 MODELLING RESULTS AND DISCUSSION

6.1 The FeO – TiO₂ binary

The model parameters were optimized using a parameter optimisation routine built into the ChemSAGE package and the following results were obtained:

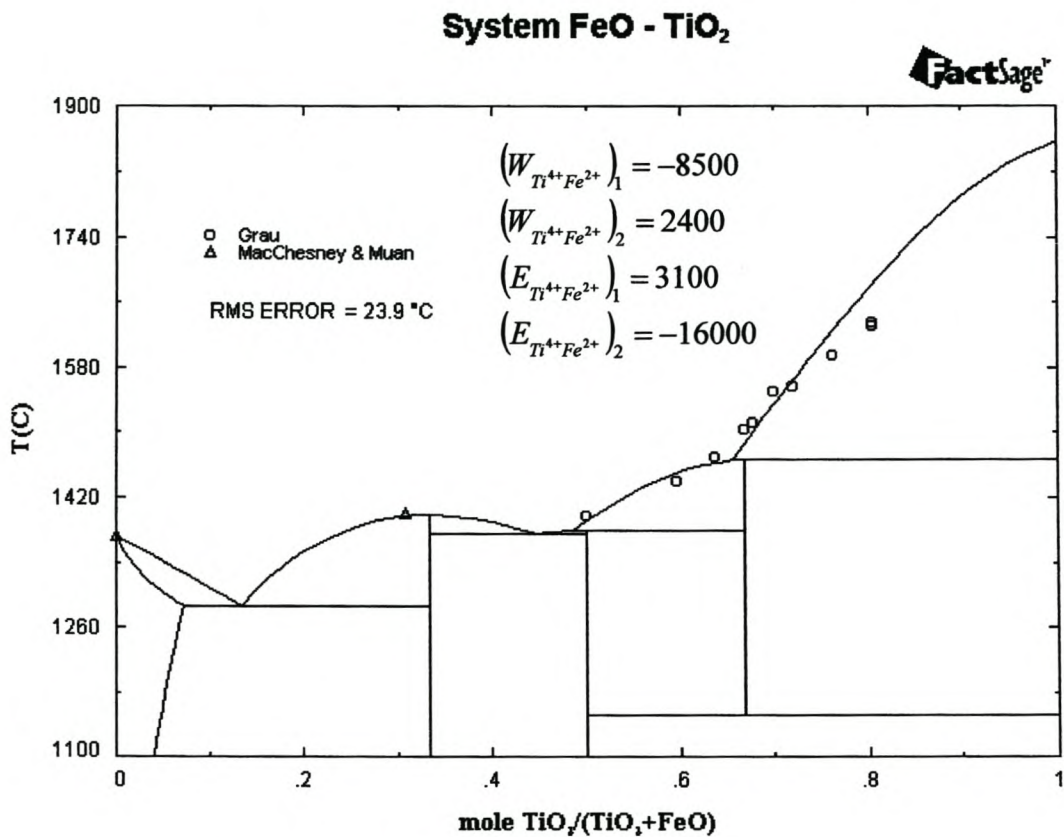


Figure 24: FeO – TiO₂ phase diagram as calculated by the cell model

Eriksson and Pelton (1993) have done the optimisation of the same system using their modified quasi-chemical model. They got a similar fit to the data (Figure 25) with also some deviation at the high titanium end. Only two quasi-chemical parameters for the liquid were required in their optimisation:

$$\omega = -12405 - 10227 Y_{TiO_2}^2 \text{ and } \eta = 0.$$

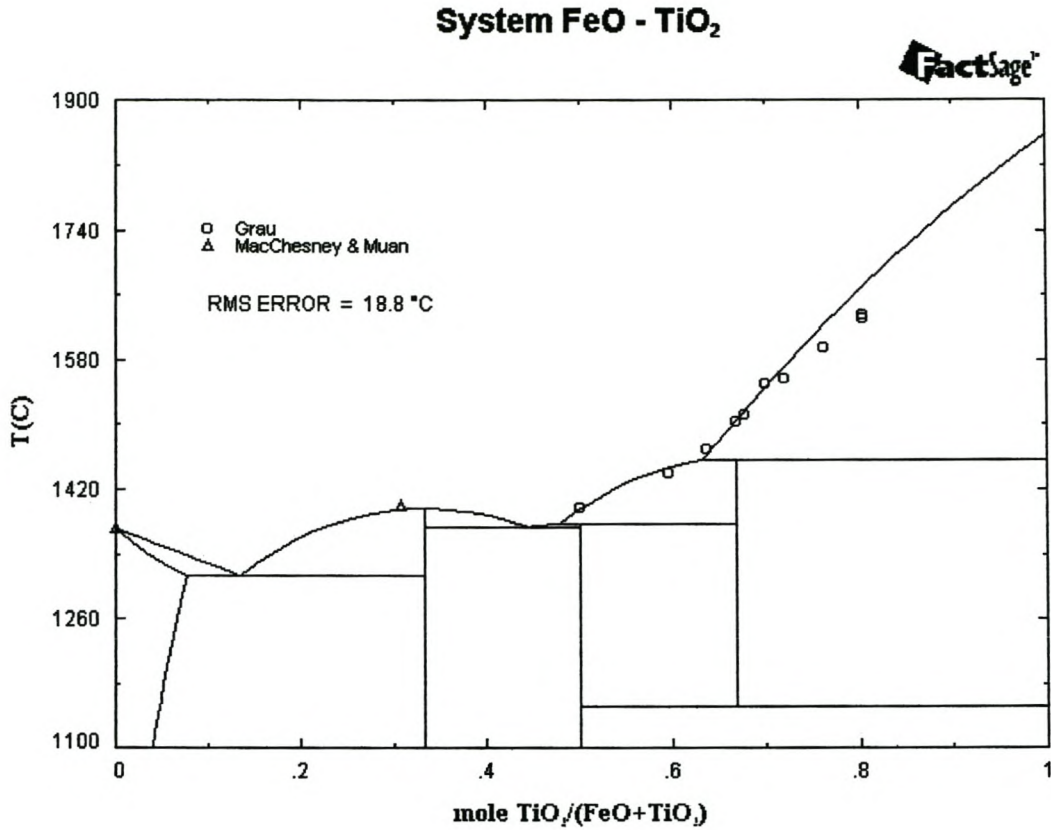


Figure 25: FeO – TiO₂ phase diagram as calculated by the modified quasi chemical model (after Eriksson and Pelton, 1993)

Both models showed some deviation at higher TiO₂ values. This could be as a result of Ti₂O₃ formation during the experiments. If this were the case, the experimental error would increase and both models would be well within the error limit. The RMS (Root Mean Square) error for the Cell model and the MQC model was 23.9 °C and 18.8 °C respectively. The experimental error is in the order of 20 °C.

6.2 The $\text{TiO}_2 - \text{Ti}_2\text{O}_3$ binary

Pelton and Eriksson (1993) again did the optimisation of the system for the MQC model. They indicated an unsure region in the low TiO_2 part of the diagram (Figure 26). The form of the curve in this region indicates a higher order expansion of the model parameters and could be interpreted as curve-fitting. The following quasi-chemical parameters were obtained from their optimisation:

$$\omega = 18913 - 175126 Y_{\text{TiO}_2} + 338410 Y_{\text{TiO}_2}^2 - 177916 Y_{\text{TiO}_2}^3 \quad 6.1$$

$$\eta = 0 \quad 6.2$$

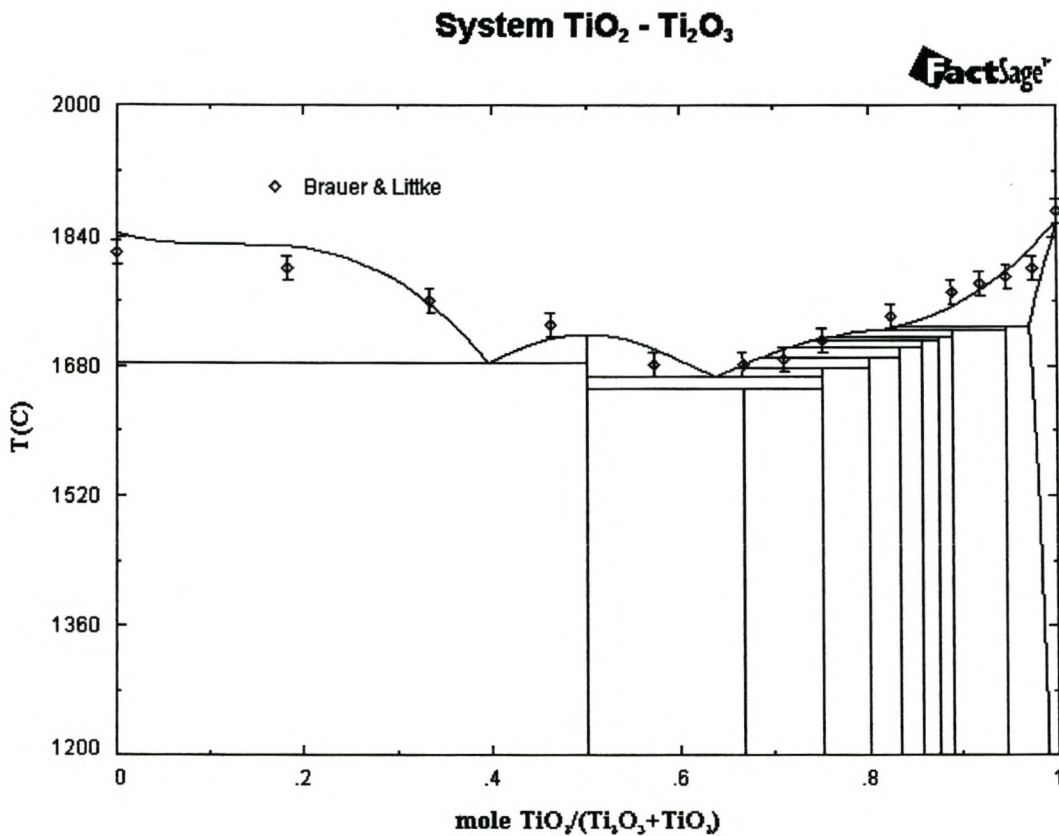


Figure 26: $\text{TiO}_2 - \text{Ti}_2\text{O}_3$ phase diagram as calculated by the modified quasi chemical model

The Cell Model (Figure 27) predicted a much wider region of Ti_3O_5 + Liquid than the MQC model and a smaller two-phase region for the Ti_2O_3 + Liquid region. The eutectic's position has shifted to 30 % TiO_2 (compared to 42 % for the MQC model). The predicted eutectic temperature shifted down from about 1680 °C to 1660 °C. The RMS (Root Mean Square) error for the Cell model and the MQC model was 32 °C and 17 °C respectively for this binary system.

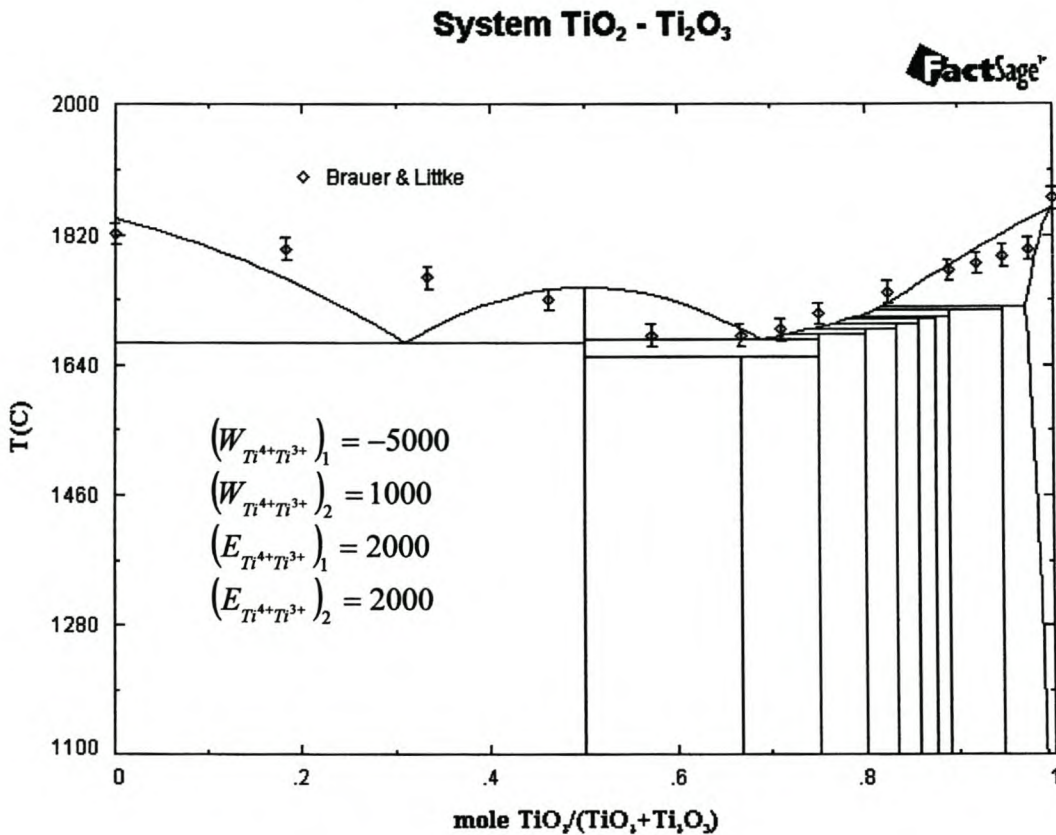


Figure 27: TiO_2 – Ti_2O_3 phase diagram as calculated by the cell model

The Cell model gave a worse fit to the data on the low TiO_2 side on the binary system. Although different starting points were used during the optimizations, it is still possible that this result is not the global minimum, but some local minimum and therefore not the optimum result. It should also be noted that only linear expansion of the binary interaction parameters were considered for the Cell model, while ω in the Modified Quasi-chemical model was expanded to a third order polynomial.

6.3 The $TiO_2 - Ti_2O_3 - FeO$ ternary

The only ternary data found in the literature was measured by Pesl and Eric (1997). They postulated the following liquidus isotherm at 1500 °C for the $TiO_2 - TiO_{1.5} - FeO$ ternary (Figure 28). They measured the liquid slag phase boundary by means of saturation experiments. The oxygen isobars within the slag phase are also indicated on the diagram.

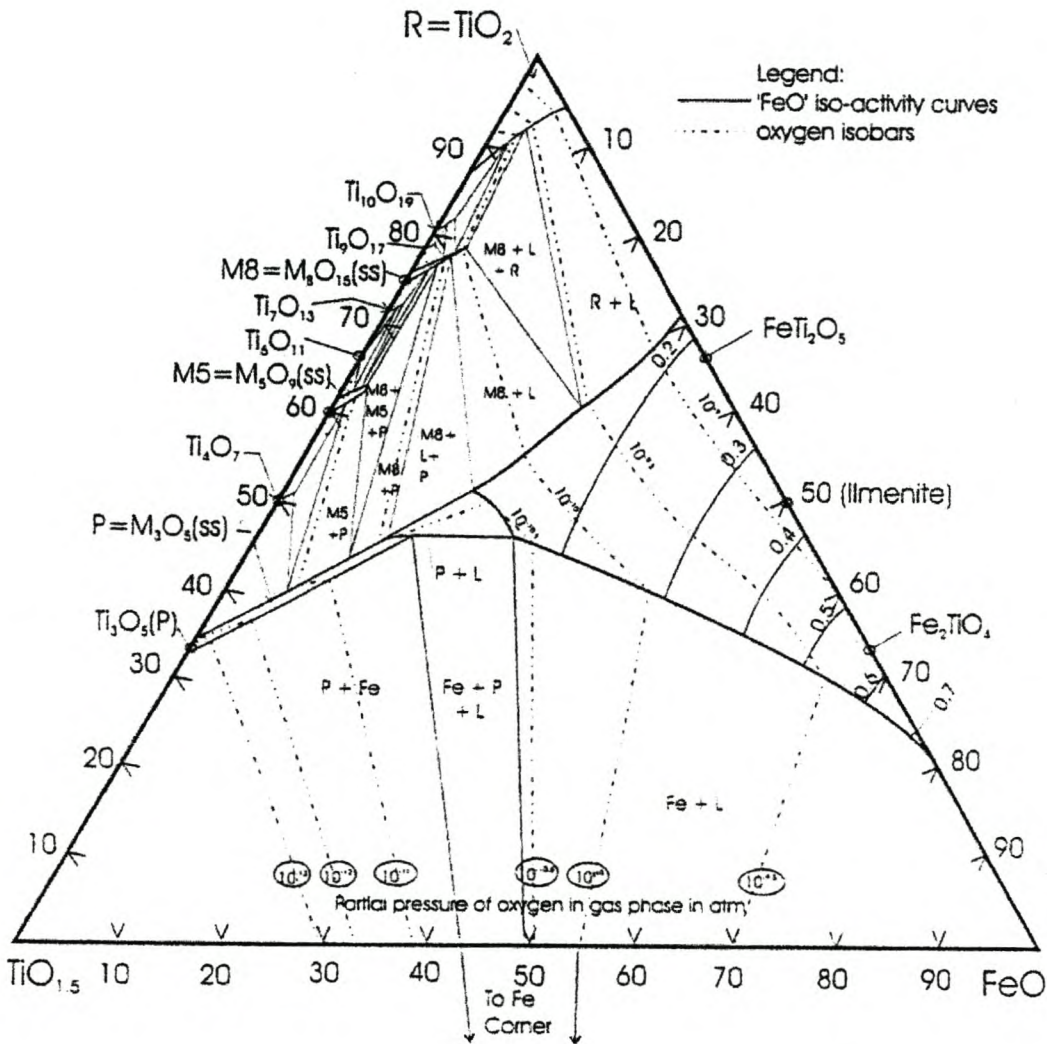


Figure 28: The liquidus isotherm at 1500 °C for the $TiO_2 - TiO_{1.5} - FeO$ ternary after Pesl and Eric (1997)

The data points measured by Pesl were plotted on a new set of co-ordinates, to be able to compare it to the diagrams produced by the software packages (Figure 29). It is more common to use Ti_2O_3 rather than $TiO_{1.5}$ used by Pesl.

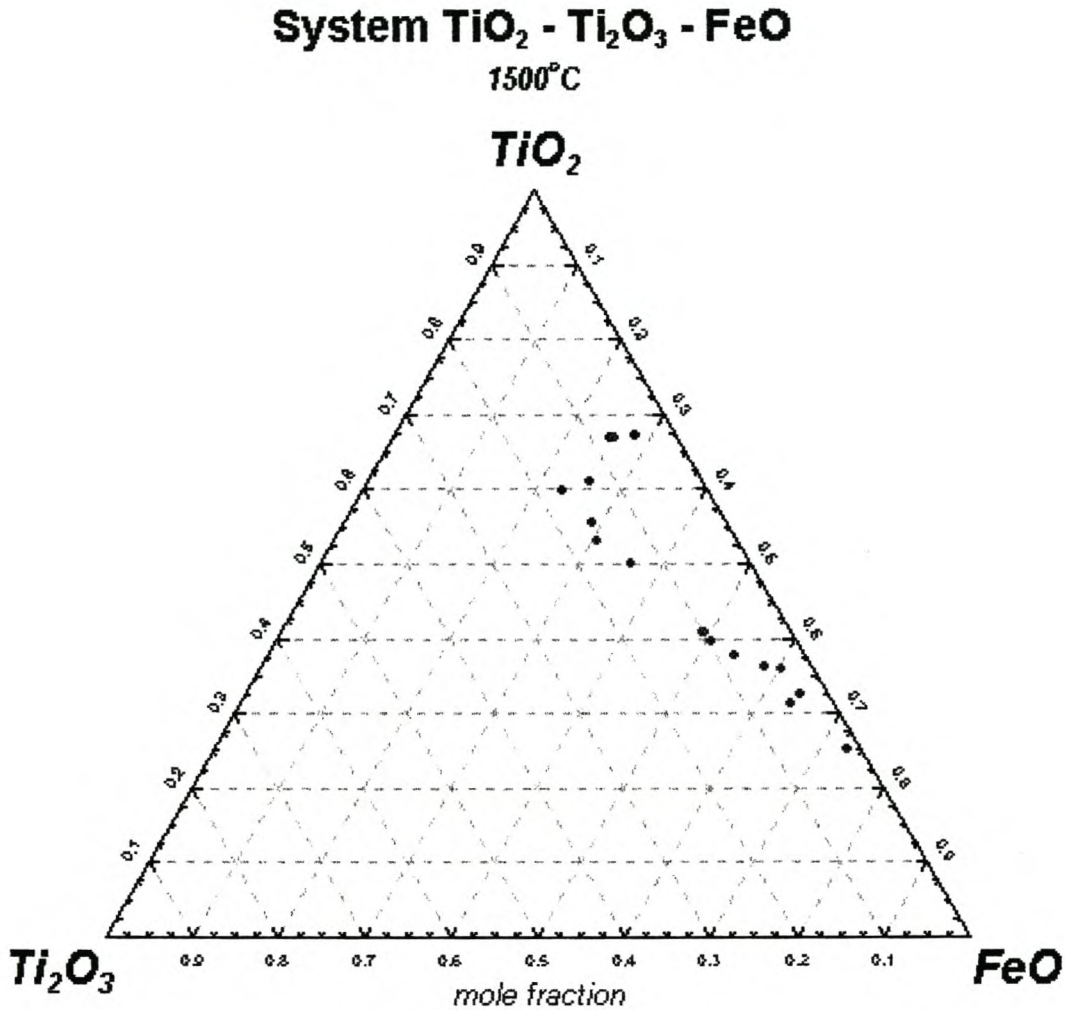


Figure 29: Data points of the 1500 isothermal section using Ti_2O_3 in stead of $TiO_{1.5}$

The liquidus isotherm for the TiO_2 - Ti_2O_3 -FeO system was calculated using the MQC model and was compared to the data points measured by Pesl and Eric (Figure 30). It can be seen that the basic form is retained, although the liquid slag region is much smaller. In this case, all the Magnéli phases, as well as the pseudo brookite phase were taken as line components and no solubility range was allowed for.

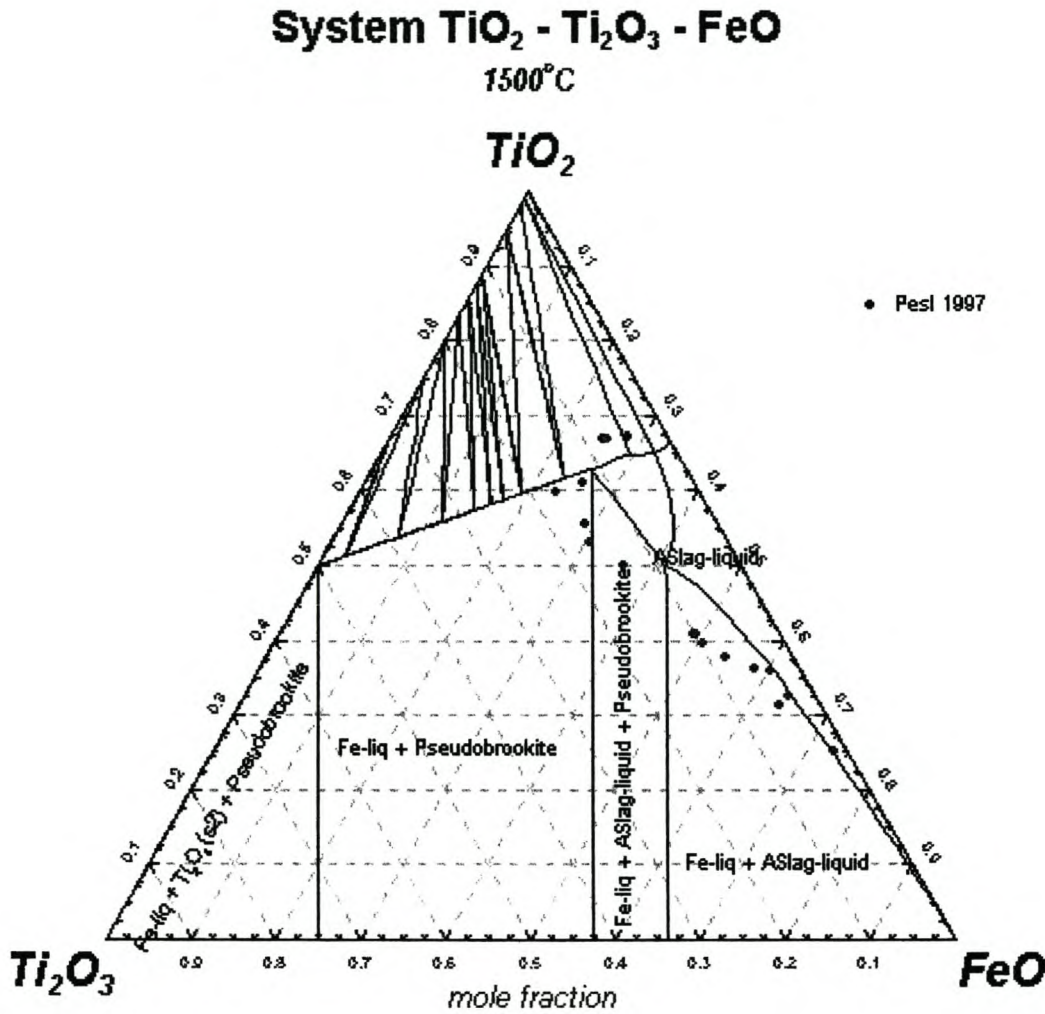


Figure 30: The liquidus isotherm at 1500 °C for the $TiO_2 - Ti_2O_3 - FeO$ ternary as calculated using the MQC model combined with the measured data points by Pesl (1997)

The remaining four interaction parameters could now be regressed by keeping the eight binary interaction parameters already optimised constant and using all the binary and ternary data points available. The interaction parameters obtained from this optimisation were then used to draw the 1500 °C isotherm for the $TiO_2 - Ti_2O_3 - FeO$ ternary system. The liquidus isotherm calculated using the MQC model (Figure 30) could now be compared directly with the same isotherm calculated using the Cell model and the newly regressed model parameters (Figure 31).

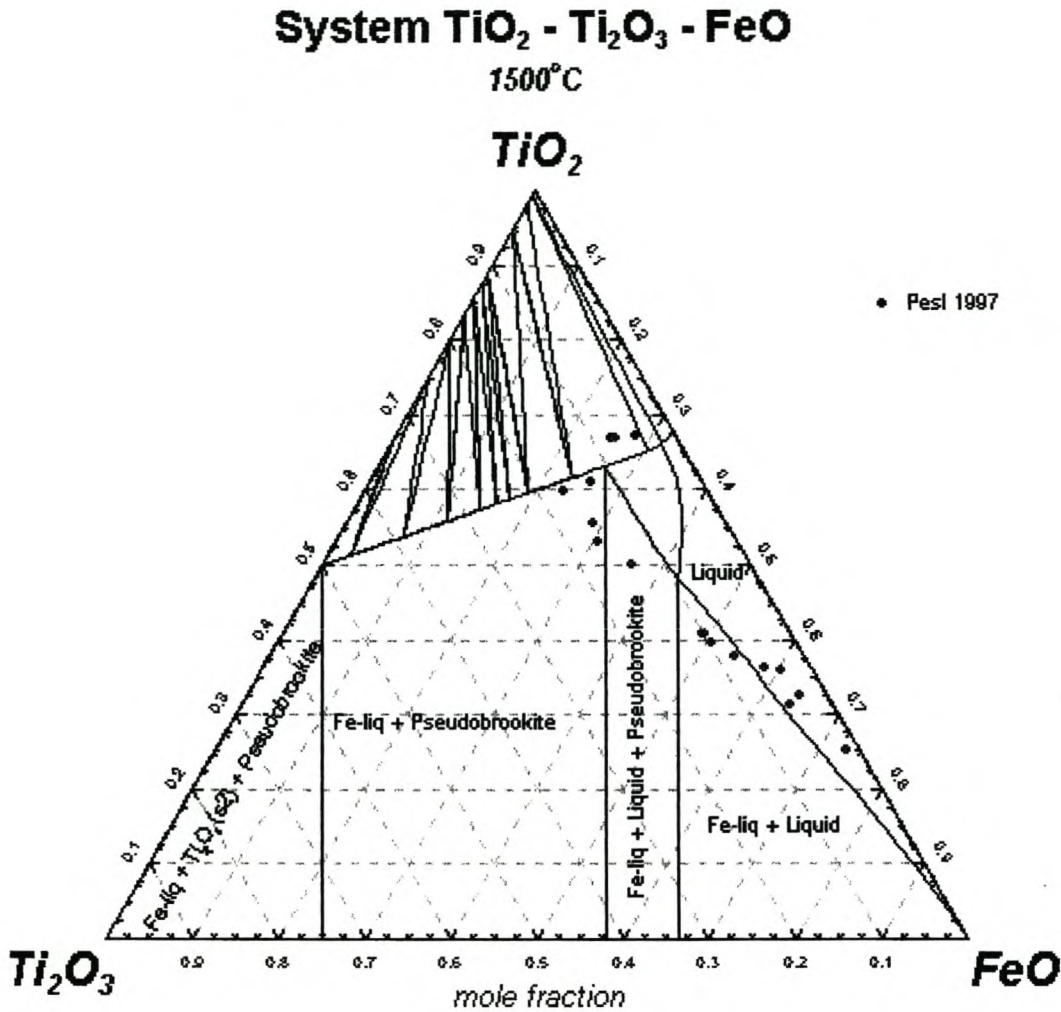


Figure 31: The liquidus isotherm at 1500 °C for the $TiO_2 - Ti_2O_3 - FeO$ ternary as calculated using the Cell model combined with the measured data points by Pesl (1997)

The two ternary phase diagrams compare very well, mostly due to the fact that the same solid solution models and pure component data were used and that all the Magnéli phases were assumed to be line components. Although the Cell model does predict a slightly larger liquid region, it must be noted that the MQC model was not optimised using the ternary data of Pesl (1997).

The optimized binary interaction parameters were then used to generate a liquidus

projection of the $\text{TiO}_2 - \text{Ti}_2\text{O}_3 - \text{FeO}$ system (Figure 32).

System $\text{TiO}_2 - \text{Ti}_2\text{O}_3 - \text{FeO}$

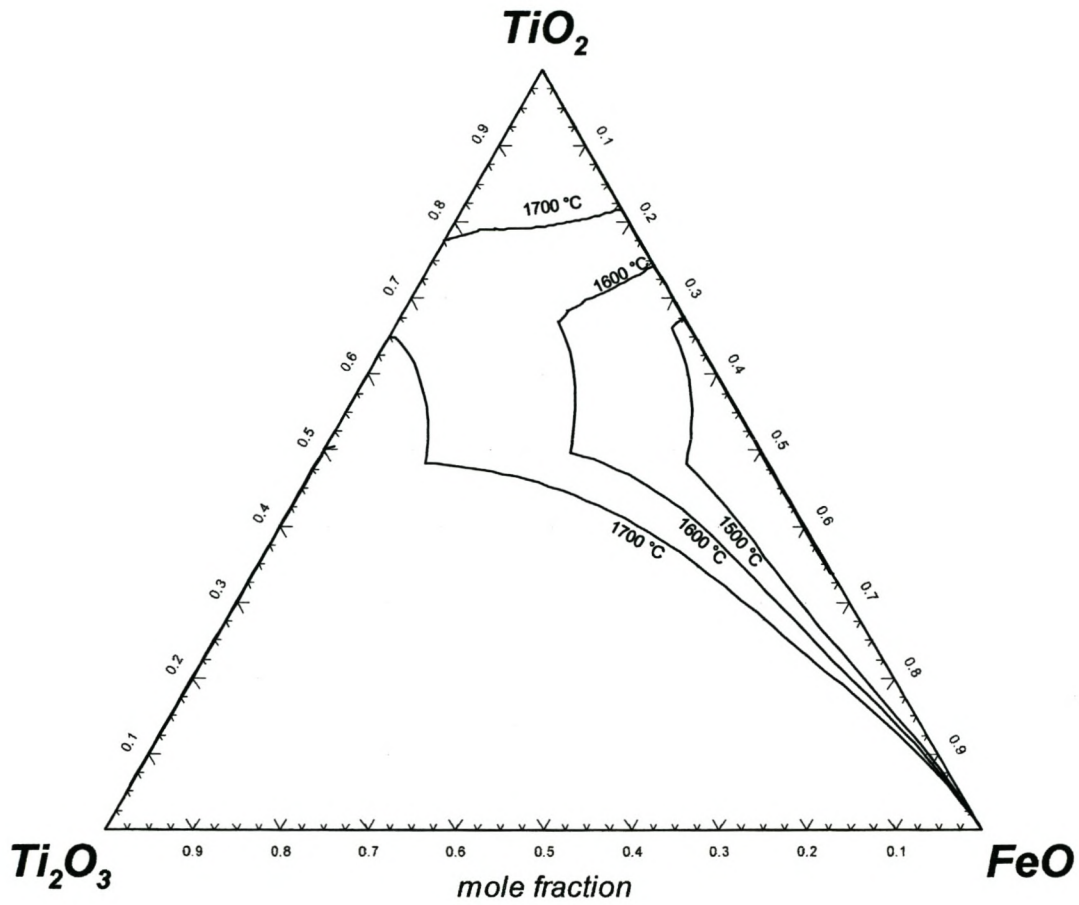


Figure 32: Liquidus projection of the $\text{TiO}_2 - \text{Ti}_2\text{O}_3 - \text{FeO}$ ternary system using the Cell model to describe the liquid slag phase.

This plot was then repeated (Figure 33) using the Modified Quasi-chemical model for the slag phase.

System TiO_2 - Ti_2O_3 - FeO

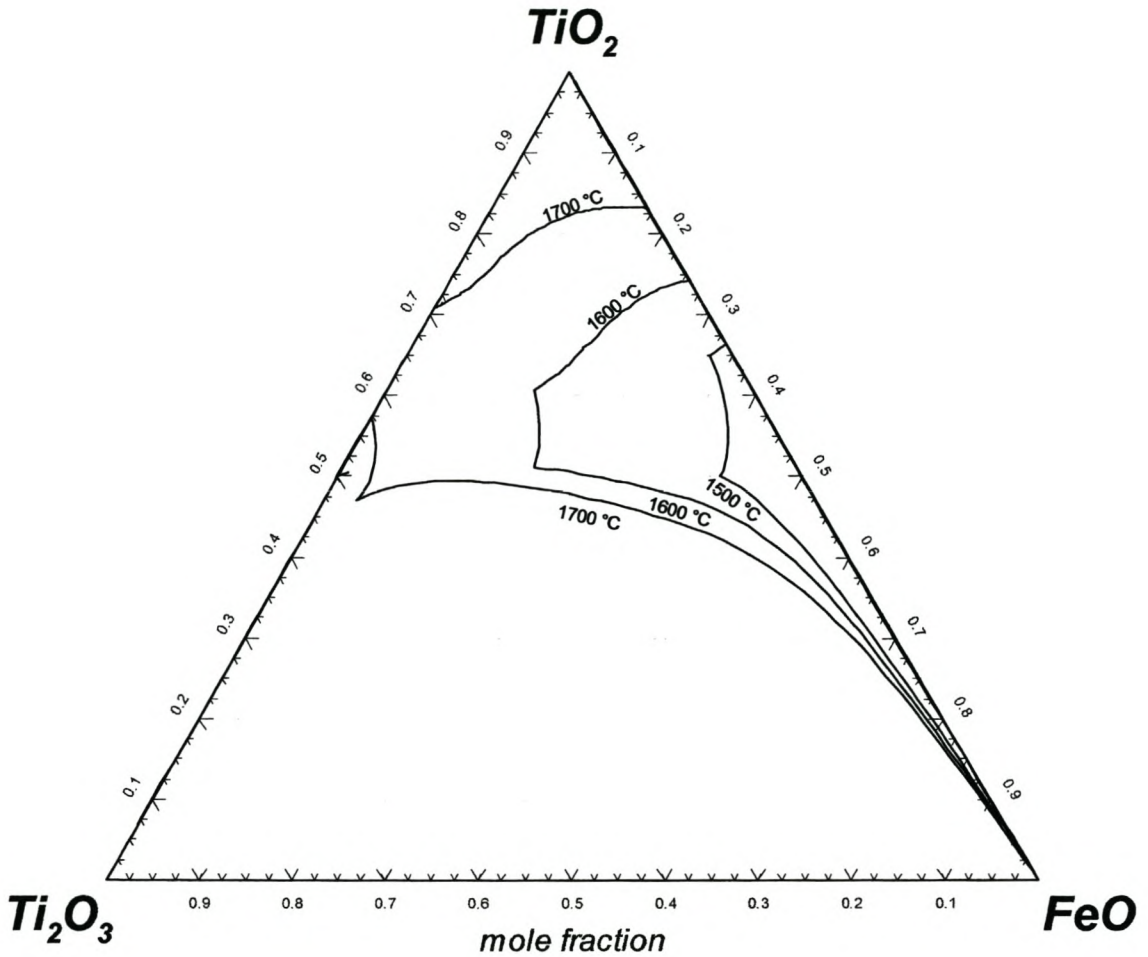


Figure 33: Liquidus projection of the TiO_2 - Ti_2O_3 - FeO system using the Modified Quasi-chemical model to describe the liquid slag phase.

Form the direct comparison between the liquidus projections using the Cell model and the Modified Quasi-chemical models (figures 32 and 33 respectively), it can be seen that the Modified Quasi-chemical model predicts a slightly bigger liquid region at higher temperatures.

7 CONCLUSIONS AND RECOMMENDATIONS

A great amount of experimental data was collected and only the most consistent and reliable liquidus data were used in the optimisations. Other thermodynamic data like partial pressures of oxygen and enthalpy of formation were not used in the optimisations and could have improved the accuracy of the results. The optimizations of this work focussed on the liquid slag solution phase and utilized the already optimized solid solution models.

The choice of the liquid state models is critical due to the long and short-range interactions of mobile ions. The quasi-chemical and cell models emerged in literature as the predominant models to model the liquid phase. These models were therefore evaluated and regressed on critically assessed data. The cell model is sometimes claimed to be more robust for higher order systems where higher order interactions are known. On the other hand, the modified quasi-chemical model is expected to perform better if all the interactions are known at all levels.

The cell model was previously only used for steelmaking slags while the modified quasi-chemical model has been optimized for a wide range of slag compositions. This work shows that results of similar accuracy were obtained. This could be expected, as these two models are mathematically very similar. The model parameters for the modified quasi-chemical model were regressed by the CRCT in Canada and incorporated in the FACT database. In this thesis, the binary interaction parameters for the cell model were regressed for two binary systems ($\text{FeO} - \text{TiO}_2$; $\text{TiO}_2 - \text{Ti}_2\text{O}_3$). The interaction parameters for the third binary subsystem, $\text{FeO} - \text{Ti}_2\text{O}_3$, were determined indirectly by using the ternary equilibrium data at 1500 °C by Pesl (1997) and keeping the already optimised binary interaction parameters constant. The $\text{FeO} - \text{TiO}_2 - \text{Ti}_2\text{O}_3$ ternary system could be described adequately using the cell model and a set of only 12 binary interaction parameters and no higher order parameters.

At the inception of the project, the emphasis was only on the FeO – TiO₂ – Ti₂O₃ system. However, it was eventually realised that this system should be studied as a subset of the Ti – Fe – O system, which lies outside the scope of an M.Sc. thesis.

In conclusion it can be said that both the cell and the modified quasi-chemical models are robust and modelled the measured data well. Table 3 Summarises the interaction parameters for the two model types.

Table 3: Summarised interaction parameters.

		<i>FeO - TiO₂</i>	<i>TiO₂ - Ti₂O₃</i>	<i>FeO - Ti₂O₃</i>
Cell Model	<i>E_{ij}</i>	<i>3100 - 16000 X_{Ti4+}</i>	<i>2000 + 2000 X_{Ti4+}</i>	<i>-10000 + 10000 X_{Ti3+}</i>
	<i>W_{ij}</i>	<i>-8500 + 2400 X_{Ti4+}</i>	<i>-5000 + 1000 X_{Ti4+}</i>	<i>- 20000</i>
MQC	<i>ω</i>	<i>- 12405 - 10227 Y²_{TiO2}</i>	<i>18913 - 175126 Y_{TiO2} + 338410 Y²_{TiO2} - 177916 Y³_{TiO2}</i>	<i>-</i>
	<i>η</i>	<i>0</i>	<i>0</i>	<i>-</i>

8 REFERENCES

- Bale, C.W and Pelton A.D.: *Metallurgical Transactions A*, Vol. 21A, 1990, pp. 1997 – 2002.
- Bale, C.W., Chartrand P., Degterov S.A., Eriksson G., Hack K., Ben Mahfoud R., Melançon J., Pelton A.D. and Petersen S.: *CALPHAD*, Vol. 26, 2002, No. 2, pp. 189-228.
- Ban-ya, S. and Shim, J.: *Canadian Metallurgical Quarterly*, vol. 21, 1982, No. 4, pp. 319 – 28.
- Ban-ya, S., Chiba, A., and Hikosaka, A.: *Tetsu-to-Hagané*, vol. 66, 1980, pp. 1484 – 93.
- Berman, R.G. and Brown, T.H.: *Contributions to Mineralogy and Petrology*, 1985, pp. 168 – 183.
- Blander, M. and Pelton, A.D.: *Geochim. Cosmochim. Acta*, vol. 51, 1987, pp. 85 – 95.
- Blander, M. and Pelton, A.D.: *Proc. 2nd International Symposium on Metallurgical Slags and Fluxes*, 1984, pp. 281 – 294.
- Blander, M. and Pelton, A.D.: *Proc. 2nd International Symposium on Metallurgical Slags and Fluxes*, 1984, pp. 295 – 304.
- Brauer, G. and Littke, W.: *Journal of Inorganic Nucl. Chem.*, Vol. 16, 1960, pp 67 to 76.
- Chang, Y. and Chen, Shuang-Lin: Thermodynamics of metallic solutions, *Advanced Physical Chemistry for Process Metallurgy*, Academic Press Ltd, 1997.

- Cho, S. and Suito, H.: *Metall. and Materials Trans. B*, vol. 25B, 1994, pp. 5 – 13.
- Darken, L.S.: *Trans. TMS-AIME*, Vol 239, 1967, pp. 90 – 96.
- de Vries, R.C. and Roy, R.: *American Ceramic Bulletin*, 1952, pp. 370 – 72.
- de Vries, R.C., Roy, R., and Osborn, E.F.: *Trans. Br. Ceram. Soc.*, vol. 53, 1954, pp. 525 – 40.
- Eriksson, G.: *Chemica Scripta*, Vol.8, 1975, pp. 100 – 103.
- Eriksson, G. and Hack, K.: *Metallurgical and Materials Transactions B*, Vol. 21B, 1990, pp. 1013 – 23.
- Eriksson, G. and Pelton, A.D.: *Metall. and Materials Trans. B*, Vol. 24B, 1993, pp. 795 – 805.
- Eriksson, G., Pelton, A.D., Woermann, E., and Ender, A.: *Ber. Bunsenges. Phys. Chem. 100*, 1996, pp. 1839 – 1849.
- Fourie, N.: *Private Communication*, 2003.
- Gaskell, D.R.: *Canadian Metallurgical Quarterly*, vol. 20, 1981, No. 1, pp. 3 – 19.
- Gaye, H. and Welfinger, J.: *Mémoires et Études Scientifiques Revue de Métallurgie – Avril 1989*.
- Gaye, H. and Welfinger, J.: *Proc. 2nd International Symposium on Metallurgical Slags and Fluxes*, 1984, pp. 357 – 75.
- Gaye, H., Lehmann, J., Matsumiya, T. and Yamada, W.: *4th International Conference on Molten Slags and Fluxes*, 1992.

Gaye, H., Lehmann, J., Riboud, P.V. and Welfinger, J.: *Mémoires et Études Scientifiques Revue de Métallurgie* – Avril 1989 , pp. 237 – 44.

Gaye, H., Lehmann, J., Rocabois, P. and Ruby-Meyer, F.: *6th International Conference on Molten Slags, Fluxes and Salts*, 2000.

Gaye, H., Riboud, P.V., and Welfringer, J.: *Ironmaking and Steelmaking*, Vol. 15, 1988, no. 6, pp. 319 – 22.

Grau, A.E.: *Canadian Metallurgical Quarterly*, Vol. 18, 1979, pp. 313 – 21.

Grey, I.E., and Merrit, R.R.: *Proc. Australia – Japan Extractive Metallurgy Simp.*, Sydney, 1980, pp. 397 – 408.

Grieve, J. and White, J.: *Journal of the Royal Technical Collage*, Vol. 4, 1939, pp 441 – 448.

Guggenheim, E.A.: The Statistical Mechanics of Regular Solutions, *Proc. Roy. Soc.*, vol. A148, 1935, pp. 304 – 312.

Guochang, J., Kuangoli, X. and Shoukun, W.: *ISIJ International*, vol. 33, 1993, no. 1, pp. 20 – 25.

Handfield, G. and Charette, G.C.: *Canadian Metallurgy Quarterly*, vol 10, 1971, no. 3, pp. 235 – 243.

Hildebrand, J.H.: *American Chemical Society Journal*, Vol 51, 1929, p. 66.

Hillert, M., Jansson, B., Sundman, B. and Agren, J.: *Metallurgical Transactions A*, Vol. 16A, 1985, pp. 261 – 266.

JANAF Thermochemical Tables, 3rd ed., *J. Phys. Chem. Ref. Data*, vol 14, 1985.

Kapoor, M.L. and Froberg, M.G.: *Chemical metallurgy of iron and steel*, 17 – 22, The Iron and Steel Institute, London, 1973.

Knacke, O., Kubaschewski, O., and Hesselmann, K.: *Thermochemical Properties of Inorganic Substances*, Second Edition, Springer-Verlag, Berlin, 1991.

Li, H. and Morris, A.E.: *Metall. and Materials Transactions B*, vol. 28B, 1997, pp. 553 – 62.

Li, H., Morris, A.E. and Robertson, D. G. C.: *Metallurgical and Materials Transactions B*, vol. 29B, 1998, pp. 1181 – 91.

Li, H., *PhD thesis*, Jan 1995, University of Tohoku, Japan.

Lin, P.L., and Pelton, A.D.: *Metallurgical Transactions B*, vol. 10B, 1979, pp. 667 – 75.

Lynch, D.C. and Bullard, D.E.: *Metall. and Materials Transactions B*, vol. 28B, 1997, pp. 447 – 53.

MacChesney, J.B. and Muan, A., *Am. Mineral.*, vol. 46, 1961, pp. 572 – 82.

Margules, M.: *Sitzungsber Wiend Akad.*, Vol 104, 1895, p 1243.

Masson, C.R.: *Proc. Roy. Soc.*, Vol A287, 1965, pp. 201 – 21.

Murray, J.L. and Wriedt, H.A., *Bulletin of Alloy Phase Diagrams*, Vol. 8, 1987, No. 2, pp. 148 – 65.

Naylor, B.F.: *American Chemical Society Journal*, Vol 68, 1946, pp. 1077 – 80.

Nell, J.: *The Journal of The South African Institute of Mining and Metallurgy*, Johannesburg, South African Institute of Mining and Metallurgy, 2000. pp. 35 – 44.

Nishimura, H. and Kimura, H.: *J. Japanese Inst. Met.*, 1956, vol. 20, pp. 524 – 27.

Pelton, A.D. and Bale, C.W.: *Metallurgical Transactions A*, 1986, vol. 17A, pp. 1211 – 15.

Pelton, A.D. and Blander, M.: *CALPHAD*, 1988, vol. 12, pp. 97 – 108.

Pelton, A.D. and Blander, M.: *Proc. AIME Symp. On Molten Salts and Slags*, 1984, pp. 281 – 94.

Pelton, A.D. and Blander, M.: *Metall. and Materials Trans. B*, 1996, vol. 17B, pp. 805 – 15.

Pelton, A.D. et al.: *Metall. and Materials Trans. B*, Vol. 31, Augustus 2000, pp. 651 – 659.

Pelton, A.D. et al.: *Metall. and Materials Trans. B*, Vol. 31, Augustus 2000, pp. 579 – 586.

Pelton, A.D., Eriksson, G., and Blander, M.: *Proc. 3rd International Symposium. on Metallurgical Slags and Fluxes*, Glasgow, UK, June (1988), p. 66.

Pelton, A.D.: *Metall. and Materials Trans. B*, 1997, vol. 28B, pp. 869 – 76.

Pelton, A.D.: Solution models, *Advanced Physical Chemistry for Process Metallurgy*, Academic Press Ltd, 1997.

Pesl, J and Eric, H.: *Minerals and Materials '96* (Conference Proceedings, 31 Jul – 2Aug. 1996, Somerset West, South Africa), Vol 1, pp. 59-66.

Pesl, J. and Eriç, R.H.: *Heavy Minerals 1997*, Johannesburg, South African Institute of Mining and Metallurgy, 1997. pp. 143 – 50.

Pesl, J. and Eriç, R.H.: *Metall. and Materials Trans. B*, 1999, vol. 30B, pp. 695 – 705.

Pesl, J.: *PhD thesis*, Jun 1997, University of the Witwatersrand, South Africa.

Pistorius, C.: *6th International Conference on Molten Slags, Fluxes and Salts*, 2000.

Sevinç, N.: *Transactions of the Institution of Mining and Metallurgy*, Sep./Dec. 1989, Vol. 98, pp. C185 – 89.

Shomate, C.H.: *American Chemical Society Journal*, 1947, Vol 69, pp. 218 – 219.

Smith, I.C. and Bell, H.B.: *Transactions Section C, Mineral Processing & Extractive Metallurgy*, 1970, vol. 79, pp. C253 - C258.

Somerville, D. and Bell, H.B.: *Canadian Metallurgical Quarterly*, 1982, vol. 21, pp. 145 – 55.

Sundman, B.: *CALPHAD*, 1991, Vol. 15, pp. 109 – 119.

Taylor, R.W.: *Journal of The American Ceramic Society*, 1963, Vol 46, pp. 276 – 279.

Temkin, M.: *Acta Phys. Chim.*, USSR, 1945, vol 20, p. 411.

Tranell, G.: *PhD thesis*, Feb 1999, University of New South Wales, Australia.

U.S. Geological Survey, *Mineral Commodity Summaries*, January 2003.

Wagner, C.: *Thermodynamics of Alloys*, Addison-Wesley, Reading, MA, 1962, p. 51.

Wahlbeck, P.G. and Gilles, P.W.: *Journal of The American Ceramic Society*, 1966, Vol. 49, No. 4, pp.180 – 83.

Waldner, P. and Eriksson, G.: *CALPHAD*, 1999, Vol. 23, No.2, pp. 189 – 218.

Yokokawa, T. and Niwa, K.: *Trans. Jap. Inst. Metals*, 1969, Vol. 10, pp. 3 and 81.

9 APPENDICES

9.1 APPENDIX A: Thermodynamic data used for calculations

Bin#1OPT.opt

C:\SAGE42\DAT\DJF1.DAT

```

4
FeO/Liq M&M
 2 1
m(FeO)
m(Rutile)
T
 2 0
Liquid
FeO
 2
Liquid
 1
1.0000000 0.0000000 1644.0000 20.000000
Ulvospinel/Liq M&M
 2 1
m(FeO)
m(Rutile)
T
 2 0
Liquid
Ulvospinel
 2
Liquid
 1
0.6930000 0.3070000 1670.0000 20.000000
Pseudobrookite/Liq Grau
 2 1
m(FeO)
m(Rutile)
T
 2 0
Liquid
Pseudobrookite
 2
Liquid
 2
0.4050000 0.5950000 1711.5000 20.000000
0.5000000 0.5000000 1669.0000 20.000000
Rutile/Liq Grau
 2 1
m(FeO)
m(Rutile)
T
 2 0
Liquid
Rutile

```

2			
Liquid			
8			
0.36400000	0.63600000	1741.5000	20.000000
0.23900000	0.76100000	1867.0000	20.000000
0.19600000	0.80400000	1906.0000	20.000000
0.28100000	0.71900000	1828.3000	20.000000
0.32300000	0.67700000	1783.0000	20.000000
0.30200000	0.69800000	1820.5000	20.000000
0.19600000	0.80400000	1902.0000	20.000000
0.33300000	0.66700000	1775.0000	20.000000

Bin#2OPT.opt

C:\SAGE42\DAT\DJF2.DAT

```

2
Liq/Ti2O3 Brauer&Littke
2 1
m(TiO2)
m(Ti2O3)
T
2 0
Liquid
Ti2O3
2
Liquid
3
0.000000000 1.000000000 2088.0000 15.000000
0.181818182 0.818181818 2068.0000 15.000000
0.333333333 0.666666667 2028.0000 15.000000
Liq/TiO2 Brauer&Littke
2 1
m(TiO2)
m(Ti2O3)
T
2 0
Liquid
TiO2
2
Liquid
6
0.750000000 0.250000000 1983.0000 15.000000
0.823529412 0.176470588 2013.0000 15.000000
0.888888889 0.111111111 2043.0000 15.000000
0.918918919 0.081081081 2053.0000 15.000000
0.947368421 0.052631579 2063.0000 15.000000
0.974358974 0.025641026 2073.0000 15.000000

```

TernaryOPT.opt

C:\SAGE42\DAT\TER.DAT

```

8
FeO/Liq M&M
 3 1
m(TiO2)
m(Ti2O3)
m(FeO)
T
 2 0
Liquid
FeO
 2
Liquid
 1
0.0000000 0.0000000 1.0000000 1644.0000 20.000000
Ulvospinel/Liq M&M
 3 1
m(TiO2)
m(Ti2O3)
m(FeO)
T
 2 0
Liquid
Ulvospinel
 2
Liquid
 1
0.3070000 0.0000000 0.6930000 1670.0000 20.000000
Pseudobrookite/Liq Grau
 3 1
m(TiO2)
m(Ti2O3)
m(FeO)
T
 2 0
Liquid
Pseudobrookite
 2
Liquid
 2
0.5950000 0.0000000 0.4050000 1711.5000 20.000000
0.5000000 0.0000000 0.5000000 1669.0000 20.000000
Rutile/Liq Grau
 3 1
m(TiO2)
m(Ti2O3)
m(FeO)
T
 2 0
Liquid
Rutile
 2
Liquid
 8
0.6360000 0.0000000 0.3640000 1741.5000 20.000000
0.7610000 0.0000000 0.2390000 1867.0000 20.000000

```

0.80400000	0.00000000	0.19600000	1906.0000	20.000000
0.71900000	0.00000000	0.28100000	1828.3000	20.000000
0.67700000	0.00000000	0.32300000	1783.0000	20.000000
0.69800000	0.00000000	0.30200000	1820.5000	20.000000
0.80400000	0.00000000	0.19600000	1902.0000	20.000000
0.66700000	0.00000000	0.33300000	1775.0000	20.000000

Liq/Ti2O3 Brauer&Littke

3 1
m(TiO2)
m(Ti2O3)
m(FeO)
T

2 0
Liquid
Ti2O3

2
Liquid
4

0.00000000	1.00000000	0.00000000	2088.0000	20.000000
0.18181818	0.81818182	0.00000000	2068.0000	20.000000
0.33333333	0.66666667	0.00000000	2028.0000	20.000000
0.46153846	0.53846154	0.00000000	2003.0000	20.000000

Liq/Rutile Brauer&Littke

3 1
m(TiO2)
m(Ti2O3)
m(FeO)
T

2 0
Liquid
Rutile

2
Liquid
6

0.75000000	0.25000000	0.00000000	1983.0000	20.000000
0.82352941	0.17647059	0.00000000	2013.0000	20.000000
0.88888889	0.11111111	0.00000000	2043.0000	20.000000
0.91891892	0.81081081E-01	0.00000000	2053.0000	20.000000
0.94736842	0.52631579E-01	0.00000000	2063.0000	20.000000
0.97435897	0.25641026E-01	0.00000000	2073.0000	20.000000

Rutile/Liq Pesl

3 1
m(TiO2)
m(Ti2O3)
m(FeO)
T

2 0
Liquid
Rutile

2
Liquid
3

0.62210000	0.14170000	0.23620000	1773.0000	20.000000
0.64370000	0.88100000E-01	0.26820000	1773.0000	20.000000
0.62200000	0.13660000	0.24140000	1773.0000	20.000000

M8015/Liq Pesl

3 1
m(TiO2)
m(Ti2O3)

m(FeO)

T
2 0

Liquid

Ti8015

2

Liquid

2

0.54130000	0.22970000	0.22900000	1773.0000	20.000000
0.51170000	0.28950000	0.19890000	1773.0000	20.000000

9.2 APPENDIX B: ChemSAGE datafiles used in the optimisations.

DJF1.dat

```

FeO-TiO2
 3 3 0 2 2 5
Ti      47.8670      Fe      55.8450      O      15.9994
 6 1 2 3 4 5 6
 2 1 2
Liquid
GAYE
TiO2
 10 2 1.0 0.0 2.0
-898725.99 72.067513
 2130.0000 77.837621 0.00000000 0.00000000 -3367841.0
-48852.840
 2 0.00000000 -0.50 0.40294067E+09 -3.00
 3000.0000 100.41600 0.00000000 0.00000000 0.00000000
 2 0.00000000 -0.50 0.00000000 -3.00
 1.00000 1 2.00000 1
FeO
 10 2 0.0 1.0 1.0
-234643.15 78.465531
 1644.0000 -18.024474 0.30608060E-01 0.00000000 -2533300.0
-13117.920
 2 1500.9000 -0.50 0.00000000 -3.00
 3000.0000 68.199200 0.00000000 0.00000000 0.00000000
 2 0.00000000 -0.50 0.00000000 -3.00
 1.00000 2 1.00000 1
 1
 1 2 0 -8500.0000 0.00000000
 1
 1 2 1 2400.0000 0.00000000
 2
 1 2 0 3100.0000 0.00000000
 2
 1 2 1 -16000.000 0.00000000
 0
FeO(ss)
RKMP
TiO2
 10 2 1.0 0.0 2.0
-944749.99 50.460007
 2130.0000 77.837621 0.00000000 0.00000000 -3367841.0
-48852.840
 2 0.00000000 -0.50 0.40294067E+09 -3.00
 3000.0000 100.41600 0.00000000 0.00000000 0.00000000
 2 0.00000000 -0.50 0.00000000 -3.00
FeO
 10 2 0.0 1.0 1.0
-265832.24 59.495798
 1644.0000 -18.024474 0.30608060E-01 0.00000000 -2533300.0
-13117.920
 2 1500.9000 -0.50 0.00000000 -3.00
 2000.0000 68.199200 0.00000000 0.00000000 0.00000000

```

```

2 0.00000000    -0.50 0.00000000    -3.00
  2
  1  2  1
0.00000000    0.00000000
  0
FeO
  10  2  0.0    1.0  1.0
-265832.24    59.495798
  1644.0000   -18.024474    0.30608060E-01 0.00000000    -2533300.0
-13117.920
2  1500.9000   -0.50 0.00000000    -3.00
  2000.0000    68.199200    0.00000000    0.00000000    0.00000000
2  1500.9000   -0.50 0.00000000    -3.00
Ulvospinel
  10  1  1.0    2.0  4.0
-1515609.7    168.87001
  2000.0000    249.63000    0.00000000    0.00000000    0.00000000
2 -1817.4000   -0.50 -54530001.    -3.00
Ilmenite
  10  1  1.0    1.0  3.0
-1233142.2    108.62751
  1650.0000    149.99950    0.00000000    0.00000000    -3323694.0
2 -441.62199  -0.50 0.34815104E+09 -3.00
Pseudobrookite
  10  1  2.0    1.0  5.0
-2152814.4    176.56940
  1728.0000    247.15400    0.00000000    0.00000000    -4502760.1
2 -1026.1500  -0.50 0.45551601E+09 -3.00
Rutile
  10  2  1.0    0.0  2.0
-944749.99    50.460007
  2130.0000    77.837621    0.00000000    0.00000000    -3367841.0
-48852.840
2 0.00000000   -0.50 0.40294067E+09 -3.00
  3000.0000    100.41600    0.00000000    0.00000000    0.00000000
2 0.00000000   -0.50 0.00000000    -3.00

```

DJF2.dat

```

Ti3Ti4
  2  3  0  2  2  11
Ti
  47.8670 15.9994
  6  1  2  3  4  5  6
  2  1  2
Liquid
GAYE
TiO2
  10  2  1.0  2.0
-898725.99 72.065130
 2130.0000 77.837621 0.00000000 0.00000000 -3367841.0
-48852.840
 2 0.40294067E+09 -3.00 0.00000000 -0.50
 3000.0000 100.41600 0.00000000 0.00000000 0.00000000
 2 0.00000000 -3.00 0.00000000 -0.50
 1.00000 1 2.00000 1
Ti2O3
  10  2  2.0  3.0
-1414375.3 130.17449
 2115.0000 169.96111 0.00000000 0.00000000 1609648.9
-23358.500
 2 -.15655210E+10 -3.00 -750.21869 -0.50
 2500.0000 156.90000 0.00000000 0.00000000 0.00000000
 2 0.00000000 -3.00 0.00000000 -0.50
 2.00000 2 3.00000 1
 1
 1  2  0 -5000.0000 0.00000000
 1
 1  2  1 1000.0000 0.00000000
 2
 1  2  0 2000.0000 0.00000000
 2
 1  2  1 2000.0000 0.00000000
 0
Rutile
RKMP
TiO2
  10  2  1.0  2.0
-944749.99 50.460007
 2130.0000 77.837621 0.00000000 0.00000000 -3367841.0
-48852.840
 2 0.40294067E+09 -3.00 0.00000000 -0.50
 3000.0000 100.41600 0.00000000 0.00000000 0.00000000
 2 0.00000000 -3.00 0.00000000 -0.50
TiO1.5
  10  3  1.0  1.5000
-760442.0 38.626487
 470.00000 730.23381 0.00000000 0.00000000 18808385.
 185.26
 2 0.00000000 -3.00 -14604.866 -0.50
 2115.0000 169.96111 0.00000000 0.00000000 1609648.9
-11679.3
 2 -.15655210E+10 -3.00 -750.21869 -0.50
 2500.0000 156.90000 0.00000000 0.00000000 0.00000000
 2 0.00000000 -3.00 0.00000000 -0.50
 2
 1  2  1

```

```

0.00000000      0.00000000
0
TiO2
 10  2   1.0   2.0
-944749.99      50.460007
 2130.0000      77.837621      0.00000000      0.00000000      -3367841.0
-48852.840
2 0.40294067E+09 -3.00 0.00000000      -0.50
 3000.0000      100.41600      0.00000000      0.00000000      0.00000000
2 0.00000000      -3.00 0.00000000      -0.50
Ti2O3
 10  3   2.0   3.0
-1520884.0      77.252974
 470.00000      730.23381      0.00000000      0.00000000      18808385.
 370.52000
2 0.00000000      -3.00 -14604.866      -0.50
 2115.0000      169.96111      0.00000000      0.00000000      1609648.9
-23358.600
2 -.15655210E+10 -3.00 -750.21869      -0.50
 2500.0000      156.90000      0.00000000      0.00000000      0.00000000
2 0.00000000      -3.00 0.00000000      -0.50
Ti3O5
 10  2   3.0   5.0
-2465422.0      129.36905
 450.00000      278.89989      0.00000000      0.00000000      7136016.6
-220.45000
2 -.21196005E+10 -3.00 -2149.4709      -0.50
 1991.0000      158.99208      0.50207946E-01 0.00000000      0.00000000
2 0.00000000      -3.00 0.00000000      -0.50
Ti4O7
 10  1   4.0   7.0
-3414316.9      197.44358
 2000.0000      364.36711      0.00000000      0.00000000      -2519517.2
2 -.14454823E+09 -3.00 -2110.8923      -0.50
Ti5O9
 10  1   5.0   9.0
-4360918.3      248.95446
 2000.0000      442.20474      0.00000000      0.00000000      -5887358.3
2 0.25839244E+09 -3.00 -2110.8923      -0.50
Ti6O11
 10  1   6.0  11.0
-5306479.3      300.50153
 2000.0000      520.04233      0.00000000      0.00000000      -9255199.2
2 0.66133312E+09 -3.00 -2110.8923      -0.50
Ti7O13
 10  1   7.0  13.0
-6251588.9      351.91071
 2000.0000      597.87996      0.00000000      0.00000000      -12623040.
2 0.10642738E+10 -3.00 -2110.8923      -0.50
Ti8O15
 10  1   8.0  15.0
-7196482.5      403.17028
 2000.0000      675.71759      0.00000000      0.00000000      -15990881.
2 0.14672145E+10 -3.00 -2110.8923      -0.50
Ti9O17
 10  1   9.0  17.0
-8141241.8      454.36516
 2000.0000      753.55522      0.00000000      0.00000000      -19358722.
2 0.18701551E+10 -3.00 2110.8923      -0.50

```


Ti10019

10	1	10.0	19.0				
-9085912.9			505.51531				
2000.0000			831.39285	0.00000000	0.00000000		-22726564.
2	0.22730958E+10	-3.00	-2110.8923		-0.50		

"Ti20039"

10	1	20.0	39.0				
-18533038.			1015.3802				
2000.0000			1609.7690	0.00000000	0.00000000		-56404973.
2	0.63025027E+10	-3.00	2110.8923		-0.50		

TER.dat

```

TiO2 - Ti2O3 - FeO (GAYE) DJF 2001
 3 5 0 3 3 3 3 15
Ti
 47.8670
6 1 2 3 4 5 6
2 1 2
Fe
55.8450
O
15.9994

Liquid
GAYE
TiO2
10 2 1.0 0.0 2.0
-898726.00 72.067510
2130.0000 77.837620 0.00000000 0.00000000 -3367841.0
-48852.840
2 0.40294070E+09 -3.00 0.00000000 -0.50
3000.0000 100.41600 0.00000000 0.00000000 0.00000000
2 0.00000000 -3.00 0.00000000 -0.50
1.00000 1 2.00000 1

Ti2O3
10 2 2.0 0.0 3.0
-1414375.3 130.17449
2115.0000 169.96111 0.00000000 0.00000000 1609648.9
-23358.500
2 -.15655210E+10 -3.00 -750.21869 -0.50
2500.0000 156.90000 0.00000000 0.00000000 0.00000000
2 0.00000000 -3.00 0.00000000 -0.50
2.00000 2 3.00000 1

FeO
10 2 0.0 1.0 1.0
-234643.15 78.465531
1644.0000 -18.024474 0.30608060E-01 0.00000000 -2533300.0
-13117.920
2 0.00000000 -3.00 1500.9000 -0.50
3000.0000 68.199200 0.00000000 0.00000000 0.00000000
2 0.00000000 -3.00 0.00000000 -0.50
1.00000 3 1.00000 1

1
1 2 0 -5000.000 0.00000000
1
1 2 1 1000.000 0.00000000
1
1 3 0 -8500.000 0.00000000
1
1 3 1 2400.000 0.00000000
1
2 3 0 -10000.00 0.00000000
1
2 3 1 10000.00 0.00000000
2
1 2 0 2000.000 0.00000000
2
1 2 1 2000.000 0.00000000
2
1 3 0 3100.000 0.00000000
2
1 3 1 -16000.00 0.00000000
2
2 3 0 -20000.00 0.00000000
    
```

```

2
2 3 1 0000.000 0.00000000
0
FeO (ss)
QKTO
TiO2
10 2 1.0 0.0 2.0
-944749.99 50.460007
2130.0000 77.837621 0.00000000 0.00000000 -3367841.0
-48852.840
2 0.40294067E+09 -3.00 0.00000000 -0.50
3000.0000 100.41600 0.00000000 0.00000000 0.00000000
2 0.00000000 -3.00 0.00000000 -0.50
1.00000 1
Ti2O3
10 1 2.0 0.0 3.0
-1519375.4 80.529126
2115.0000 169.96111 0.00000000 0.00000000 1609648.9
2 -.15655210E+10 -3.00 -750.21869 -0.50
1.00000 1
FeO
10 2 0.0 1.0 1.0
-265832.24 59.495798
1644.0000 -18.024474 0.30608060E-01 0.00000000 -2533300.0
-13117.920
2 0.00000000 -3.00 1500.9000 -0.50
2000.0000 68.199200 0.00000000 0.00000000 0.00000000
2 0.00000000 -3.00 0.00000000 -0.50
1.00000 1
2
1 3 1 0 6171.3740 0.00000000
0
Rutile
QKTO
TiO2
10 1 1.0 0.0 2.0
-944749.99 50.460007
2130.0000 77.837621 0.00000000 0.00000000 -3367841.0
2 0.40294067E+09 -3.00 0.00000000 -0.50
1.00000 1
Ti2O3
10 1 2.0 0.0 3.0
-1519375.4 80.529126
2115.0000 169.96111 0.00000000 0.00000000 1609648.9
2 -.15655210E+10 -3.00 -750.21869 -0.50
1.00000 1
FeO
10 2 0.0 1.0 1.0
-265832.24 59.495798
1644.0000 -18.024474 0.30608060E-01 0.00000000 -2533300.0
-13117.920
2 0.00000000 -3.00 1500.9000 -0.50
2000.0000 68.199200 0.00000000 0.00000000 0.00000000
2 0.00000000 -3.00 0.00000000 -0.50
1.00000 1
2
1 2 0 1 27785.930 0.00000000
0

```

FeLQ

WAGN

Fe

10 1 0.0 1.0 0.0
 406173.01 172.850821
 6000.0000 27.062112 0.00000000 0.00000000 0.00000000
 2 0.00000000 -3.00 0.00000000 -0.50

Ti

10 3 1.0 0.0 0.0
 -265832.24 38.11187
 1166.0000 22.191346 0.00604957920 0.00000000 0.00000000
 -1404.820
 2 0.00000000 -3.00 0.00000000 -0.50
 1939.0000 31.232443 -0.00940355216 0.000000661637959 -24586.381
 -93310.910
 2 0.00000000 -3.00 0.00000000 -0.50
 2500.0000 -32.545778 0.0294202209 0.00000000 50260428.00
 2 0.00000000 -3.00 0.00000000 -0.50

O

10 2 0.0 0.0 1.0
 249173.00 160.948556
 2200.0000 19.964968 0.000263898925 -0.0000000369535916 58654.878
 19725.710
 2 0.00000000 -3.00 20.952464 -0.50
 6000.0000 38.050669 0.00000000 0.00000000 -24241478.000
 2 70811.4360 -1.00 -2082.7134 -0.50

2
 1 1 15733.000 0.000
 2
 3 3 -115309.00 50.790985
 2
 3 1 -413933.00 0.000
 2
 3 0 -14086.000 2.947999
 2
 1 0 -6593.0000 -0.93300015

FeO

10 2 0.0 1.0 1.0
 -265832.24 59.495798
 1644.0000 -18.024474 0.30608060E-01 0.00000000 -2533300.0
 -13117.920
 2 0.00000000 -3.00 1500.9000 -0.50
 2000.0000 68.199200 0.00000000 0.00000000 0.00000000
 2 0.00000000 -3.00 0.00000000 -0.50

Ulvospinel

10 1 1.0 2.0 4.0
 -1515609.7 168.87001
 2000.0000 249.63000 0.00000000 0.00000000 0.00000000
 2 -54530001. -3.00 -1817.4000 -0.50

Ilmenite

10 1 1.0 1.0 3.0
 -1233142.2 108.62751
 1650.0000 149.99950 0.00000000 0.00000000 -3323694.0
 2 0.34815104E+09 -3.00 -441.62199 -0.50

Pseudobrookite

10 1 2.0 1.0 5.0
 -2152814.4 176.56940
 1728.0000 247.15400 0.00000000 0.00000000 -4502760.1

```

2 0.45551601E+09 -3.00 -1026.1500 -0.50
TiO2
10 1 1.0 0.0 2.0
-944749.99 50.460007
2130.0000 77.837621 0.00000000 0.00000000 -3367841.0
2 0.40294067E+09 -3.00 0.00000000 -0.50
Ti2O3
10 1 2.0 0.0 3.0
-1519375.4 80.529126
2115.0000 169.96111 0.00000000 0.00000000 1609648.9
2 -.15655210E+10 -3.00 -750.21869 -0.50
Ti3O5
10 1 3.0 0.0 5.0
-2452465.0 157.61698
1991.0000 158.99208 0.50207946E-01 0.00000000 0.00000000
2 0.00000000 -3.00 0.00000000 -0.50
Ti4O7
10 1 4.0 0.0 7.0
-3414316.9 197.44358
2000.0000 364.36711 0.00000000 0.00000000 -2519517.2
2 -.14454823E+09 -3.00 -2110.8923 -0.50
Ti5O9
10 1 5.0 0.0 9.0
-4360918.3 248.95446
2000.0000 442.20474 0.00000000 0.00000000 -5887358.3
2 0.25839244E+09 -3.00 -2110.8923 -0.50
Ti6O11
10 1 6.0 0.0 11.0
-5306479.3 300.50153
1963.0000 520.04235 0.00000000 0.00000000 -9255199.0
2 0.66133310E+09 -3.00 -2110.8923 -0.50
Ti8O15
10 1 8.0 0.0 15.0
-7196482.4 403.17028
1983.0000 675.71759 0.00000000 0.00000000 -15990881.
2 0.14672144E+10 -3.00 -2110.8923 -0.50
Ti9O17
10 1 9.0 0.0 17.0
-8141241.7 454.36515
1989.0000 753.55521 0.00000000 0.00000000 -19358722.
2 0.18701551E+10 -3.00 -2110.8923 -0.50
Ti10O19
10 1 10.0 0.0 19.0
-9085912.9 505.51533
1997.0000 831.39283 0.00000000 0.00000000 -22726564.
2 0.22730958E+10 -3.00 -2110.8923 -0.50
"Ti20O39"
10 1 20.0 0.0 39.0
-18533039. 1015.3802
2001.0000 1609.7690 0.00000000 0.00000000 -56404974.
2 0.63025026E+10 -3.00 -2110.8923 -0.50
Ti7O13
10 1 7.0 0.0 13.0
-6251589.1 351.91071
1976.0000 597.87997 0.00000000 0.00000000 -12623040.
2 0.10642738E+10 -3.00 -2110.8923 -0.50

```

9.3 APPENDIX C: Pure component data used in the optimisations.

FeO

FeO Units: P(atm) Energy(J)
Name: iron monoxide

Formula Weight: 71.8464

Phase	Cp_Range,_K	Density,_g/ml	Ref.
S wustite	298.15 - 1644.15	5.865	130 149
S wustite	1644.15 - 2000.00	5.865	130 149
L liquid	298.15 - 1644.15	5.865	130
L liquid	1644.15 - 2000.00	5.865	130
G gas	298.15 - 1600.00	ideal	128
G gas	1600.00 - 3900.00	ideal	128
G gas	3900.00 - 6000.00	ideal	128

$$C_p(T) = \sum_{i=1}^8 C(i) \times T^{P(i)} \quad (J/K)$$

	DH(298.15) (J)	S(298.15) (J/K)	C(i)	P(i)	C(i)	P(i)	Cp (K)
S	1 -265832.24	59.495798	-18.024474	0	3.06080599E-02	1	298 - 1644
S	1		-2533300.0	-2	1500.9000	-0.5	298 - 1644
S	2 -278950.16	39.512270	68.199200	0			1644 - 2000
L	3 -234643.15	78.465531	-18.024474	0	3.06080599E-02	1	298 - 1644
L	3		-2533300.0	-2	1500.9000	-0.5	298 - 1644
L	4 -247761.07	58.482003	68.199200	0			1644 - 2000
G	5 251040.00	241.811703	45.086391	0	-4.83422859E-03	1	298 - 1600
G	5		507276.22	-2	1.31685370E-06	2	298 - 1600
G	5		-5386.0381	-1			298 - 1600
G	6 285494.73	327.401532	140.03746	0	-2.73711719E-03	1	1600 - 3900
G	6		-62347823.	-2	253414.30	-1	1600 - 3900
G	6		-9285.3097	-0.5			1600 - 3900
G	7 -174342.21	-694.759881	2.4118912	0	3.02185632E+08	-2	3900 - 6000
G	7		-436463.46	-1	8192.9317	-0.5	3900 - 6000

G(T) J/mol - 1 atm

	G(T)	G(T)	G(T)	T(K)
S	1 - 322147.542	- 330.687435	T - 1.530402997E-02 T^2	298 - 1644
S	1 + 1266650.00	+ 6003.60001	T^0.5 + 18.0244741 T ln(T)	298 - 1644
S	2 - 299283.753	+ 417.258468	T - 68.1992000 T ln(T)	1644 - 2000
L	3 - 290958.454	- 349.657168	T - 1.530402997E-02 T^2	298 - 1644
L	3 + 1266650.00	+ 6003.60001	T^0.5 + 18.0244741 T ln(T)	298 - 1644
L	4 - 268094.665	+ 398.288735	T - 68.1992000 T ln(T)	1644 - 2000
G	5 264803.572	+ 73.9875439	T + 2.417114297E-03 T^2	298 - 1600
G	5 - 253638.108	- 2.194756174E-07	T^3 - 5386.03812 ln(T)	298 - 1600
G	5 - 45.0863911	T ln(T)		298 - 1600
G	6 - 835030.307	+ 1185.92621	T + 1.368558597E-03 T^2	1600 - 3900
G	6 + 31173911.5	+ 253414.297	ln(T) - 37141.2387 T^0.5	1600 - 3900
G	6 - 140.037464	T ln(T)		1600 - 3900
G	7 2605868.55	- 473.856883	T - 151092816. T^-1	3900 - 6000
G	7 - 436463.463	ln(T) + 32771.7268	T^0.5 - 2.41189124 T ln(T)	3900 - 6000

H(T) J/mol

	H(T)	H(T)	H(T)	T(K)

S	1	- 322147.542	- 18.0244741	T	+ 1.530402997E-02	T ²	298 - 1644
S	1	+ 2533299.99	T ⁻¹	+ 3001.80001	T ^{0.5}		298 - 1644
S	2	- 299283.753	+ 68.1992000	T			1644 - 2000
L	3	- 290958.454	- 18.0244741	T	+ 1.530402997E-02	T ²	298 - 1644
L	3	+ 2533299.99	T ⁻¹	+ 3001.80001	T ^{0.5}		298 - 1644
L	4	- 268094.665	+ 68.1992000	T			1644 - 2000
G	5	270189.610	+ 45.0863911	T	- 2.417114297E-03	T ²	298 - 1600
G	5	- 507276.216	T ⁻¹	+ 4.389512348E-07	T ³	- 5386.03812	ln(T) 298 - 1600
G	6	- 1088444.60	+ 140.037464	T	- 1.368558597E-03	T ²	1600 - 3900
G	6	+ 62347822.9	T ⁻¹	+ 253414.297	ln(T)	- 18570.6193	T ^{0.5} 1600 - 3900
G	7	3042332.01	+ 2.41189124	T	- 302185632.	T ⁻¹	3900 - 6000
G	7	- 436463.463	ln(T)	+ 16385.8634	T ^{0.5}		3900 - 6000

S(T) J/mol-K - 1 atm

	S(T)	S(T)	S(T)	T(K)
S	1 312.662961	- 18.0244741	ln(T)	+ 3.060805995E-02 T 298 - 1644
S	1 + 1266650.00	T ⁻²	- 3001.80001	T ^{-0.5} 298 - 1644
S	2 - 349.059268	+ 68.1992000	ln(T)	1644 - 2000
L	3 331.632694	- 18.0244741	ln(T)	+ 3.060805995E-02 T 298 - 1644
L	3 + 1266650.00	T ⁻²	- 3001.80001	T ^{-0.5} 298 - 1644
L	4 - 330.089535	+ 68.1992000	ln(T)	1644 - 2000
G	5 - 28.9011528	+ 45.0863911	ln(T)	- 4.834228595E-03 T 298 - 1600
G	5 - 253638.108	T ⁻²	+ 6.584268522E-07	T ² + 5386.03812 T ⁻¹ 298 - 1600
G	6 - 1045.88874	+ 140.037464	ln(T)	- 2.737117195E-03 T 1600 - 3900
G	6 + 31173911.5	T ⁻²	- 253414.297	T ⁻¹ + 18570.6193 T ^{-0.5} 1600 - 3900
G	7 476.268774	+ 2.41189124	ln(T)	- 151092816. T ⁻² 3900 - 6000
G	7 + 436463.463	T ⁻¹	- 16385.8634	T ^{-0.5} 3900 - 6000

Fe₂O₅Ti

Fe2O5Ti Units: P(atm) Energy(J)
Name: Iron Titanium Oxide

Formula Weight: 239.571

Phase	Cp_Range,_K	Density,_g/ml
S ferric pseudobrookite	298.15 - 2000.00	

$$Cp(T) = \sum_{i=1}^8 C(i) \times T^{P(i)} \quad (J/K)$$

	DH(298.15) (J)	S(298.15) (J/K)	C(i)	P(i)	C(i)	P(i)	Cp (K)
S 1	-1738786.72	171.962400	192.58952	0	2.20078400E-02	1	298 - 2000
S 1			-3100344.0	-2			298 - 2000

G(T) J/mol - 1 atm

	G(T)	G(T)	G(T)	T(K)
S 1	- 1807584.07	+ 1141.92472	T - 1.100392000E-02 T ²	298 - 2000
S 1	+ 1550172.00	T ⁻¹ - 192.589520	T ln(T)	298 - 2000

H(T) J/mol

	H(T)	H(T)	H(T)	T(K)
S 1	- 1807584.07	+ 192.589520	T + 1.100392000E-02 T ²	298 - 2000
S 1	+ 3100344.00	T ⁻¹		298 - 2000

S(T) J/mol-K - 1 atm

	S(T)	S(T)	S(T)	T(K)
S 1	- 949.335200	+ 192.589520	ln(T) + 2.200784000E-02 T	298 - 2000
S 1	+ 1550172.00	T ⁻²		298 - 2000

FeTi₂O₄

FeTi2O4 Units: P(atm) Energy(J)
Name: Iron titanate

Formula Weight: 215.6046

Phase	Cp_Range,_K	Density,_g/ml	Ref.
S solid	298.15 - 1818.00		130

$$Cp(T) = \sum_{i=1}^8 C(i) \times T^{P(i)} \quad (J/K)$$

	DH(298.15) (J)	S(298.15) (J/K)	C(i)	P(i)	C(i)	P(i)	Cp (K)
S	1 -1824402.78	139.443293	359.77796	0	-3.06080599E-02	1	298 - 1818
S	1		7510790.0	-2	-4068.5188	-0.5	298 - 1818
S	1		-2.02299170E+09	-3			298 - 1818

G(T) J/mol - 1 atm

	G(T)	G(T)	G(T)	T(K)
S	1 - 1775995.19	+ 2715.52290	T + 1.530402997E-02 T ²	298 - 1818
S	1 - 3755395.01	T ⁻¹ - 16274.0750	T ^{0.5} + 337165283.	T ⁻² 298 - 1818
S	1 - 359.777959	T ln(T)		298 - 1818

H(T) J/mol

	H(T)	H(T)	H(T)	T(K)
S	1 - 1775995.19	+ 359.777959	T - 1.530402997E-02 T ²	298 - 1818
S	1 - 7510790.03	T ⁻¹ - 8137.03751	T ^{0.5} + 1.011495849E+09 T ⁻²	298 - 1818

S(T) J/mol-K - 1 atm

	S(T)	S(T)	S(T)	T(K)
S	1 - 2355.74494	+ 359.777959	ln(T) - 3.060805995E-02 T	298 - 1818
S	1 - 3755395.01	T ⁻² + 8137.03751	T ^{-0.5} + 674330566.	T ⁻³ 298 - 1818

Fe₂TiO₄

(FeO)₂(TiO₂) Units: P(atm) Energy(J)
 Name: Iron orthotitanate (Ulvospinel)

Formula Weight: 223.5716

Phase	Cp_Range,_K	Density,_g/ml	Ref.
S ulvospinel	298.15 - 2000.00	4.775523	130 132
L liquid	298.15 - 2000.00	4.776	130

$$C_p(T) = \sum_{i=1}^8 C(i) \times T^{P(i)} \quad (J/K)$$

	DH(298.15) (J)	S(298.15) (J/K)	C(i)	P(i)	C(i)	P(i)	Cp (K)
S	1 -1515609.69	168.870006	249.63000	0	-1817.4000	-0.5	298 - 2000
S	1		-54530001.	-3			298 - 2000
L	2 -1376824.32	252.074665	249.63000	0	-1817.4000	-0.5	298 - 2000
L	2		-54530001.	-3			298 - 2000

G(T) J/mol - 1 atm

	G(T)	G(T)	G(T)	T(K)
S	1 - 1527581.43	+ 1714.24222	T - 7269.59992	T ^{0.5} 298 - 2000
S	1 + 9088333.48	T ⁻² - 249.630000	T ln(T)	298 - 2000
L	2 - 1388796.05	+ 1631.03756	T - 7269.59992	T ^{0.5} 298 - 2000
L	2 + 9088333.48	T ⁻² - 249.630000	T ln(T)	298 - 2000

H(T) J/mol

	H(T)	H(T)	H(T)	T(K)
S	1 - 1527581.43	+ 249.630000	T - 3634.79996	T ^{0.5} 298 - 2000
S	1 + 27265000.4	T ⁻²		298 - 2000
L	2 - 1388796.05	+ 249.630000	T - 3634.79996	T ^{0.5} 298 - 2000
L	2 + 27265000.4	T ⁻²		298 - 2000

S(T) J/mol-K - 1 atm

	S(T)	S(T)	S(T)	T(K)
S	1 - 1464.61222	+ 249.630000	ln(T) + 3634.79996	T ^{-0.5} 298 - 2000
S	1 + 18176667.0	T ⁻³		298 - 2000
L	2 - 1381.40756	+ 249.630000	ln(T) + 3634.79996	T ^{-0.5} 298 - 2000
L	2 + 18176667.0	T ⁻³		298 - 2000

FeTiO₃

(FeO)(TiO₂) Units: P(atm) Energy(J)
 Name: Iron metatitanate (Ilmenite)

Formula Weight: 151.7252

Phase	Cp_Range,_K	Density,_g/ml
S ilmenite	298.15 - 1650.00	4.789

$$C_p(T) = \sum_{i=1}^8 C(i) \times T^{P(i)} \quad (J/K)$$

	DH(298.15) (J)	S(298.15) (J/K)	C(i)	P(i)	C(i)	P(i)	Cp (K)
S	1 -1233142.16	108.627506	149.99950	0	-3323694.0	-2	298 - 1650
S	1		-441.62199	-0.5	3.48151037E+08	-3	298 - 1650

G(T) J/mol - 1 atm

	G(T)	G(T)	G(T)	T(K)
S	1 - 1271802.99	+ 961.476891	T + 1661847.00	T ⁻¹ 298 - 1650
S	1 - 1766.48798	T ^{0.5} - 58025172.9	T ⁻² - 149.999500	T ln(T) 298 - 1650

H(T) J/mol

	H(T)	H(T)	H(T)	T(K)
S	1 - 1271802.99	+ 149.999500	T + 3323694.00	T ⁻¹ 298 - 1650
S	1 - 883.243990	T ^{0.5} - 174075519.	T ⁻²	298 - 1650

S(T) J/mol-K - 1 atm

	S(T)	S(T)	S(T)	T(K)
S	1 - 811.477390	+ 149.999500	ln(T) + 1661847.00	T ⁻² 298 - 1650
S	1 + 883.243990	T ^{-0.5} - 116050346.	T ⁻³	298 - 1650

FeTi₂O₅

FeTi2O5 Units: P(atm) Energy(J)
 Name: Iron titanate (Pseudobrookite)

Formula Weight: 231.604

Phase	Cp_Range,_K	Density,_g/ml	Ref.
S pseudobrookite	298.15 - 1728.00		130

$$C_p(T) = \sum_{i=1}^8 C(i) \times T^{P(i)} \quad (J/K)$$

	DH(298.15) (J)	S(298.15) (J/K)	C(i)	P(i)	C(i)	P(i)	Cp (K)
S 1	-2152814.44	176.569402	247.15400	0	-4502760.1	-2	298 - 1728
S 1			-1026.1500	-0.5	4.55516013E+08	-3	298 - 1728

G(T) J/mol - 1 atm

	G(T)	G(T)	G(T)	T(K)
S 1	- 2203606.48	+ 1617.22281	T + 2251380.07	T ⁻¹ 298 - 1728
S 1	- 4104.60006	T ^{0.5} - 75919335.5	T ⁻² - 247.154001	T ln(T) 298 - 1728

H(T) J/mol

	H(T)	H(T)	H(T)	T(K)
S 1	- 2203606.48	+ 247.154001	T + 4502760.13	T ⁻¹ 298 - 1728
S 1	- 2052.30003	T ^{0.5} - 227758006.	T ⁻²	298 - 1728

S(T) J/mol-K - 1 atm

	S(T)	S(T)	S(T)	T(K)
S 1	- 1370.06881	+ 247.154001	ln(T) + 2251380.07	T ⁻² 298 - 1728
S 1	+ 2052.30003	T ^{-0.5} - 151838671.	T ⁻³	298 - 1728

Ti₂O₃

Ti2O3 Units: P(atm) Energy(J)
Name: titanium sesquioxide

Formula Weight: 143.7582

Phase	Cp_Range,_K	Density,_g/ml
S1 solid-a	298.15 - 470.00	4.6
S1 solid-a	470.00 - 2115.00	4.6
S1 solid-a	2115.00 - 2500.00	4.6
S2 solid-b	298.15 - 2115.00	4.6
S2 solid-b	2115.00 - 2500.00	4.6
L liquid	298.15 - 2115.00	4.6
L liquid	2115.00 - 2500.00	4.6

$$Cp(T) = \sum_{i=1}^8 C(i) \times T^{P(i)} \quad (J/K)$$

	DH(298.15) (J)	S(298.15) (J/K)	C(i)	P(i)	C(i)	P(i)	Cp (K)
S1	1 -1520884.00	77.252974	730.23381	0	18808385.	-2	298 - 470
S1	1		-14604.866	-0.5			298 - 470
S1	2 -1520513.48	78.107546	169.96111	0	1609648.9	-2	470 - 2115
S1	2		-750.21869	-0.5	-1.56552100E+09	-3	470 - 2115
S1	3 -1543872.02	38.666441	156.90000	0			2115 - 2500
S2	4 -1519375.38	80.529126	169.96111	0	1609648.9	-2	298 - 2115
S2	4		-750.21869	-0.5	-1.56552100E+09	-3	298 - 2115
S2	5 -1542733.92	41.088021	156.90000	0			2115 - 2500
L	6 -1414375.30	130.174487	169.96111	0	1609648.9	-2	298 - 2115
L	6		-750.21869	-0.5	-1.56552100E+09	-3	298 - 2115
L	7 -1437733.84	90.733382	156.90000	0			2115 - 2500

G(T) J/mol - 1 atm

	G(T)	G(T)	G(T)	T(K)
S1	1 - 1171154.54	+ 6399.41546	T	- 9404192.70
S1	1 - 58419.4632	- 730.233813	T ln(T)	T^-1
S1	2 - 1548686.12	+ 1157.75518	T	298 - 470
S1	2 - 3000.87476	+ 260920167.	- 804824.470	T^-1
S1	3 - 1590651.75	+ 1012.18648	T	470 - 2115
S2	4 - 1547548.01	+ 1155.33360	- 169.961109	T ln(T)
S2	4 - 3000.87476	+ 260920167.	T	2115 - 2500
S2	5 - 1589513.65	+ 1009.76490	- 804824.470	T^-1
L	6 - 1442547.94	+ 1105.68824	T	298 - 2115
L	6 - 3000.87476	+ 260920167.	- 156.900000	T ln(T)
L	7 - 1484513.58	+ 960.119543	T	2115 - 2500

H(T) J/mol

	H(T)	H(T)	H(T)	T(K)
S1	1 - 1171154.54	+ 730.233813	T	- 18808385.4
S1	1 - 29209.7316	T^0.5	T	T^-1
S1	2 - 1548686.12	+ 169.961109	- 1609648.94	298 - 470
S1	2 - 1500.43738	+ 782760502.	T^-2	T^-1
S1	3 - 1590651.75	+ 156.900000	T	470 - 2115
S2	4 - 1547548.01	+ 169.961109	- 1609648.94	2115 - 2500
S2	4 - 1500.43738	+ 782760502.	T^-2	T^-1
S2	5 - 1589513.65	+ 156.900000	T	298 - 2115
L	6 - 1442547.94	+ 169.961109	- 1609648.94	2115 - 2500
L	6 - 1500.43738	+ 782760502.	T^-2	T^-1
L	7 - 1484513.58	+ 156.900000	T	298 - 2115

S(T) J/mol-K - 1 atm

	S(T)	S(T)	S(T)	T (K)
S1	1 - 5669.18165	+ 730.233813	ln(T) - 9404192.70	T ⁻² 298 - 470
S1	1 + 29209.7316	T ^{-0.5}		298 - 470
S1	2 - 987.794067	+ 169.961109	ln(T) - 804824.470	T ⁻² 470 - 2115
S1	2 + 1500.43738	+ 521840335.	T ⁻³	470 - 2115
S1	3 - 855.286484	+ 156.900000	ln(T)	2115 - 2500
S2	4 - 985.372487	+ 169.961109	ln(T) - 804824.470	T ⁻² 298 - 2115
S2	4 + 1500.43738	+ 521840335.	T ⁻³	298 - 2115
S2	5 - 852.864903	+ 156.900000	ln(T)	2115 - 2500
L	6 - 935.727126	+ 169.961109	ln(T) - 804824.470	T ⁻² 298 - 2115
L	6 + 1500.43738	+ 521840335.	T ⁻³	298 - 2115
L	7 - 803.219543	+ 156.900000	ln(T)	2115 - 2500

Ti₃O₅

Ti305 Units: P(atm) Energy(J)

Name: Titanium pentoxide

Formula Weight: 223.637

Phase	Cp_Range,_K	Density,_g/ml	Ref.
S1 solid-a	298.15 - 450.00		128 130
S1 solid-a	450.00 - 1991.00		128 130
S2 solid-b	298.15 - 1991.00		128 130

$$Cp(T) = \sum_{i=1}^8 C(i) \times T^{P(i)} \quad (J/K)$$

	DH(298.15) (J)	S(298.15) (J/K)	C(i)	P(i)	C(i)	P(i)	Cp (K)
S1	1	-2465422.00	129.369046	278.89989	0	7136016.6	-2 298 - 450
S1	1			-2149.4709	-0.5	-2.11960051E+09	-3 298 - 450
S1	2	-2465642.45	128.404484	158.99208	0	5.02079456E-02	1 450 - 1991
S2	3	-2452465.03	157.616983	158.99208	0	5.02079456E-02	1 298 - 1991

G(T) J/mol - 1 atm

	G(T)	G(T)	G(T)	T(K)
S1	1 - 2462333.91	+ 1974.07831	T - 3568008.30	T ⁻¹ 298 - 450
S1	1 - 8597.88352	T ^{0.5} + 353266752.	T ⁻² - 278.899892	T ln(T) 298 - 450
S1	2 - 2515277.51	+ 951.429844	T - 2.510397280E-02	T ² 450 - 1991
S1	2 - 158.992079	T ln(T)		450 - 1991
S2	3 - 2502100.10	+ 922.217346	T - 2.510397280E-02	T ² 298 - 1991
S2	3 - 158.992079	T ln(T)		298 - 1991

H(T) J/mol

	H(T)	H(T)	H(T)	T(K)
S1	1 - 2462333.91	+ 278.899892	T - 7136016.60	T ⁻¹ 298 - 450
S1	1 - 4298.94176	T ^{0.5} + 1.059800255E+09	T ⁻²	298 - 450
S1	2 - 2515277.51	+ 158.992079	T + 2.510397280E-02	T ² 450 - 1991
S2	3 - 2502100.10	+ 158.992079	T + 2.510397280E-02	T ² 298 - 1991

S(T) J/mol-K - 1 atm

	S(T)	S(T)	S(T)	T(K)
S1	1 - 1695.17842	+ 278.899892	ln(T) - 3568008.30	T ⁻² 298 - 450
S1	1 + 4298.94176	T ^{-0.5} + 706533503.	T ⁻³	298 - 450
S1	2 - 792.437765	+ 158.992079	ln(T) + 5.020794561E-02	T 450 - 1991
S2	3 - 763.225266	+ 158.992079	ln(T) + 5.020794561E-02	T 298 - 1991

Ti₄O₇

Ti4O7 Units: P(atm) Energy(J)
 Name: Titanium heptaoxide

Formula Weight: 303.5158

Phase	Cp_Range,_K	Density,_g/ml
S solid	298.15 - 2000.00	

$$C_p(T) = \sum_{i=1}^8 C(i) \times T^{P(i)} \quad (J/K)$$

	DH(298.15) (J)	S(298.15) (J/K)	C(i)	P(i)	C(i)	P(i)	Cp (K)
S	1 -3414316.92	197.443579	364.36711	0	-2519517.2	-2	298 - 2000
S	1		-2110.8923	-0.5	-1.44548234E+08	-3	298 - 2000

G(T) J/mol - 1 atm

	G(T)	G(T)	G(T)	T(K)
S	1 - 3459318.88	+ 2503.42979	T + 1259758.59	T ⁻¹ 298 - 2000
S	1 - 8443.56923	T ^{0.5} + 24091372.3	T ⁻² - 364.367109	T ln(T) 298 - 2000

H(T) J/mol

	H(T)	H(T)	H(T)	T(K)
S	1 - 3459318.88	+ 364.367109	T + 2519517.19	T ⁻¹ 298 - 2000
S	1 - 4221.78462	T ^{0.5} + 72274116.8	T ⁻²	298 - 2000

S(T) J/mol-K - 1 atm

	S(T)	S(T)	S(T)	T(K)
S	1 - 2139.06268	+ 364.367109	ln(T) + 1259758.59	T ⁻² 298 - 2000
S	1 + 4221.78462	T ^{-0.5} + 48182744.6	T ⁻³	298 - 2000

Ti₂O₃

Ti509 Units: P(atm) Energy(J)
Name: Titanium nonoxide

Formula Weight: 383.3946

Phase	Cp_Range,_K	Density,_g/ml
S solid	298.15 - 2000.00	

$$C_p(T) = \sum_{i=1}^8 C(i) \times T^{P(i)} \quad (J/K)$$

	DH(298.15) (J)	S(298.15) (J/K)	C(i)	P(i)	C(i)	P(i)	Cp (K)
S	1 -4360918.35	248.954456	442.20474	0	-5887358.3	-2	298 - 2000
S	1		-2110.8923	-0.5	2.58392443E+08	-3	298 - 2000

G(T) J/mol - 1 atm

	G(T)	G(T)	G(T)	T(K)
S	1 - 4438156.96	+ 2987.11938	T + 2943679.14	T ⁻¹ 298 - 2000
S	1 - 8443.56923	T ^{0.5} - 43065407.1	T ⁻² - 442.204742	T ln(T) 298 - 2000

H(T) J/mol

	H(T)	H(T)	H(T)	T(K)
S	1 - 4438156.96	+ 442.204742	T + 5887358.28	T ⁻¹ 298 - 2000
S	1 - 4221.78462	T ^{0.5} - 129196221.	T ⁻²	298 - 2000

S(T) J/mol-K - 1 atm

	S(T)	S(T)	S(T)	T(K)
S	1 - 2544.91464	+ 442.204742	ln(T) + 2943679.14	T ⁻² 298 - 2000
S	1 + 4221.78462	T ^{-0.5} - 86130814.3	T ⁻³	298 - 2000

Ti₆O₁₁

Ti6O11 Units: P(atm) Energy(J)
Name: Titanium endecaoxide

Formula Weight: 463.2734

Phase Cp_Range,_K Density,_g/ml

S solid 298.15 - 2000.00

$$Cp(T) = \sum_{i=1}^8 C(i) \times T^{P(i)} \quad (J/K)$$

	DH(298.15) (J)	S(298.15) (J/K)	C(i)	P(i)	C(i)	P(i)	Cp (K)
S 1	-5306479.34	300.501528	520.04233	0	-9255199.2	-2	298 - 2000
S 1			-2110.8923	-0.5	6.61333123E+08	-3	298 - 2000

G(T) J/mol - 1 atm

	G(T)	G(T)	G(T)	T(K)
S 1	- 5415954.60	+ 3470.77247	T + 4627599.60	T ⁻¹ 298 - 2000
S 1	- 8443.56923	T ^{0.5} - 110222187.	T ⁻² - 520.042330	T ln(T) 298 - 2000

H(T) J/mol

	H(T)	H(T)	H(T)	T(K)
S 1	- 5415954.60	+ 520.042330	T + 9255199.21	T ⁻¹ 298 - 2000
S 1	- 4221.78462	T ^{0.5} - 330666562.	T ⁻²	298 - 2000

S(T) J/mol-K - 1 atm

	S(T)	S(T)	S(T)	T(K)
S 1	- 2950.73014	+ 520.042330	ln(T) + 4627599.60	T ⁻² 298 - 2000
S 1	+ 4221.78462	T ^{-0.5} - 220444374.	T ⁻³	298 - 2000

Ti₇O₁₃

Ti7O13 Units: P(atm) Energy(J)
Name: Heptatitanium oxide

Formula Weight: 543.1522

Phase	Cp_Range,_K	Density,_g/ml	Ref.
S solid	298.15 - 2000.00		130

$$Cp(T) = \sum_{i=1}^8 C(i) \times T^{P(i)} \quad (J/K)$$

	DH(298.15) (J)	S(298.15) (J/K)	C(i)	P(i)	C(i)	P(i)	Cp (K)
S	1 -6251588.87	351.910705	597.87996	0	-12623040.	-2	298 - 2000
S	1		-2110.8923	-0.5	1.06427375E+09	-3	298 - 2000

G(T) J/mol - 1 atm

	G(T)	G(T)	G(T)	T(K)
S	1 - 6393300.79	+ 3954.56374	T + 6311520.07	T ⁻¹ 298 - 2000
S	1 - 8443.56923	T ^{0.5} - 177378958.	T ⁻² - 597.879960	T ln(T) 298 - 2000

H(T) J/mol

	H(T)	H(T)	H(T)	T(K)
S	1 - 6393300.79	+ 597.879960	T + 12623040.1	T ⁻¹ 298 - 2000
S	1 - 4221.78462	T ^{0.5} - 532136873.	T ⁻²	298 - 2000

S(T) J/mol-K - 1 atm

	S(T)	S(T)	S(T)	T(K)
S	1 - 3356.68378	+ 597.879960	ln(T) + 6311520.07	T ⁻² 298 - 2000
S	1 + 4221.78462	T ^{-0.5} - 354757915.	T ⁻³	298 - 2000

Ti₈O₁₅

Ti8O15 Units: P(atm) Energy(J)
Name: Octatitanium oxide

Formula Weight: 623.031

Phase	Cp_Range,_K	Density,_g/ml
S solid	298.15 - 2000.00	

$$Cp(T) = \sum_{i=1}^8 C(i) \times T^{P(i)} \quad (J/K)$$

	DH(298.15) (J)	S(298.15) (J/K)	C(i)	P(i)	C(i)	P(i)	Cp (K)
S	1 -7196482.51	403.170282	675.71759	0	-15990881.	-2	298 - 2000
S	1		-2110.8923	-0.5	1.46721445E+09	-3	298 - 2000

G(T) J/mol - 1 atm

	G(T)	G(T)	G(T)	T(K)
S	1 - 7370431.09	+ 4438.50460	T + 7995440.53	T ⁻¹ 298 - 2000
S	1 - 8443.56923	T ^{0.5} - 244535742.	T ⁻² - 675.717590	T ln(T) 298 - 2000

H(T) J/mol

	H(T)	H(T)	H(T)	T(K)
S	1 - 7370431.09	+ 675.717590	T + 15990881.1	T ⁻¹ 298 - 2000
S	1 - 4221.78462	T ^{0.5} - 733607226.	T ⁻²	298 - 2000

S(T) J/mol-K - 1 atm

	S(T)	S(T)	S(T)	T(K)
S	1 - 3762.78701	+ 675.717590	ln(T) + 7995440.53	T ⁻² 298 - 2000
S	1 + 4221.78462	T ^{-0.5} - 489071484.	T ⁻³	298 - 2000

Ti₉O₁₇

Ti9O17 Units: P(atm) Energy(J)
Name: Nonatitanium oxide

Formula Weight: 702.9098

Phase	Cp_Range,_K	Density,_g/ml
S solid	298.15 - 2000.00	

$$C_p(T) = \sum_{i=1}^8 C(i) \times T^{P(i)} \quad (\text{J/K})$$

	DH(298.15) (J)	S(298.15) (J/K)	C(i)	P(i)	C(i)	P(i)	Cp (K)
S	1 -8141241.84	454.365162	753.55522	0	-19358722.	-2	298 - 2000
S	1		-2110.8923	-0.5	1.87015512E+09	-3	298 - 2000

G(T) J/mol - 1 atm

	G(T)	G(T)	G(T)	T(K)
S	1 - 8347427.08	+ 4922.51016	T + 9679361.20	T ⁻¹ 298 - 2000
S	1 - 8443.56923	T ^{0.5} - 311692519.	T ⁻² - 753.555220	T ln(T) 298 - 2000

H(T) J/mol

	H(T)	H(T)	H(T)	T(K)
S	1 - 8347427.08	+ 753.555220	T + 19358722.4	T ⁻¹ 298 - 2000
S	1 - 4221.78462	T ^{0.5} - 935077558.	T ⁻²	298 - 2000

S(T) J/mol-K - 1 atm

	S(T)	S(T)	S(T)	T(K)
S	1 - 4168.95494	+ 753.555220	ln(T) + 9679361.20	T ⁻² 298 - 2000
S	1 + 4221.78462	T ^{-0.5} - 623385038.	T ⁻³	298 - 2000

Ti₁₀O₁₉

Ti10019 Units: P(atm) Energy(J)
Name: Decatitanium oxide

Formula Weight: 782.7886

Phase	Cp_Range,_K	Density,_g/ml
S solid	298.15 - 2000.00	

$$C_p(T) = \sum_{i=1}^8 C(i) \times T^{P(i)} \quad (J/K)$$

	DH(298.15) (J)	S(298.15) (J/K)	C(i)	P(i)	C(i)	P(i)	Cp (K)
S	1 -9085912.90	505.515315	831.39285	0	-22726564.	-2	298 - 2000
S	1		-2110.8923	-0.5	2.27309578E+09	-3	298 - 2000

G(T) J/mol - 1 atm

	G(T)	G(T)	G(T)	T(K)
S	1 - 9324334.79	+ 5406.56045	T + 11363282.1	T ⁻¹ 298 - 2000
S	1 - 8443.56923	T ^{0.5} - 378849297.	T ⁻² - 831.392849	T ln(T) 298 - 2000

H(T) J/mol

	H(T)	H(T)	H(T)	T(K)
S	1 - 9324334.79	+ 831.392849	T + 22726564.2	T ⁻¹ 298 - 2000
S	1 - 4221.78462	T ^{0.5} - 1.136547890E+09	T ⁻²	298 - 2000

S(T) J/mol-K - 1 atm

	S(T)	S(T)	S(T)	T(K)
S	1 - 4575.16760	+ 831.392849	ln(T) + 11363282.1	T ⁻² 298 - 2000
S	1 + 4221.78462	T ^{-0.5} - 757698593.	T ⁻³	298 - 2000

Ti₂₀O₃₉

Ti20O39 Units: P(atm) Energy(J)
Name: Higher Magneli phases

Formula Weight: 1581.5766

Phase	Cp_Range,_K	Density,_g/ml
S higher magneli phases (composite)	298.15 - 2000.00	

$$Cp(T) = \sum_{i=1}^8 C(i) \times T^{P(i)} \quad (J/K)$$

	DH(298.15) (J)	S(298.15) (J/K)	C(i)	P(i)	C(i)	P(i)	Cp (K)
S 1	-18533038.46	1015.380191	1609.7690	0	-56404973.	-2	298 - 2000
S 1			-2110.8923	-0.5	6.30250271E+09	-3	298 - 2000

G(T) J/mol - 1 atm

	G(T)	G(T)	G(T)	T(K)
S 1	- 19093826.9	+ 10248.6988	T + 28202486.3	T ⁻¹ 298 - 2000
S 1	- 8443.56923	T ^{0.5} - 1.050417119E+09	T ⁻² - 1609.76898	T ln(T) 298 - 2000

H(T) J/mol

	H(T)	H(T)	H(T)	T(K)
S 1	- 19093826.9	+ 1609.76898	T + 56404972.6	T ⁻¹ 298 - 2000
S 1	- 4221.78462	T ^{0.5} - 3.151251356E+09	T ⁻²	298 - 2000

S(T) J/mol-K - 1 atm

	S(T)	S(T)	S(T)	T(K)
S 1	- 8638.92987	+ 1609.76898	ln(T) + 28202486.3	T ⁻² 298 - 2000
S 1	+ 4221.78462	T ^{-0.5} - 2.100834237E+09	T ⁻³	298 - 2000

TiO₂

TiO2 Units: P(atm) Energy(J)
Name: titanium dioxide (Rutile)

Formula Weight: 79.8788

Phase	Cp_Range,_K	Density,_g/ml
S1 rutile	298.15 - 2130.00	4.245
S1 rutile	2130.00 - 3000.00	4.245
S2 anatase	298.15 - 2100.00	3.84
S2 anatase	2100.00 - 3000.00	3.84
L liquid	298.15 - 2130.00	4.245
L liquid	2130.00 - 3000.00	4.245

$$Cp(T) = \sum_{i=1}^8 C(i) \times T^{P(i)} \quad (J/K)$$

	DH(298.15) (J)	S(298.15) (J/K)	C(i)	P(i)	C(i)	P(i)	Cp (K)	
S1	1	-944749.99	50.460007	77.837621	0	-3367841.0	-2	298 - 2130
S1	1			4.02940672E+08	-3			298 - 2130
S1	2	-993602.83	-7.453545	100.41600	0			2130 - 3000
S2	3	-933032.00	49.915120	75.035856	0	-1762719.2	-2	298 - 2100
S2	4	-983836.01	-9.344290	100.41600	0			2100 - 3000
L	5	-898725.99	72.067513	77.837621	0	-3367841.0	-2	298 - 2130
L	5			4.02940672E+08	-3			298 - 2130
L	6	-947578.83	14.153962	100.41600	0			2130 - 3000

G(T) J/mol - 1 atm

	G(T)	G(T)	G(T)	T(K)			
S1	1	-976986.650	+ 484.740378	T	+ 1683920.51	T ⁻¹	298 - 2130
S1	1	-67156778.7	- 77.8376214	T ln(T)			298 - 2130
S1	2	-1023541.86	+ 679.999417	T	- 100.416000	T ln(T)	2130 - 3000
S2	3	-961316.130	+ 462.559573	T	+ 881359.600	T ⁻¹	298 - 2100
S2	3	-75.0358560		T ln(T)			298 - 2100
S2	4	-1013775.04	+ 681.890162	T	- 100.416000	T ln(T)	2100 - 3000
L	5	-930962.650	+ 463.132871	T	+ 1683920.51	T ⁻¹	298 - 2130
L	5	-67156778.7	- 77.8376214	T ln(T)			298 - 2130
L	6	-977517.858	+ 658.391910	T	- 100.416000	T ln(T)	2130 - 3000

H(T) J/mol

	H(T)	H(T)	H(T)	T(K)			
S1	1	-976986.650	+ 77.8376214	T	+ 3367841.01	T ⁻¹	298 - 2130
S1	1	-201470336.		T ⁻²			298 - 2130
S1	2	-1023541.86	+ 100.416000	T			2130 - 3000
S2	3	-961316.130	+ 75.0358560	T	+ 1762719.20	T ⁻¹	298 - 2100
S2	4	-1013775.04	+ 100.416000	T			2100 - 3000
L	5	-930962.650	+ 77.8376214	T	+ 3367841.01	T ⁻¹	298 - 2130
L	5	-201470336.		T ⁻²			298 - 2130
L	6	-977517.858	+ 100.416000	T			2130 - 3000

S(T) J/mol-K - 1 atm

	S(T)	S(T)	S(T)	T(K)			
S1	1	-406.902756	+ 77.8376214	ln(T)	+ 1683920.51	T ⁻²	298 - 2130
S1	1	-134313557.		T ⁻³			298 - 2130

S1	2 - 579.583417	+ 100.416000	ln(T)		2130 - 3000
S2	3 - 387.523717	+ 75.0358560	ln(T) + 881359.600	T ⁻²	298 - 2100
S2	4 - 581.474162	+ 100.416000	ln(T)		2100 - 3000
L	5 - 385.295250	+ 77.8376214	ln(T) + 1683920.51	T ⁻²	298 - 2130
L	5 - 134313557.	T ⁻³			298 - 2130
L	6 - 557.975910	+ 100.416000	ln(T)		2130 - 3000

NOMENCLATURE

A	–	Arrhenius constant
R	–	Universal gas constant
T	–	absolute temperature
κ	–	electrical conductivity
E_{κ}	–	energy of activation for viscous flow
μ	–	viscosity
i, j	–	components
$i - j$	–	nearest-neighbour pairs
α, β	–	constants (Regular solution model)
${}^k L_{ij}$	–	empirical constant (Sub-regular solution model)
χ_i	–	charge of the ion of component i (Two-Sublattice model)
P, Q	–	number of sites on the sub-lattices (Two-Sublattice model)
y_i	–	site fraction of component i
y_{Va}	–	site fraction of vacancies
m	–	number of components
a_i	–	activity of component i
σ_{ij}	–	pair bond non-configurational entropy
n_i	–	number of moles of i
n_{ij}	–	number of moles of $i - j$ pairs
v_i, u_i	–	stoichiometric indexes
$R_{ib}, 2R_{ij}$	–	numbers of $i - O - i, i - O - j$ cells
$R_{ij}^* = (v_i v_j X_i X_j) / D_i$	–	fraction of $i - O - j$ cells for a random distribution of cations on their sublattice

$$D_i = \sum_{k=i+1}^m v_k X_k$$

$$Q_i = \sum_{k=i+1}^m (v_k X_k / D_i) (E_{ik} / RT)$$

$$P_{ij} = \begin{matrix} 1 & \text{if } (j = i) \\ \exp(Q_i) \cdot \exp(Q_j) \exp(-W_{ij}/RT) & \text{if } (j \neq i) \end{matrix}$$

Ω_i	–	$\Omega_i = n_i!/(n_{ii}!(n_i - n_{ii})!)$
ε_{ij}	–	pair bond energies
ϕ_{ijk}	–	adjustable ternary parameters
$\delta_{ij} = \begin{matrix} 1 & (i = j) \\ 0 & (i \neq j) \end{matrix}$	–	KRONECKER's delta
η	–	molar non-configurational entropy change (MQC model)
ω	–	molar enthalpy change (MQC model)
z	–	lattice co-ordination number
a, b	–	integers
$r = a/(a + b)$		
$E_{ij} = (E_{ij})_1 + (E_{ij})_2 \cdot X_i$	–	energy parameters for cells interaction (cell model)
$W_{ij} = (W_{ij})_1 + (W_{ij})_2 \cdot X_i$	–	energy parameters for asymmetric cells formation (cell model)
k	–	constant
k_b	–	Boltzmann's constant
N^0	–	Avogadro's number
T_{mA}	–	melting temperature of A
X_i	–	mole fractions
X_{ij}	–	mole fractions of each type of pair in solution
Y_i	–	equivalent fractions
Δ	–	change in
C_P	–	heat capacity at constant pressure
H	–	enthalpy
S	–	entropy
H^E	–	excess enthalpy

S^E	–	excess entropy
H^{id}	–	enthalpy (ideal solution)
S^{id}	–	entropy (ideal solution)
H^{reg}	–	enthalpy (regular solution)
S^{reg}	–	entropy (regular solution)
H_{fus}°	–	enthalpy of fusion
S_{fus}°	–	entropy of fusion
H_m	–	enthalpy of melting of the pure component
S_m	–	entropy of melting of the pure component
H_{298}°	–	enthalpy of formation at 298 K
S_{298}°	–	entropy of formation at 298 K
H_{mix}	–	enthalpy of mixing
S_{mix}	–	entropy of mixing
S_{config}	–	configurational entropy
$S_{nonconfig}$	–	non-configurational entropy
\bar{G}_i	–	partial molar Gibbs free energy of component i
p_i	–	partial pressure of component i in solution
p_i^0	–	partial pressure of pure component i
f_i	–	fugacity of component i in solution
f_i^θ	–	fugacity pressure of pure component i
γ_i	–	activity coefficient of component i